SAG AND SWELL OF EXTRUDATE FROM ANNULAR DIES

by

Neşe Orbey

A thesis submitted to the Faculty of Graduate Studies and
Research in partial fulfillment of the requirements for
the degree of Doctor of Philosophy

Departement of Chemical Engineering
McGill University
Montreal, Canada

Ph.D. Nesе Orbey Copy 1

To Hasan

ABSTRACT

In the extrusion blow molding process the shape and thickness distribution of the finished container depend on the dimensions of the parison at the time of inflation. In particular, the processes of swell and sag act to cause a variation of parison dimensions between the time the melt emerges from the die and the moment of inflation.

In the present study the effects of die geometry, extrusion velocity and the rheological properties of the resin on parison behavior were studied. Four annular dies (a straight, a diverging and two converging dies) and three high density polyethylene resins were used. To study the individual contributions of swell and sag to the overall parison behavior, two types of experiments were carried out. First, swell was studied in the absence of sag by extruding the parison into an isothermal oil bath. Both diameter and thickness swells were measured as functions of time. Then combined effect of swell and sag was studied by extruding the parison into an isothermal air oven.

A simple lumped parameter model was developed to predict the length of the parison using the swell data, storage modulus and process variables.

RESUME

Dans le moulage par extrusion-soufflage, la forme et la répartition de l'épaisseur des parois des articles finis sont determinées par les diménsions du paraison avant le soufflage. En particulier, les phénomènes de gonflement et d'étirage, entre les temps de formation et de gonflement, determinent les diménsions du paraison.

Dans l'étude présente, les effets de la géometrie de la filière, de la vitesse d'extrusion et les propriétés rhéologiques ont été étudiés. Quatre filières annulaires (une filière rectilique, une filière divergente et deux filierès convergentes) et trois résines de polyéthylène à haute densité ont été utilisées. Pour l'étude des contributions individuelles d'étirage et de gonflement au comportement total du paraison, deux sortes d'expériences ont été utilisées. Premièrement, l'étirage du paraison a été éliminé en extrudant dans un bain d'huile isotherme. Le gonflement de l'épaisseur et du diamètre ont été determinés en fonction du temps. L'effet combiné de gonflement et d'étirage a été étudie en extrudant dans un four isotherme à circulation d'air.

Un modèle simple pour la prédiction de la longueur du paraison a été proposé. Ce modèle utilise les données expérimentales de gonflement, le composante du module en phase et certaines variables d'opération du procédé.

ACKNOWLEDGEMENTS

I am particularly indebted to my thesis supervisor Professor J.M. Dealy, for his advice and guidance throughout all the facets of the project.

I would also like to express my appreciation to the following people and orginizations:

I am grateful to Professor M.R Kamal for his helpful comments.

I am grateful to my colleagues Ms. S.S. Soong, Mr. P.G. Lafleur and Dr. V. Tan for many helpful discussions.

I am indebted to Messrs. A. Krish, H. Alexander and W. Greenland for their diligent work in constructing the dies, and to Messrs. J. Dumont and W. Hoogendoorn for their assistance with equipment and instrumental problems.

I am grateful to Mr. D. Parks of Union Carbide and his associates for their help in the blow molding experiments and to Union Carbide of Canada Limited for their permission to use their facilities.

I wish to thank to the National Sciences and Engineering Research Council of Canada and to the Chemical Engineering Department of McGill University for financial support.

TABLE OF CONTENTS

Page

LIST OF FIGURES

LIST OF TABLES

CHAPTER 1

INTRODUCTION

1.1 General

The extrusion blow molding process is an important polymer processing method for manufacturing hollow articles such as bottles and containers. It is a method borrowed from the glass industry. The process is made up of two stages. The first stage is the parison formation stage in which a cylindrical tube of molten polymer called a "parison" is formed by extruding the polymer melt through an annular die. In the second stage, the parison is enclosed by two mold halves and air is blown into it causing the parison to take the shape of the mold. The polymer quickly solidifies upon contacting the cold mold, and the finished hollow article is ejected.

Basically there are two methods of extruding the parison: continuous and intermittent (Hoechst Plastics,1976). Continuous extrusion is used to manufacture containers up to 30 l capacity. This is achieved by a system of rotating molds or by parison transfer to the blow molding tool with the aid of a gripping device. Output can be raised considerably with minimum space requirement through the use of multiple die heads, molds and clamping units. Intermittent extrusion is employed in the production of larger and heavier products. In this type of operation the plastication unit supplies an accumulator with the required volume of melt and the melt is forced out of the die by the application of hydraulic pressure employing a ram or a reciprocating screw acting as a ram.

Two phenomena govern parison dimensions prior to mold closing: sag and swell. Swell is the enlargement both in thickness and diameter, of the polymer melt as it emerges from the die. It is widely accepted to be a manifestation of the elastic nature of the melt as it recovers from the deformations it has experienced during its flow in the die. Sag is caused by the effect of gravity on the freely hanging parison.

The melt is subjected to shear flow in the die and in the extruder and to extensional flow in the die entrance and in the converging sections within the die. Therefore, the blow molding process is a combination of shear and extensional deformations as well as the elastic recovery of the material from such deformations.

The dimensions of the parison prior to mold closing is of central importance in the blow molding process. From both the product design and the economic point of view, the shape and the thickness of the parison throughout its entire length and before mold closing must be controllable so that acceptable product strength levels can be achieved with minimum product weight. The parison diameter must also be controlled, not only because it contributes to the product thickness uniformity but also for two additional reasons. First, its "lay flat" width (defined as half the perimeter of the parison) should not exceed the mold diameter since this will interfere with mold closing. Second, if the blown product has a handle the diameter of the parison should be large enough to accomodate it, since handle pinch off occurs before any appreciable radial stretching of the parison. Therefore a thorough understanding of the parison formation is necessary to control and optimize the extrusion blow molding process.

Parison swell is influenced by system parameters such as die design, extrusion velocity and temparature and by the rheological properties of the polymeric resin. Most of the work done on swell has been carried out using capillary and slit dies. Relatively little research is done on dies of complex geometry. Typical die designs used in industry include dies with cylindirically parallel annular gaps and dies having converging and diverging channels (Hoechst Plastics, 1976; Tadmor and Gogos, 1979). Dies having converging or diverging channels are preferred since these geometries facilitate parison programming, a procedure widely used in industry to adjust the thickness distribution along the length of the parison. This is achieved by varying the die gap as a function of time as extrusion speed is held constant. Another method of parison programming is achieved by varying the material flow rate as a function of time while keeping the die gap constant. These techniques, although sophisticated, still require costly trial and error procedures to obtain the right thickness distribution in the parison.

From the above discussion we can conclude that the study of parison behavior is essential to gain a better understanding of the process. Also the evaluation of resins for possible use in a blow molding process would be greatly facilitated if the phenomenon were well understood, and correlations could be established between rheological properties and parison behavior.

1.2 Scope and Objectives of the Present Work

In most general terms, this study is aimed at understanding parison behavior in the extrusion blow molding process.

The specific objectives of the present work can be summarized as follows:

1. To study the relation between parison behavior and die design, extrusion velocity and the rheological properties

of the resin under well controlled experimental conditions.

2. To develop a simple lumped parameter model to predict parison dimensions.

1.3 Organization of Thesis

The organization of the thesis is as follows: In Chapter 2 the resins used are described and their rheological characterization is presented. In Chapters 3 and 4 previous experimental and theoretical work done on swell and sag are reviewed. The experimental methods employed to study sag and swell are described and the results obtained are presented and discussed in Chapter 5. In Chapter 6 the derivation and performance of the proposed model are described. Finally in Chapter 7, the conclusions of the present work and recommendations for future work are presented.

CHAPTER 2

RHEOLOGICAL PROPERTIES OF THE RESINS USED

Parison behaviour in the extrusion blow molding process is governed by the process variables as well as the rheological properties of the resin. Therefore, a complete rheological characterization is essential to be able to understand the parison behaviour.

This chapter is devoted to a description of the materials used and their rheological properties. The following properties were measured.

a) Molecular weight distribution

b) Viscometric functions (viscosity, $\eta(\dot{\gamma})$ and first normal stress difference, $N_1(\dot{\gamma})$)

c) Linear viscoelastic functions (complex viscosity, $\eta^*(\omega)$, and storage modulus, $G'(\omega)$)

2.1 Desciption of the Resins

Three high density polyethylene resins were used in the present study. These are:

a) Resin 22A, "Sclair 59A". Made by DuPont of Canada.

b) Resin 27, "DMDJ 5140". Made by Union Carbide of Canada.

c) Resin 29, "Dow 80060". Made by Dow Canada.

The numbers used to identify the resins refer to McGill Polymer Engineering Laboratories stock numbers. All three resins were designed for use in the blow molding industry in the production of bottles for non-stress cracking liquids such as vinegar and bleach; i.e. they are all competing for the same market.

Resin 27 is manufactured by use of a gas phase polymerization. Catalyst is fed into a fluidized bed reactor where it contacts with the ethylene gas, and a fluid bed of polymer particles is formed. Resins 22A and 29 are manufactured via a solution phase polymerization process. Modified Ziegler type catalyst is used in the manufacture of both resins. All the resins are homopolymers.

In industry, blow molding resins are specified in terms of their solid density and melt index. Melt index is the amount of polymer (in grams) extruded in 10 minutes under specified conditions. These specifications are given under the condition "E" of the test ASTMD1238 . Values of melt index and density supplied by the resin manufacturers for the materials used in this study are listed in Table 2.1. Inspection of the table shows that all three resins have similar values of density and melt index. This reflects the fact that they are intended for the same end use .

TABLE 2.1 Various Properties of the Resins

Resin	Density (g/cm^3)	Melt Index (g/10 min)	$\bar{M}_w$	$\bar{M}_n$	$\bar{M}_z$	$\bar{M}_w/\bar{M}_n$
Resin 22A	0.960	0.70	119057	11660	444330	10.2
Resin 27	0.962	0.72	107615	15747	370015	6.8
Resin 29	0.960	0.80	104411	16329	327030	6.4

2.2 Molecular Characterization

A polymer is a large molecule built up by the repetition of small simple chemical units. Since the polymerization process is subject to a multitude of random events, it is quite improbable that all the chain molecules in a polymer sample would have the same length. Rather there exists a distribution of molecular weights, which may be narrow or quite broad. As with any distributed quantity, the " molecular weight " is characterized in terms of some average value and one or more moments of distribution.

Two average molecular weights are commonly used, depending on how the contributions of sample chains having the same length are taken into account statistically. These are the number average molecular weight, $\bar{M}_n$ and the weight average molecular weight, $\bar{M}_w$. These are defined by the following equations:

$$\bar{M}_n = (\Sigma N_i M_i)/(\Sigma N_i) \qquad 2.2.1$$

$$\bar{M}_w = (\Sigma w_i M_i)/(\Sigma w_i) = (\Sigma N_i M_i^2)/(\Sigma N_i M_i) \qquad 2.2.2$$

where N_i denotes the number of moles of the fraction having a molecular weight M_i, and w_i is the mass of the i'th fraction. The number average molecular weight is particularly sensitive to species at the lower end of the molecular weight distribution, whereas $\bar{M}_w$ is influenced by the presence of higher molecular weight species. Other average molecular weights are also defined, such as the "z average" and "z+1 average" molecular weights. These are very sensitive to the presence of small fractions of high molecular weight material. The ratio $\bar{M}_w/\bar{M}_n$ is called the polydispersity index. The relationship $\bar{M}_w/\bar{M}_n \geq 1$ holds for all polymers, with the equality representing a "monodispersed" sample, in which all the chains have the same molecular weight. The polydispersity index is used as a measure of the breadth of the molecular weight distribution. Two polymers having significantly different molecular weight distributions can have similar average molecular weights. Therefore, it is better to consider the entire molecular distribution curve rather than the averages.

The molecular weight of polymers can be determined by chemical or physical methods. These methods are described elsewhere (Billmeyer, 1971).

Molecular weight determinations of the resins used in the present study were carried out by Dr. D. Axelson at the Kingston Research Center of DuPont Canada Inc. . A DuPont 830 Liquid Choromatograph was employed together with a Wilkes Infrared Detector. The reported values of molecular weight averages and the polydispersity index are presented in Table 2.1. The standard deviations of number and weight average molecular weights are between ±500-1000 and that for the z-average molecular weight is around ±10000. It is seen from Table 2.1 that Resins 27 and 29 have very similar values of the polydispersity index, $\bar{M}_w$ and $\bar{M}_n$. Resin 22A has higher $\bar{M}_w$ and polydispersity index than the other two resins. The molecular weight distribution curves for the resins are given in Appendix A1.

2.3 Viscometric Functions

A viscometric flow is a flow in which the deformation as seen in a corotating frame (a frame which translates and rotates , but does not deform with a fluid element) is indistinguishable from simple shear. Simple shear is a unidirectional flow with a linear velocity gradient. If the velocity is constant with time, the motion is called steady simple shear. In a steady simple shear, the stress and the strain are constant in space. The three physically measurable quantities of the flow are shear stress, τ_{12} , and two normal stress differences, $(\tau_{11}-\tau_{22})$ and $(\tau_{22}-\tau_{33})$. It is common practice to report values of these material functions in terms of the following ratios:

$$\eta(\dot{\gamma}) = \tau_{12} / \dot{\gamma} \qquad 2.3.1$$

$$\Psi_1(\dot{\gamma}) = (\tau_{11}-\tau_{22}) / \dot{\gamma}^2 \qquad 2.3.2$$

$$\Psi_2(\dot{\gamma}) = (\tau_{22}-\tau_{33})/\dot{\gamma}^2 \qquad 2.3.3$$

These are called viscometric functions and are functions of shear rate. Viscometric functions are usually measured by use of cone and plate flow and capillary flow. Due to the neglect of inertia terms in the derivation of the rheometric equations for cone and plate flow, the use of this flow is limited to relatively low shear rates. For higher shear rates, capillary flow is used, although only the viscosity can be reliably determined in this case. These flows will be discussed below.

2.3.1 Cone and Plate Flow

Cone and plate flow is used to measure the viscometric and linear viscoelastic material functions. In this type of flow, the sample is sheared between a cone and a plate, one of which is rotating. The flow is actually rather complex and certain assumptions have to be made in order to be able to use the cone-plate geometry for measuring rheological properties. These assumptions are as follows:

1. "Inertia" effects are small, so that the second-order terms in the equation of motion are negligible.

2. The cone angle is very small so that certain approximate trigonometric relationships can be used to simplify equations.

3. Edge effects are negligible, i.e., the free surface of the liquid is spherical with a radius of curvature equal to the cone radius and the flow is uniform right up to this surface.

4. Surface tension forces acting on the free surface are negligible.

With these assumptions, the flow is approximately viscometric and the shear rate, and hence the shear stress, is uniform throughout the gap. The following equations are thus obtained for the shear rate, $\dot{\gamma}$, the viscosity, η and the first normal stress difference, N_1:

$$\dot{\gamma} = \Omega/\theta_o \qquad 2.3.4$$

$$\eta(\dot{\gamma}) = 3\ M/2\pi R^2 \dot{\gamma} \qquad 2.3.5$$

$$N_1(\dot{\gamma}) = 2\ F/\ \pi R^2 \qquad 2.3.6$$

where Ω is the rotational speed, θ_o is the cone angle, R is the radius of the cone and the plate, M is the torque required to rotate the cone and F is the total normal force on the plate. Thus, the measurements of the torque and the total normal force as functions of rotational speed can be used to determine the viscosity and the first normal stress difference as functions of shear rate. The detailed derivation of these equations is given elsewhere (Walters, 1975).

An important consideration in the application of this flow geometry to measure the rheological properties is the extent to which the above assumptions are valid in practical situations and the limitations they impose on the operating conditions. Viscous heating, secondary flows, shear rate nonuniformity and the deformation of the shape of the free surface can be minimized by the proper selection of cone angle and radius and by operating at low shear rates. As cone angle decreases, the errors mentioned above decrease but the errors due to the geometrical nonidealities (such as the deviations in the flow geometry from that of a perfectly shaped, aligned and positioned cone and plate) will increase. Extreme caution should be exercised at shear rates between 1 and 10 s^{-1} and especially at shear rates above 10 s^{-1} (Dealy, 1982). The sources of error in cone and plate geometry have been described in detail by Dealy (1982) and Walters (1975).

2.3.2 Capillary Flow

In the previous section we saw that cone and plate flow can be conveniently used to measure viscometric functions provided the various potential sources of error are kept under control. Many of these error sources are related to the shear rate and regardless of the precautions taken to minimize these errors, there is, for any given liquid, a maximum shear rate at which reliable results can be obtained. At the present time only capillary and slit rheometers are suitable for the measurement of viscosity at high shear rates.

Capillary flow is a shear flow which can be easily generated in a laboratory. The sample is forced from a cylindrical reservoir through the capillary by applying pressure above the reservoir fluid. The steady shear flow velocity profile develops over a certain entrance length. In the succeeding fully developed flow region, the streamlines are always parallel to the axis of the tube, but the velocity profile depends on the nature of the fluid. Unless a specific constitutive equation is known to be valid for the fluid, as in the case of a Newtonian or a power law fluid, special computational techniques are required. It can be shown that the shear stress and shear rate at the tube wall, τ_w and $\dot{\gamma}_w$ respectively, are given by the following expressions (Dealy, 1982) :

$$\tau_w = -(\Delta P R)/2L \qquad 2.3.7$$

$$\dot{\gamma}_w = \dot{\gamma}_A (3/4 + (1/4)(d\ln \dot{\gamma}_A / d\ln \tau_w)) \qquad 2.3.8$$

where ΔP is the axial pressure gradiant in a tube of radius

R and length L; $\dot{\gamma}_A \equiv 4Q/\pi R^3$ is the apparent shear rate, and Q is the volumetric flow rate. In the derivation of the above equations the flow is assumed to be steady, isothermal, unidirectional and symmetrical, and end effects are neglected. The term in brackets in equation 2.3.8 is known as the Rabinowitsch correction factor for the shear rate, and it represents the deviation from Newtonian behavior. Measuring ΔP and Q in a series of experiments will enable the shear viscosity to be determined. In actual practice, the driving pressure in the barrel, P_d, is measured and the pressure at the outlet is taken to be the ambient pressure. Since for polymer melts P_d is nearly always much larger than the ambient pressure, the pressure drop ΔP in equation 2.3.7 is replaced by P_d. However, this is clearly not the wall pressure drop that one would observe for fully developed flow in a capillary of length L. In the entrance region of the capillary the fluid undergoes a change in velocity distribution and the wall shear stress is larger than for the case of fully developed flow, causing a larger wall pressure gradient. The excess pressure drop thus caused is called the " entrance pressure drop ". At the exit of the capillary the velocity profile of the fluid may change (in anticipation of the disappearence of the confining wall) leading to a larger pressure drop than that in a fully developed flow. The type of pressure distribution observed for capillary flow of molten polymers is shown in Figure 2.1. Although flow patterns in the entrance and the exit regions are not known precisely, some emprical methods have been proposed to get around this problem. Bagley (1957) proposed to use an end correction, e, defined by the following equation.

$$\tau_w = P_d/2(e + L/R) \qquad 2.3.9$$

The product of e and R is the length of capillary for which the pressure drop in fully developed flow is equal to the excess pressure drop resulting from end effects. Bagley (1957) carried out a series of experiments with capillaries of different L/R ratios and a straight line was obtained when ΔP was plotted versus L/R, apparent shear rate being the parameter. This line cuts the L/R axis at −e. (Note that e is a function of shear rate). The appearance of such a graph is sketched in Figure 2.2. Curvature of the lines on a "Bagley plot", often observed at large values of L/R, may be due to viscous heating and pressure dependence of viscosity. In such cases the value of e should be obtained by extrapolating the straight portion of the curve. In order to obtain the true viscosity from capillary flow the following procedure should be used.

1. For capillaries with different L/R ratios, ΔP and $\dot{\gamma}_A$ are measured.

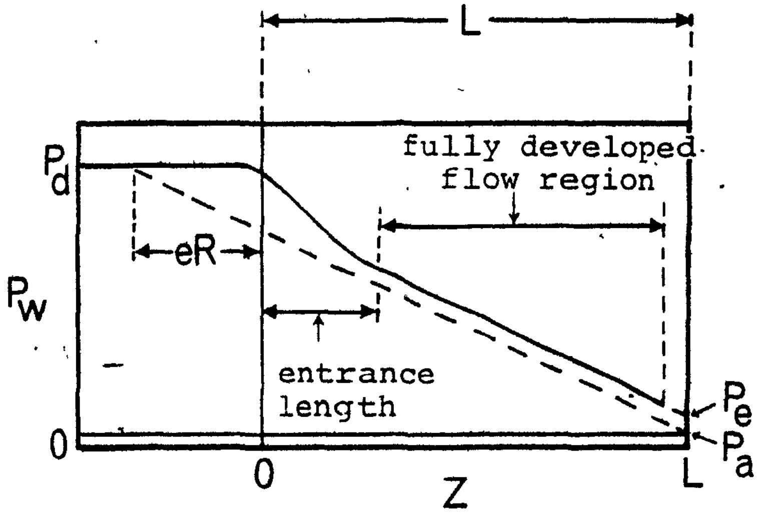

Figure 2.1 Wall Pressure Distribution for Capillary Flow

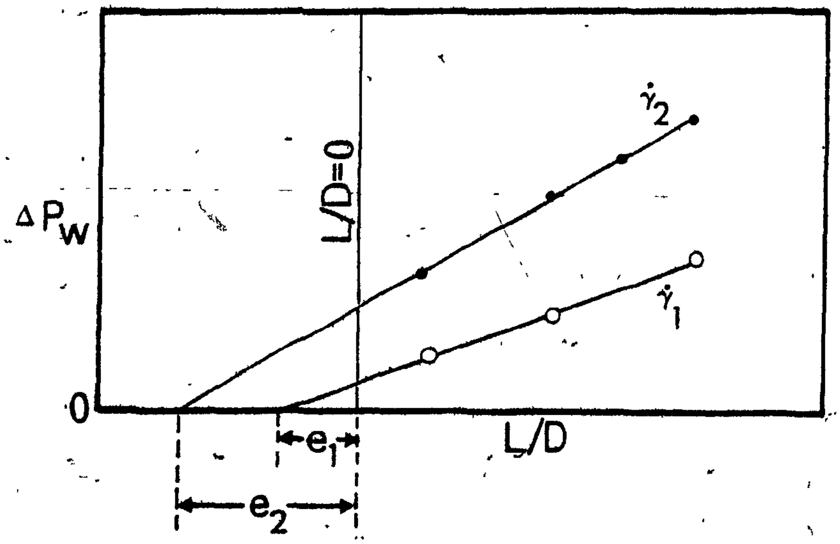

Figure 2.2 Bagley Plots for Different Shear Rates

2. The end correction term e is obtained for each shear rate using Bagley plots.

3. The true value of shear stress at the wall is calculated by use of equation 2.3.9.

4. The Rabinowitsch correction is used to obtain the true shear rate at the wall using equation 2.3.8.

5. The viscosity is calculated using the following relation:

$$\eta(\dot{\gamma}) = \tau_w / \gamma_w \qquad 2.3.10$$

In capillary flow viscous heating and pressure effects can be troublesome since these affect the viscosity of the molten polymer. The analysis of these two phenomena is rather complex and no simple formulae are available to estimate them. To reduce such effects, it is better to use a capillary of smaller diameter and intermediate L/R ratio. The sources of error in capillary flow are discussed in detail in the book by Dealy (1982).

2.3.3 Experimental Equipment

Cone and plate flow was generated by use of a Rheometrics Mechanical Spectrometer (Model RMS-605). The spectrometer is furnished with a forced air convection oven to heat the sample to the desired temperature. A platinum resistance thermocouple located in the oven is used to provide temperature stability to 0.5° C. The torque and normal force were measured by a TC-2000 transducer having a very low compliance. To reduce the baseline drift an oil circulation system is used to thermostat the transducer. The strain, torque and normal force signals are fed to the central processor where they are used together with sample geometry to compute the viscosity and first normal stress difference. Further information on the Mechanical Spectrometer can be found elsewhere (Rheometrics Manual, 1980). The cone and plate fixtures had the following dimensions:

Radius (R) =12.5 mm.
Cone angle =0.04 radian
Gap =0.05 mm.

A small portion of the apex of the cone has been removed. The amount removed is 0.05 mm. This necessitates the setting of this gap in the experimental procedure.

For each speed two measurements of the force were taken: one when the cone was rotating in the clockwise direction, the other in the counterclockwise direction. The two values were then averaged.

The capillary flow tests were performed in a constant flow rate capillary viscometer manufactured by the Instron Corporation. This system consists of a hardened stainless steel barrel with an accurately ground 9.525 mm inside diameter, mounted on a special support assembly underneath the moving crosshead of the Instron tester. A hardened plunger, which is also accurately ground to fit the inside of the barrel is driven by the moving crosshead of the machine. The crosshead can be driven at speeds in the range of 0.5-50 cm/min. The force on the sample is detected by a strain gauge load cell (type CFM). The capillary is inserted in the bottom of the barrel and is held in place with a clamping nut. The barrel and the capillary are heated using a 3-zone heating system in the extrusion barrel. Temperature control is provided with a " Speedomax H " current adjusting type controller, and the system is capable of maintaining the temperature within ±0.5°C of the set point. Further information on Instron Capillary Rheometer is given elsewhere (Instron Manual, 1976). Four capillary dies having L/D ratios of 5, 10, 20 and 40 were used. The dies had a diameter of 1.321 mm. Bagley plots were prepared by plotting the measured force value as a function of L/D for each shear rate. Due to the curvature of the lines at L/D = 40, the Bagley correction term was obtained by extrapolating the straight portion of the curve, i.e., using values at L/D = 5, 10 and 20. It was observed that Bagley's correction became significant for values of apparent shear rate equal to 100 s^{-1} and above. Therefore, Bagley's correction was not used for apparent shear rates below 100 s^{-1}. The viscosity values were calculated following the procedure described in section 2.3.2. Measurements were carried out at 170°C for all the resins and the range of shear rate used was approximately 2–2000 s^{-1}. However at high shear rates (exact value of which depends on the resin) no reliable viscosity data could be obtained due to the onset of melt instabilities such as melt fracture.

2.3.4 Results

The viscosity shear rate curves for the three resins are shown in Figure 2.3. Data in the shear rate range of 0.06–1.6 s^{-1} are obtained from the Mechanical Spectrometer whereas the rest of the data are obtained from the capillary rheometer. At low shear rate values the viscosity function did not show a Newtonian region, so that the zero shear viscosity could not be determined. Figure 2.3 shows that all the resins have similar viscosity curves. Resin 29 has the highest viscosity values at lower shear rates. At higher shear rates, Resin 22A has the lowest viscosity values and Resins 27 and 29 have nearly the same values. Melt fracture characteristics of the resins were also similar. Melt fracture was observed at approximately 1000 s^{-1}.

First normal stress difference results are presented in Figure 2.4. Data were obtained for shear rates between

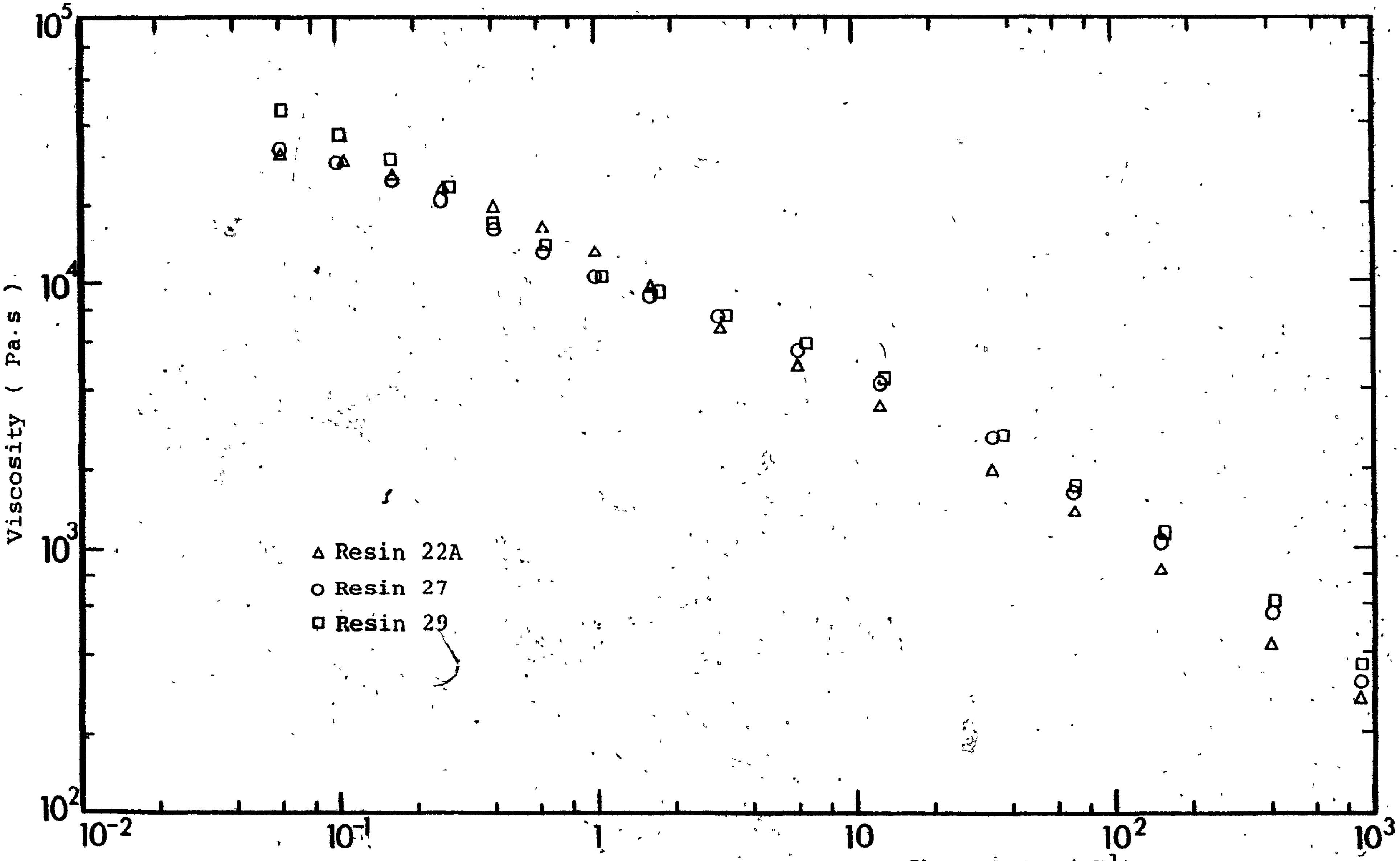

Figure 2.3 Shear Viscosity at 170° C

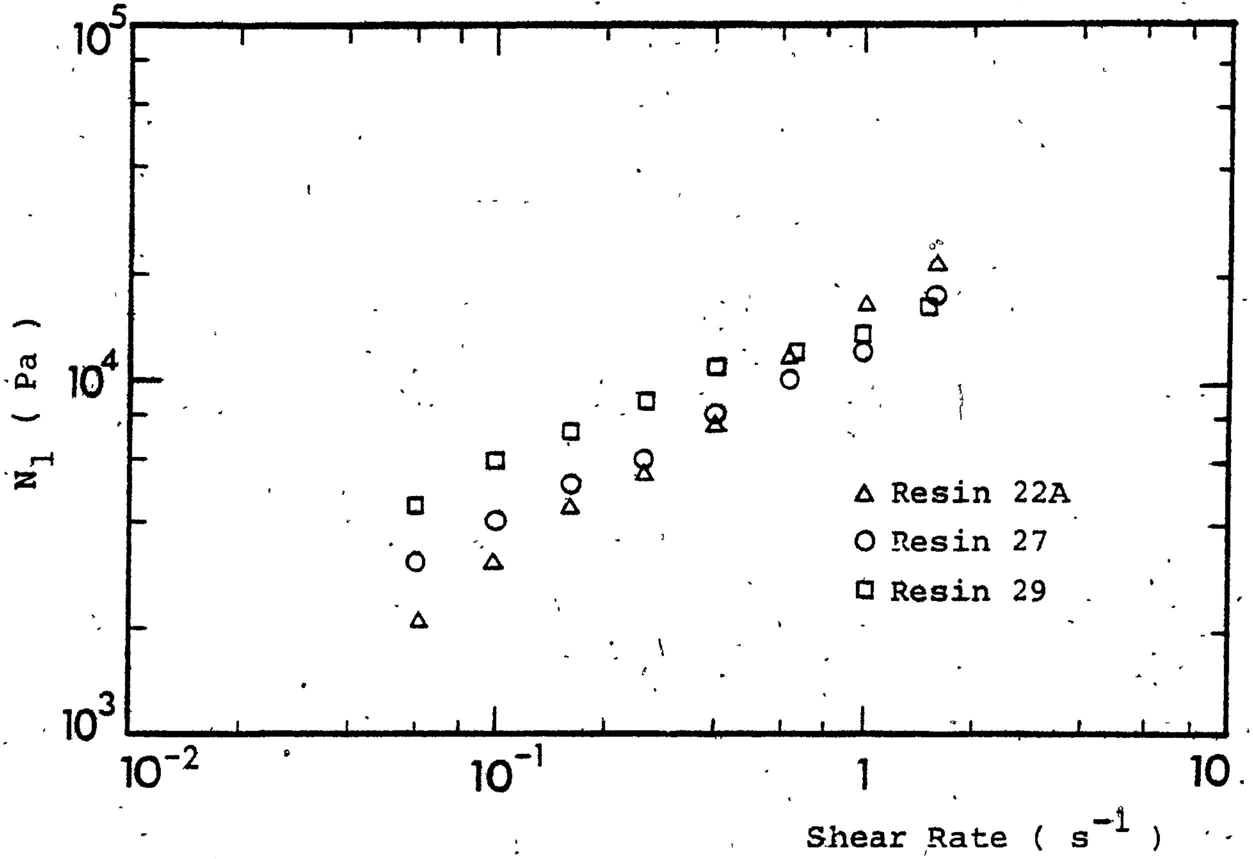

Figure 2.4 First Normal Stress Difference (N_1) at 170°C

$0.06-1.6\ s^{-1}$. At the lower shear rates studied Resin 29 has the highest N_1 values and Resin 22A the lowest. At higher shear rates the resins seem to have similar values. It is widely accepted that first normal stress difference is a measure of elasticity and that the higher the value of N_1 the more elastic the material. However at high shear rates that are of relevance in the actual blow molding process, no N_1 data can be obtained, and the relationship between N_1 and swell could not be studied.

The values of viscosity and first normal stress difference are tabulated in Appendix A2.

2.4 Linear Viscoelastic Properties

Linear viscoelasticity refers to the behavior exhibited when a material is deformed in such a way that its structure and the configuration of its molecules are not significantly different from those characteristic of its equilibrium rest state. Linear viscoelastic properties are used as fundamental physical measures of the nature of the material. There are many types of experiments one can perform to determine the linear viscoelastic properties of polymeric materials. Examples are stress growth, stress relaxation after cessation of steady shear, creep and small amplitude oscillatory shear. The material functions obtained from these experiments are interrelated by well established mathematical formulas. It is therefore necessary to determine only one material function and the others can, in theory, be calculated. These methods are summarized in the book by Ferry (1980).

In the present study, the complex viscosity, η^*, and storage modulus, G', were determined.

2.4.1 Small Amplitude Oscillatory Flow

A small amplitude oscillatory shear flow can be achieved in a number of geometries. One of these is the cone and plate geometry. The cone is allowed to undergo sinusoidal oscillation, and the lower plate is kept fixed. The angular position of the cone, ϕ, is given by:

$$\phi = \phi_o \sin \omega t \qquad 2.4.1$$

where ϕ_o is the amplitude and ω the frequency of oscillation. If the amplitude of oscillation is sufficiently small to satisfy the linearity approximation, the resulting torque on the plate, M, is given by:

$$M = M_o \sin(\omega t+\delta) \qquad 2.4.2$$

where M_o is the amplitude of the torque and δ is the phase lag of the torque behind the position. Equation 2.4.2 can also be written in the following way:

$$M = (M_0\cos\delta)\sin\omega t + (M_0\sin\delta)\cos\omega t \qquad 2.4.3$$

where the first term on the right hand side of the equation is the in-phase (elastic) component of the torque to the strain and the second term is the out-of-phase (viscous) component. If the same assumptions described in section 2.3.1 are applied, the dynamic viscosity and the dynamic modulus can be calculated by the following equations:

$$\eta' = (3M_0\theta_0/2\pi R^3\phi_0\omega)\sin\delta \qquad 2.4.4$$

$$G' = (3M_0\theta_0/2\pi R^3\phi_0)\cos\delta \qquad 2.4.5$$

The dynamic viscosity, η', is an indication of the viscous aspects of the viscoelastic material and the storage modulus, G', is an indication of the elastic aspects. The " absolute magnitude of complex viscosity " , η^*, is defined as follows:

$$\eta^* = ((\eta')^2 + (\eta'')^2)^{1/2} \qquad 2.4.6$$

where $\eta'' = G'/\omega$.

2.4.2 Experimental Equipment and Results

In the present study, dynamic data were obtained by the use of cone and plate fixtures in the Rheometrics Mechanical Spectrometer (see section 2.3.3). The dimensions of the cone and plate were:

Radius (R) =12.5 mm.
Cone angle =0.04 radian
Gap=0.05 mm.

Dynamic mechanical testing is accomplished by controlling the amplitude and frequency of the sinusoidal deformation applied to the test sample and measuring the resulting torque. The strain and the torque are amplified and fed to the computer where they are used, together with sample geometry, to compute the dynamic viscosity and shear modulus. The computer contains a sampling sine wave correlator which is used in dynamic mode to reject both harmonics and noise and to separate the viscous and elastic components of the deformation force.

Strain sweep experiments were carried out at several frequencies to determine the linear viscoelastic range of the materials used. The measurements of dynamic viscosity and storage modulus as functions of frequency were carried out at a value of strain which was found to give linear viscoelastic behavior. The values of $G'(\omega)$ and $\eta^*(\omega)$ are shown in Figures 2.5 and 2.6 and are tabulated in Appendix A2. The results

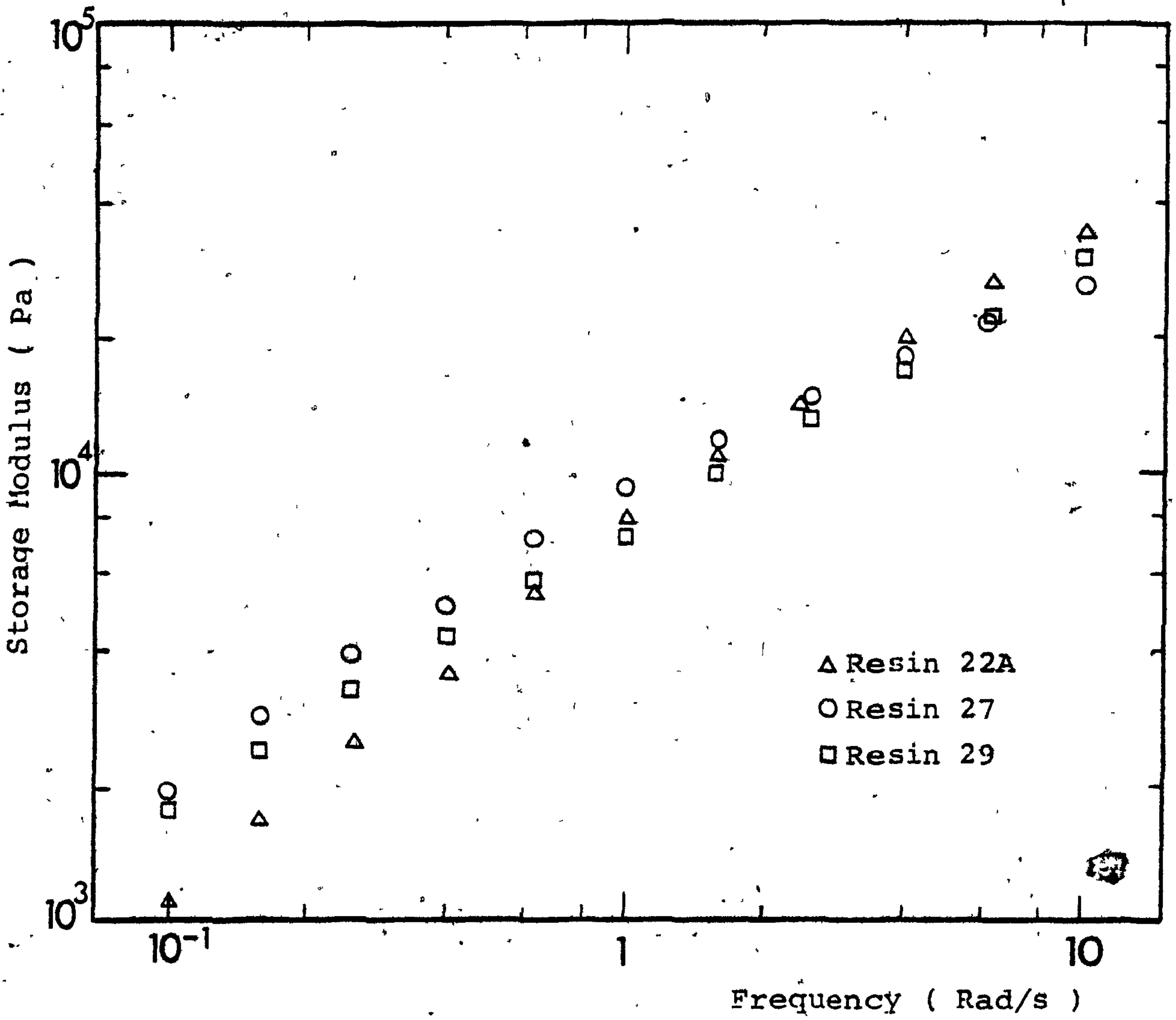

Figure 2.5 Storage Modulus at 170°C

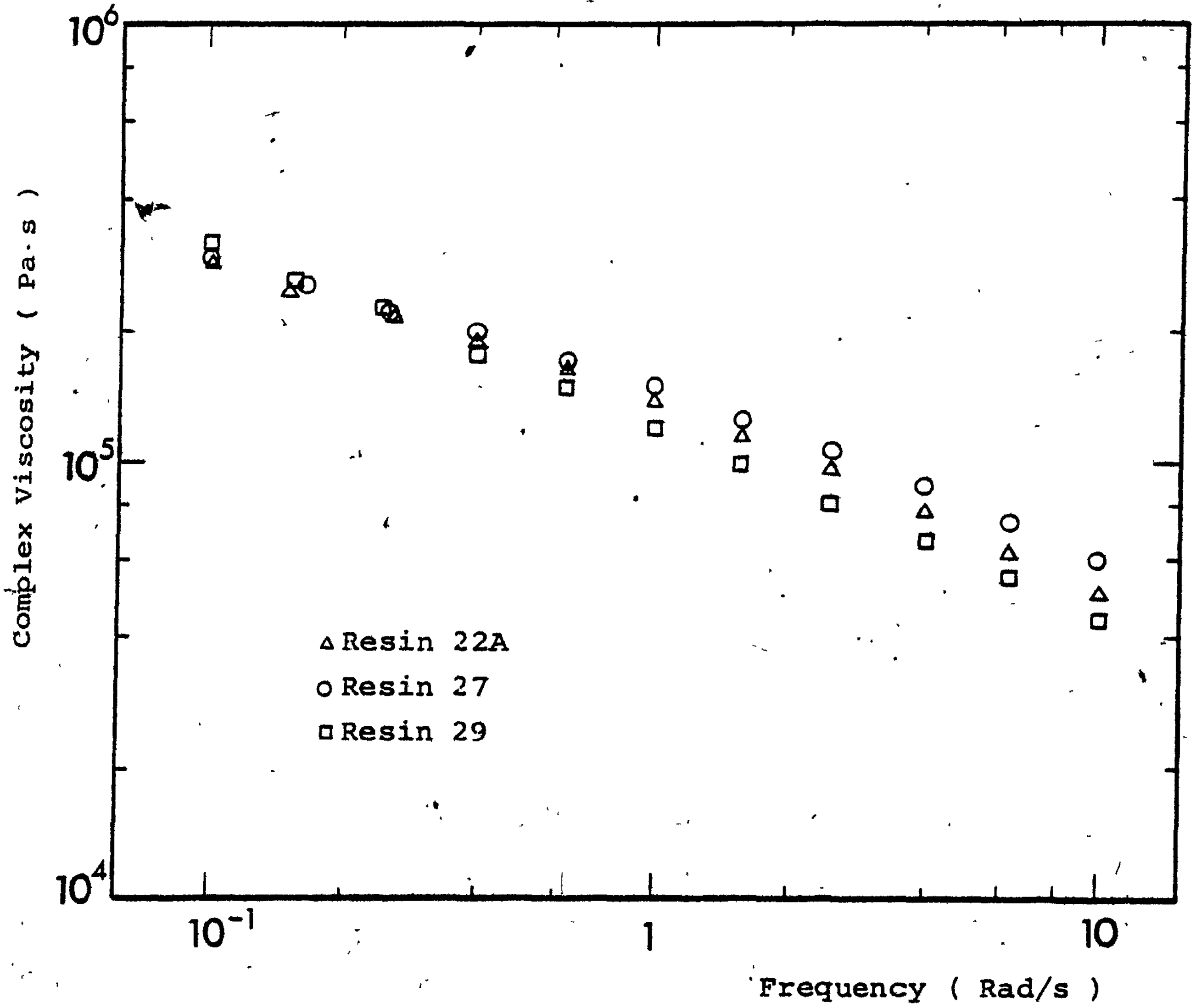

Figure 2.6 Complex Viscosity at 170°C

for all the resins are similar. These data are useful in determining the linear relaxation spectrum.

2.4.3 Determination of the Linear Relaxation Spectrum

In the present study, the linear relaxation spectrum was obtained from the experimentally determined storage modulus data.

The approximation procedures used to obtain spectra from experimental functions usually involve taking derivatives of the function either graphically or by a numerical differencing procedure. These methods are reviewed by Ferry (1980). In the present work, Tschoegl's second approximation formula was used. In log-log form this formula is (Tschoegl, 1971; Tschoegl, 1973) :

$$H_O(\lambda_O)=G'[(d\log G'/d\log\omega)-0.5(d\log G'/d\log\omega)^2 + (1/4.606)(d^2\log G'/d(\log\omega)^2)] \qquad 2.4.7$$

$$\frac{1}{\omega}=\frac{\lambda_O}{\sqrt{2}}$$

The G'(ω) data were first converted to a logarithmic form and then fitted by a fourth order polynomial. The derivatives were then calculated analytically and the spectrum was obtained using equation 2.4.7. The values obtained are shown in Table 2.2.

In actual calculations a discrete relaxation spectrum is used in place of a continuous one. For example one can

TABLE 2.2 Linear Relaxation Spectrum of Resin 27 at 170°C

λ_o (s)	H_o (Pa)
0.100	9403
0.178	8666
0.316	7364
0.562	5962
1.000	4692
1.780	3626
3.160	2761
5.621	2055
10.000	1474
17.800	997
31.600	617
56.210	334
100.000	148

λ_{ok} (s)	G_{ok} (Pa)
0.316	16956
3.160	6357
31.600	1420

subdivide the $\ln\lambda_o$ axis into equal intervals, $\Delta\ln\lambda_o$, and take a discrete set of relaxation times λ_{ok} and corresponding values of H_{ok}. Then:

$$G_{ok} = H_{ok}\Delta\ln\lambda_{ok} \quad . \qquad 2.4.8$$

In order to check the procedure used, the storage modulus $G'(\omega)$ was backcalculated using the discrete relaxation spectrum obtained. For this purpose the following expression was used.

$$G'(\omega) = \sum_k \frac{G_{ok}(\omega\lambda_{ok})^2}{1 + (\omega\lambda_{ok})^2} \qquad 2.4.9$$

The agreement between the experimental data and backcalculated values is found to be good.

In summary, all the resins had very similar behavior in terms of their viscometric and linear viscoelastic functions. Resins 27 and 29 had very similar molecular weight distribution curves whereas Resin 22A had a higher weight-average molecular weight and polydispersity index than the other two. Since the actual blow molding process involves high shear rates, if the rheological characterization of the resins could be carried out at these shear rates, the evaluation of the resins would be improved. Also, elongational properties of the resins play an important role in the process (Dealy and Garcia-Rejon , 1980).

CHAPTER 3

PREVIOUS EXPERIMENTAL WORK ON SAG AND SWELL

At the exit of a capillary, slit or die of any shape, an emerging stream of polymeric liquid undergoes a substantial change in cross-sectional area from that of the channel in which it has been flowing. This phenomenon is called " die swell ". If the channel is noncircular, then the extrudate will also undergo a change of shape. Die swell can occur even in the case of Newtonian liquids at low Reynolds numbers (Middleman, 1977), but the effects are much more pronounced in the case of viscoelastic liquids. From the structural point of view, it is believed that die swell occurs as a result of a disorientation of the molecules that have been oriented within the capillary by the shear and/or elongational flow fields. From the rheological point of view, on the other hand, it is believed that die swell occurs as a result of the recovery of the elastic deformation imposed in the die. The swelling of viscoelastic fluids is connected with a sudden recovery of stored elastic energy and a subsequent slow relaxation.

Die swell is a very complex phenomenon which depends on die design (the geometry and dimensions of the die, the design of the die entrance), temperature, extrusion velocity and the rheological characteristics of the polymer.

Understanding swell is important since it is one of the key phenomena which govern parison behavior in extrusion blow molding process. Due to the complexity of the problem, most of the work done on swell is experimental. A limited number of theoretical results have been reported. These include calculations based on the theory of rubber elasticity and, more recently, finite element methods. In this chapter, experimental contributions will be reviewed, and their contributions and limitations will be highlighted.

3.1 Methods of Measuring Swell

It should be emphasized that the results obtained by different workers should be analyzed carefully due to the different experimental techniques employed. When the melt emerges from the die, there is a rapid swelling which occurs almost immediately; then the material continues to swell at a lower rate for some period of time. For this reason the results are dependent on the method of measurement.

White and Roman (1976) compared capillary swell values of HDPE obtained using four different techniques. These were the following:

1. The frozen extrudate diameter was measured using a micrometer.

2. Direct photographs of the extrudate were taken as it

emerged from the capillary.

3. The solidified extrudates were annealed in hot silicone oil at temperatures above the melting or glass transition temperature until they reached constant diameter. The extrudates were then removed and measured with a micrometer.

4. The melt was extruded into a bath of silicon oil which was at the same temperature as the extrusion temperature. Photographs of the extrudates in the bath were taken between 5-10 minutes after the extrudate emerged from the capillary.

All these methods gave substantially different results. The first two methods represent extrudates with frozen-in residual stresses, while the last two represent completely recovered samples. Also, unless the melt is extruded into a medium which has nearly the same density as the melt, it is subjected to sagging which causes a decrease in the cross sectional area (actually, the density of the medium should be slightly less than the melt so that the parison flows smoothly (Garcia-Rejon, 1979)). The third method has another problem associated with it; it tends to flatten the extrudate on one side due to the procedure used in annealing. Swell was found to increase in the order of listing, i.e., the lowest swell value was obtained with the frozen extrudate and highest value was obtained with the fourth method. A correction factor for density variation with temperature is necessary when measuring the diameter of frozen extrudates.

Utracki et al. (1975) designed a thermostating chamber to measure capillary die swell. The extrudates were extruded directly into silicone mixture having the same density as the melt and the same temperature as the extrusion temperature. Thus the gravitational effects were eliminated. The samples were allowed to relax completely and then their photographs were taken through a side window on the chamber.

Dealy and Garcia-Rejon (1980) used the same technique to study the time dependency of swell. Capillary and annular dies were used. In the case of annular dies, the transparency of the parison in the oil enabled them to measure directly both the thickness and the diameter of the parison.

In the experimental studies that have been done on commercial blow molding machines, the most commonly employed technique for the characterization of polymer swell behavior is the parison pinch-off technique, which was developed by Sheptak and Beyer (1965). They designed a special multiple pinch-off device, consisting of a series of thirteen blades, which pinched a parison into twelve 2.54 cm segments and held them until the parison solidified. Cutting and weighing the segments gave the weight distribution of the material in the parison. Parison weight swell was defined to be :

$$B_w = 4W_i \; \Delta L/\pi(D_o^2-D_i^2) \; \Delta L\rho \qquad 3.1.1$$

where W_i is the weight of a parison segment with length L and D_o and D_i are the outside and inside diameters of the die, respectively. The width of the pinched-off parison segment, W, was assumed to represent one-half of the circumference of the parison before pinch-off, and the diameter swell was obtained to be:

$$B_1 = 2W/\pi D_o \qquad 3.1.2$$

Sheptak and Beyer employed a photographic technique in conjunction with the pinch-off mold for purposes of calibration. There are certain disadvantages associated with the parison pinch-off technique: the data obtained are not continuous in time, the measurements involve errors due to subsequent shrinkage or distortion of specimens, and there is an uncertainty in estimation of the exact time of pinch-off.

Kalyon (1980) used cinematography together with a pinch-off mold to eliminate the above difficulties. The diameter swell values obtained from the two techniques were found to give different results. The thickness distribution was calculated using the weight distribution obtained from the pinch-off technique and the diameter swell obtained from cinematography. This was compared with the thickness distribution calculated on the basis of pinch-off experiments alone, and a substantial discrepancy was noted. It was concluded that the use of cinematography along with pinch-off measurements is essential to obtain reliable results.

There is also a commercial instrument designed to measure die swell (Dealy, 1982). It is called the Monsanto Automatic Die Swell Detector and is based on the use of a sweeping laser beam to measure the extrudate profile.

3.2 Results of Previous Studies on Swell and Sag

Due to its relative simplicity, capillary die swell has received the most attention from the melt rheologists. In the case of capillary extrudate there is no change of shape so that the swell can be described in terms of the extrudate diameter alone. The " die swell ratio ", B is defined as the ratio of the diameter of the extrudate, D_p, divided by that of the die or capillary, D.

$$B \equiv D_p/D \qquad 3.2.1$$

For a given die entry shape, this ratio is a function of wall shear rate $\dot{\gamma}_w$, the L/D ratio, L being the length of the die, and the time elapsed after exiting the die. There is a general agreement in the literature as to the effects of these parameters on die swell. Die swell decreases with decreasing wall shear rate and with increasing L/D ratio, approaching a constant value at values of L/D often around 30. The results for capillary die swell have been reviewed elsewhere (Han, 1976; Leblanc, 1981; Vlachopoulos, 1981a).

Relatively few studies related to the die swell of viscoelastic liquids flowing between infinitely wide parallel rectangular plates (slit) are reported in literature. Theoretically, swell is expected to be in one direction only, since the plates are assumed to be infinitely wide, and the swell is defined as the ratio of the thickness of the extrudate to the thickness of the die (h/H). However, this is not usually the case, and the extrudate swells in two directions.

A comparative study of die swell from capillary and slit dies has been carried out by Huang and White (1979, 1980). HDPE and PP resins were used. The extrudate swell ratio (h/H) of the polymer emerging from the slit die was measured at the center of the cross section, where the swell was greatest. The ratio was found to be an increasing function of shear rate for both geometries. Swell from the slit die (h/H) was observed to be higher than capillary swell and was found to increase more rapidly with extrusion rate. Values of 7-8 were obtained for the slit die and 3-4 for the capillary die. The influence of die entry geometry on swell was studied by changing the entrance angle at a constant L/D or L/H ratio. Swell was found to decrease with decreasing entrance angle. Although the cross section of the extrudate obtained from the slit die shows swell in both directions, only thickness swell was considered.

In a subsequent paper, White and Huang (1981) studied swell from a rectangular and a trapezoidal die. In both cases swell was measured at the centerline of the extrudate. In the case of the rectangular die both the thickness and the width swell were measured. The swell values thus obtained were found to be very close to the values obtained from the slit die in the previous study (Huang and White, 1979).

Huang et al. (1982) compared die swell from a conical capillary and a converging slit die using LDPE. Both the thickness and width swell values were obtained for the slit die, and measurements were taken at the centerline of the extrudate. The thickness swell was found to be much greater than the width swell, and the capillary swell values fell between these two. They also observed that for the capillary and slit dies used, the same area swell was obtained.

Chee and Rudin (1980) studied the flow behavior of a polystyrene and a polyethylene melt during extrusion through successive capillaries arranged to produce converging and diverging flow patterns. For the polyethylene melt, with a given orifice pair, the diverging flow arrangement produced a smaller swell value than the converging flow sequence when both values were measured at a fixed shear rate in the second die of the sequence. This was attributed to the effect of the contraction ratio, defined as the ratio of the diameter of the reservoir to that of the die. Especially at lower shear rates an increase in contraction ratio increased die swell.

Suto and Fujimura (1980) also studied the effect converging slit channels formed by arranging in series several slit dies with different gaps. HDPE resin was used. The swell ratio was found to depend only on the final die. However Chee and Rudin (1980) observed a higher swell for the converging die having a lower L/D ratio in the first die, the second die being the same.

3.2.1 Extrudate Swell From Annular Dies

Most of the work done on annular dies has been carried out by industrial research teams using commercial blow molding machines (Sheptak and Beyer, 1965; Terenzi et al., 1968; Clifford, 1969; Wilson et al., 1970; Cancio et al., 1970; Chao and Wu, 1971; Henze and Wu, 1973; Blower and Standish, 1973; Worth and Parnaby, 1974). The parison behavior in these tests are described in terms of swell and sag.

Sheptak and Beyer (1965) obtained pure swell data from the bottom of the parison, assuming the first extruded segment to be free of drawdown effects since no weight is acting below it. The drawdown contribution was then obtained by subtracting the pure swell contribution to the incremental weight from the experimental incremental weight.

Chao and Wu (1971) also assumed that the bottom portion of the parison is free from drawdown effects and that it represents the contribution of pure swell. The top segment was considered to incorporate the combined effects of sag and swell. The net effect of drawdown was obtained by subtracting the weight of the bottom element from that of the top element.

Wilson et al. (1970) were the first researchers to study the effect of die design variables on parison swell characteristics. A commercial blow molding machine was used in conjunction with a pinch-off mold to obtain data for several HDPE resins. The diameter swell and weight swell values were obtained using the following equations:

$$B_1 = (D_p/D_o - 1)100 \qquad 3.2.2$$

$$B_2 = (W_A/W_T - 1)100 \qquad 3.2.3$$

where D_p and D_o are the diameter of the parison and the outer diameter of the die respectively, W_A is the actual parison weight per unit length and W_T is the theoretical weight per unit length. Three different die geometries were used. These were a straight die, a 30° diverging die and a 30° converging die. The diameter swell and weight swell ratios were found to increase in going from the diverging die to the straight die to the converging die. The increase in swell in changing from the diverging die to the straight die or converging die was found to be 6% and 30% respectively.

Henze and Wu (1973) presented the first attempt to relate diameter swell ratio, B_1 and weight swell ratio, B_W. The experimental set-up consisted of a commercial blow molding machine and a 30° diverging die. The parison pinch-off technique was used to obtain diameter and weight swell data. The following relation was proposed:

$$B_1 = B_W^a \qquad 3.2.4$$

Using the experimental data they obtained, the value of "a" was found to be 0.25. The exponent a, is an indication of the anisotropy of the deformation in the circumferential and radial directions. A value of a = 0.5 corresponds to the isotropic case.

Garcia-Rejon (1979) also attempted to find a correlation between the diameter swell ratio and area swell ratio using a modified version of the equation proposed by

Henze and Wu (1973).

$$B_1 = A\,B_w^{a} \simeq A(B_1 B_2)^{a} \qquad 3.2.5$$

A straight annular die was used and the diameter swell ratio, B_1, and thickness swell ratio, B_2, were obtained from completely relaxed samples extruded into an isothermal oil bath. Using the experimental data, values of a = 0.38 and a ≐ 0.52 were found for the HDPE resins and for the polypropylene resin respectively. The straight die seems to give results which are closer to the isotropic case than the diverging die used by Henze and Wu (1973). It was concluded that the relationship between diameter swell and thickness swell at a given shear rate depends on the die geometry.

Miller (1975) tried to develop a correlation between the rheological properties of the resin and its swell behavior. HDPE resins were used. Rheological characterization was obtained by measuring the shear viscosity, dynamic functions like dynamic viscosity, storage modulus and complex viscosity, and molecular weight distribution. The diameter and weight swell values were obtained from blow molded bottles obtained at preset operating conditions. These conditions were determined by use of a particular blow molding resin. Large differences in swelling behavior were found but these differences could not be explained in the light of the differences in the rheological properties.

Garcia-Rejon (1979) also characterized the HDPE and the PP resin used in his study. Both shear (viscosity, first normal stress difference, dynamic data) and elongational (elongational viscosity, stress growth in uniaxial elongation) properties were measured, but no qualitative correlation could be found between the swell and the above mentioned rheological properties.

Garcia-Rejon (1979) used a long annular die of cylindrical geometry to analyze the effect of sag and swell on parison behavior. Three HDPE and one PP resin were used. Pure swell and the combined effect of sag and swell were studied separately. To obtain the pure swell values the parisons were extruded into an isothermal oil bath having nearly the same density as the melt. Thickness and diameter swell values were measured simultaneously (the parison was transparent inside the oil) as functions of time. Both swell ratios were found to be composed of a quick recovery period accounting nearly 80% of the total swell potential and a delayed recovery period at the end of which the ultimate swell value was obtained. For the HDPE resins the diameter swell was found to be greater than the thickness swell. The opposite result was obtained with the polypropylene. The combined effect of sag and swell was studied by extruding the parison directly into an isothermal air oven. It was found that the sag contribution could be correlated with the stress growth function in uniaxial elongation. This finding appears to be the first quantitative indication of the role played by the extensional flow properties in parison behavior.

3.3 Effect of Molecular Weight on Swell

Several researchers have studied the relation between capillary die swell and molecular parameters.

Graessley et al. (1970) used polystyrenes with different molecular weights. Swell data were obtained by measuring the diameter of the hardened extrudates with a micrometer. Polydispersity was found to be the primary molecular variable affecting die swell. Samples with higher molecular weights and broadar molecular weight distributions gave higher swell values. Moreover, the narrow distribution samples displayed a constant swelling over a wider range of low shear stresses than samples with broader distributions. A relation between die swell and molecular parameters was developed assuming swell to be due to the release of elastic energy stored in the fluid inside the capillary. The following equation was obtained:

$$B^2+2/B-3 = (J_o \tau_w^2/2G_s)\left[\frac{\int_0^1 \xi^5 d\xi/(\eta/\eta_o)}{\int_0^1 \xi^3 d\xi/(\eta/\eta_o)}\right] \qquad 3.3.1$$

where ξ is the dimensionless radial position, J_o is the shear compliance, G_s is the modulus of elasticity and τ_w is the shear stress at the wall. The term in the parentheses accounts for the velocity and stress distribution across the capillary. Measurements on concentrated solutions and melts of PS showed that J_o could be obtained from the follwing expression:

$$J_o = 2.2 J_R/(1+2.1*10^{-5}c\bar{M}_w) \qquad 3.3.2$$

where $\bar{M}_w$ is the weight average molecular weight and J_R is the steady state shear compliance given by the following equation according to Rouse theory:

$$J_R = (2/5)(\bar{M}_w/cRT)(\bar{M}_z\bar{M}_{z+1}/\bar{M}_w^2) \qquad 3.3.3$$

$\bar{M}_w$, $\bar{M}_z$ and $\bar{M}_{z+1}$ are the average molecular weights defined as the ratios of the moments of the molecular weight distribution. The experimental data and predictions of equation 3.3.1 were found to be in good agreement.

It is apparent from equations 3.3.2 and 3.3.3 that an increase in $\bar{M}_w$ and/or molecular weight distribution $(\bar{M}_z\bar{M}_{z+1}/\bar{M}_w^2)$ will increase the shear compliance J_o. For molecular weights exceeding several hundred thousand (as in the case of polymer melts) the additive factor of 1 in the denominator of equation 3.3.2 may be neglected and J_o becomes independent of $\bar{M}_w$ and depends only on the distribution of molecular weight. Since swell is directly proportional to J_o through equation 3.3.1, an increase in molecular weight distribution will also increase swell values. The results of Graessley et al. (1970) are in agreement with the above argument. However, since the theories on die swell based on elastic solid analysis are successful only in certain cases, one must be cautious in making a generalization.

The work done by Vlachopoulos and Alam (1972a) with PS melts confirms the results obtained by Graessley et al. (1970). They also observed that the broader the molecular weight distribution, the larger the extrudate swell.

Mendelson and Finger (1975) attempted to determine the die swell behavior of HDPE comparing samples with different molecular characteristics. These samples were either prepared by fractionation, removing or adding component molecular species, or by small scale batch polymerization wherein one or another molecular parameter was held constant while other parameters were modified. Contrary to the results previously obtained, swell was seen to decrease with increasing $\bar{M}_w$ and with broadening molecular weight distribution over the entire range of shear rates used. Mendelson and Finger (1975) pointed out the importance of considering overall molecular distribution curves rather than specific moments or combinations of moments.

Shroff and Shida (1977) studied the swell of HDPE, PP and PS samples. For all the samples, swell was found to decrease with increasing molecular weight. Contradictory results were obtained regarding the effect of molecular weight distribution: for some HDPE resins swell increased with MWD whereas for some others the value decreased. This was explained by the effect of viscosity of the polymer. They claimed that swell increased with broadening MWD when such broadening also caused a reduction in viscosity.

Racin and Bogue (1979) studied several PS samples with different molecular structures. As in the previous studies carried out with PS, swell was found to increase markedly with broadening MWD and increasing $\bar{M}_w$. Also, the low shear asymptote for the die swell was found to depend significantly on MWD.

We can conclude that the relation between die swell and molecular parameters is not very well understood. This is partly due to the difficulty in obtaining molecular weight data. The precision with which the MWD can be measured is limited. In particular, the higher moments, $\bar{M}_z$ and $\bar{M}_{z+1}$ can not be accurately determined since these are very sensitive to the presence of small fractions of higher molecular weight material. Also two polymers having significantly different molecular weight distributions can have similar average molecular weights. Therefore, it is better to consider the entire molecular distribution curve rather than the averages.

All the work discussed in this chapter contributed in one way or another to our understanding of parison behavior. However, experimental data for dies similar to those used in industry seem to be missing and the relation between die geometry and swell is not clearly understood. Also, nonisothermal effects and effects of sag on swell have not been studied in detail. Future work should be focused on these points to develop a better understanding of the parison formation stage in blow molding process.

CHAPTER 4

METHODS FOR PREDICTING SWELL

4.1 Models Based on the Theory of Rubber Elasticity

There seems to be a general agreement that die swell is an elastic recoil phenomenon. Several theories based on elastic solid analysis have been proposed in the literature to predict die swell. These theories have in common the fact that die swell is related to the recoverable shear strain, S_R, defined as:

$$S_R = J_o \tau \qquad 4.1.1$$

where J_o is the steady state shear compliance. Since this equation is based on linear viscoelasticity it cannot be relied upon except at low shear rates, but it is often observed that it continues to fit data even at higher shear rates (Dealy, 1982). It has been shown (Stratton and Butcher, 1971) that S_R can be calculated from normal stress measurements in the limiting low shear rate region where the viscosity is Newtonian and the first normal stress difference, N_1 varies as $\dot{\gamma}^2$. For this particular case we have:

$$S_R = N_1/2\tau \qquad 4.1.2$$

In deriving die swell relations based on elastic solid analysis, geometric assumptions are made to relate the unconstrained recoil that occurs in extrudate swell to the constrained recoil that occurs in creep recovery.

Nakajima and Shida (1966) considered extrudate swelling to be similar to the behavior of ideal rubber under isothermal conditions. They hypothesized a process in which the swollen extrudate is pulled lengthwise until its diameter is equal to the diameter of the capillary. The tensile strain is then taken as a quantitative expression for the recoverable strain in the flow.

Nakajima (1974) later extended this work. He defined a time constant λ, which relates strain, S_R to shear rate by the following relation:

$$\lambda = S_R/\dot{\gamma} \qquad 4.1.3$$

From the previous study of Nakajima and Shida (1966) strain was related to the swell by:

$$S_R = B^2 - 1/B^4 \qquad 4.1.4$$

To calculate swell, strain must be evaluated. Therefore, three time constants were introduced. Emprical correlations were used to relate the time constants to the melt index of the resin. However, it is well known that melt index alone is not sufficient to characterize resins in terms of swell. The model does not have a practical application since the parameters cannot be related to measurable rheological properties.

Bagley and Duffey (1970) followed essentially the analysis of Nakajima and Shida (1966) but used a one-constant stored energy function. The following relation was obtained:

$$S_R^2 = B^4 - B^{-2}. \qquad 4.1.5$$

Another relation was obtained using the strain energy function in shear inside the capillary.

$$S_R^2 = B^4 + 2/B^2 - 3 \qquad 4.1.6$$

The two equations were found to give similar results for large values of swell. The experimental data did not correlate very well with the above equations.

Locati (1976) proposed a model assuming that the deformation undergone by the melt entering the capillary from the reservoir is essentially elastic and the deformation within the capillary is essentially viscous. The basic ideas proposed by Nakajima and Shida (1966) were reworked and the following equation was obtained:

$$B^2 = 1+(\Delta P_e/3G)e^{-t_p/\zeta} \qquad 4.1.7$$

where B is the capillary die swell, ΔP_e the entrance pressure, G is an elastic modulus, t_p the transit time in the capillary and ζ is a characteristic relaxation time. Experiments were carried out with HDPE resins and the extrudates were annealed in silicone oil after extrusion. The loss modulus (G") was taken to be the elastic modulus and was obtained using a shift factor. It was concluded that if ζ could be defined in a better way, the model would be complete.

Mendelson et al. (1971) also assumed that the viscoelastic liquid can be treated in terms of the solid state rubber behavior described by Treloar (1958). They developed 3 models, two of which are applicable to dies having small L/D ratios since it was assumed that the extrudate had undergone perfectly elastic recovery from a homogeneous tensile deformation. In the third approach the recoverable energy stored in simple shear and recovered in tensile contraction was considered. This approach is well suited for dies having high L/D ratios, where entrance effects are negligible. The results were the same as those obtained by Bagley and Duffey (1970).

Tanner (1970) developed a model based on unconstrained elastic recovery from Poiseuille flow. The flow at the exit was approximated by a sudden strain which takes the fluid from the viscometric stress state inside the tube instantaneously to the zero stress state (atmospheric pressure) outside the tube. Inertia forces in the sample were completely neglected. As a constitutive equation the K-BKZ model (Bernstein et al., 1963) was used. For a material with a single relaxation time the relation was found to be:

$$S_R^2 = 2(B^6-1) \qquad 4.1.8$$

In order to account for the Newtonian die swell the above equation was rearranged and the term 0.1 was added.

$$B = (1+S_R^2/2)^{1/6} + 0.1 \qquad 4.1.9$$

The model predictions were compared with some experimental data and results were found to be satisfactory.

Huang and White (1979, 1980, 1981) extended Tanner's approach (1970) to different die geometries. For slit dies, die swell (defined as the ratio of the thickness of the extrudate to the thickness of the die) was found to be given by the following relation (Huang and White, 1979):

$$B_S = (1+S_R^2/3)^{1/4} \qquad 4.1.10$$

To evaluate the recoverable strain, an empirical equation relating normal stresses to molecular parameters was used. Equation 4.1.10 predicts the swell from the slit die to be larger than the capillary swell and to increase more rapidly with extrusion rate. Their experimental results obtained from capillary and slit dies supported these predictions.

In a subsequent study Huang and White (1980) applied the unconstrained recovery theory of Tanner (1970) to the problem of die swell from short dies. The flow in the entry region was considered to be elongational in character and shear flow contributions were considered to be small. The models were found to predict the qualitative trend of the experimental data taken from short capillary and slit dies, but quantitative predictions were poor. They also applied this theory to rectangular and trapezoidal dies (White and Huang, 1981). Although the model underestimated swell, the predicted extrudate shape was consistent with the observed shape.

Cogswell (1970) derived expressions for capillary swell and annular area swell considering the unconstrained elastic recovery of the material caused by shear flow in the die.

The material was assumed to follow Hooke's law in shear. The following relations were obtained:

Capillary:

$$B^2 = (2/3)S_R\{(1+1/S_R^2)^{3/2} - 1/S_R^2\} \qquad 4.1.11$$

Annular:

$$B_1B_2 = 0.5\ \{(1+S_R^2)^{1/2} + (1/S_R)\ln[(S_R + (1+S_R^2)^{1/2}]\} \qquad 4.1.12$$

Garcia-Rejon (1979) combined the above two equations to eliminate S_R. Thus a relation between annular area swell and capillary area swell based on a theoretical model was obtained. Good agreement was found between the predictions of the resulting equation and the experimental results for the HDPE resins used in that study. However for the PP resin the results were poor.

Theories based on rubber elasticity have been reviewed by Vlachopoulos et al. (1972b) and by Utracki et al. (1975).

The theories discussed above neglect velocity and stress field rearrangements at the end of the die. The work carried out by Whipple and Hill (1978) showed that pronounced nonlinearities in the velocity profile can exist at the die exit and that what happens is grossly different from what is assumed to occur in elastic like fluid theories. Another problem that is associated with these theories is that recovery (swell) is assumed to be instantaneous whereas in reality recovery is time dependent, and only some part of it takes place instantaneously. Finally, in order to be able to use these theories, seperate measurements of N_1 at the same shear rate as in the die are required. In most cases the values of N_1 are available only at quite low shear rates, and the equations relating N_1 to molecular parameters are empirical and do not have a general validty. Therefore, we can say that relations based on elastic-solid analysis are only partially successful and that they do not constitute a fundamental theory in the sense that for given material properties die swell cannot be predicted in advance.

4.2 Models Based on Numerical Methods

Newtonian fluids also exhibit die swell. The value of capillary die swell for them varies only from 1.12 at low shear rates (Batchelor et al., 1973; Horsfall, 1973; Middleman and Gavis, 1961; Tanner, 1973; Reddy and Tanner, 1978) to 0.87 at high rates (Middleman, 1977). Polymer melts exhibit the same low shear rate swell value in the Newtonian plateau region (Batchelor et al., 1973). Theories on die swell based on elastic solid analysis cannot explain this behavior. In recent years, several studies were carried out to evaluate die swell of Newtonian and viscoelastic fluids by means of the finite element method.

Tanner (1973) and Nickell et al. (1974) solved the dynamic and continuity equations for a Newtonian fluid in the neighborhood of the capillary exit by a numerical technique. In the limit of low Reynolds number they obtained a die swell of 1.13 which is in good agreement with the experimental value.

The swell value of 0.87, valid at high Reynolds numbers, can be predicted by theory using a simple combination of mass and momentum balances (Middleman, 1977). Thus the Newtonian flow problem is well understood, and the theory is in good agreement with the data at both low and high Reynolds numbers.

The numerical calculation of die swell of a viscoelastic fluid has been considered only recently by several authors (Chang et al., 1979; Coleman, 1981; Crochet and Keunings, 1980, 1981, 1982a; Reddy and Tanner, 1978). Only limited success has been achieved at the present time, since the calculations extend over a very limited range of elastic forces.

Crochet and Keunings (1980, 1981) carried out a series of studies to calculate the die swell of a viscoelastic fluid extruded from different die geometries. They used an upper convected Maxwell fluid with a single relaxation time. This model was selected since it predicts satisfactory qualitative behavior in terms of only two material constants. It is assumed that the upstream velocity field corresponds to a fully developed viscometric flow and that the contact forces vanish on the free surfaces. The work is limited to creeping viscoelastic flow, and the finite element method of calculation is used. Several different die geometries were studied; capillary, slit, straight annular, converging and diverging annular dies. Results could be obtained up to $\lambda\dot{\gamma}_w$= 0.75, where λ is the relaxation time and $\dot{\gamma}_w$ is the shear rate at the wall. This dimensionless number, $\lambda\dot{\gamma}_w$, is a measure of elasticity. The results for capillary die swell (Crochet and Keunings, 1980) were compared with the predictions of Tanner's (1970) model based on elastic solid analysis and good agreement was found.

The converging and diverging dies on which their calculations were based were the ones designed and used for the present study. Crochet and Keunings (1981) carried out their numerical analysis for these dies for creeping flow of a Newtonian, a power law and a Maxwell fluid. The effect of shear-thinning was found to cause the outer and inner radii of the parison to approach the corresponding radii of the die lips. Elasticity enhanced swelling, and higher values were obtained than for Newtonian and power law fluids. However, their predictions are not in agreement with the experimental data obtained in the present study. Experimentally, higher diameter swell values are obtained for a converging die, whereas their calculations predict the reverse. This will be discussed in section 5.3.3. The case of annular dies is more complicated since it requires the simultaneous calculation of two free surfaces. Values of die swell were calculated on the assumption that the flow is fully developed a few diameters above the exit. To study the effect of capillary length upon swell, L/D ratios ranging from 0 to 1 were investigated (Crochet and Keunings, 1981). Similar swell values were obtained with all the L/D ratios studied.

In a subsequent paper Crochet and Keunings (1982a) used the Oldroyd three constant model rather than Maxwell model. The Oldroyd three constant model introduces a retardation time and reduces to the Maxwell fluid for viscometric flows. They observed that the addition of a retardation time has a considerable impact upon the quality of the finite element calculation of die swell and that higher elasticity (values of $\lambda\dot{\gamma}_w = 4$) could be accomodated. Capillary and slit die swell values were calculated and compared with Tanner's (1970) elastic-solid theory predictions. Good agreement was obtained. Capillary die swell predictions were also in agreement with the experimental data obtained by Vlachopoulos et al. (1981) and by Racin and Bogue (1979).

Reddy and Tanner (1978) studied the swelling of a sheet of fluid modelled by the second order fluid equation. Finite element computer methods were utilized. No comparison with experimental data was given.

Coleman (1981) calculated slit die swell for a Maxwell fluid using a finite element method different from that used by Crochet and Keunings (1980). He was able to obtain convergence up to $\lambda\dot{\gamma}_W = 1.25$, which is higher than the maximum value reached by Crochet and Keunings (1980) using the same constitutive equation. Similar swell values were obtained in these two studies.

Chang et al. (1979) also applied the finite element method to the calculation of slit and capillary die swell of a generalized Maxwell fluid and obtained higher swell values than others.

All of the models described above share the same convergence failure of the numerical method when the elastic contributions, measured by a dimensionless number, $\lambda\dot{\gamma}_W$, exceed a certain critical value. Several researchers (Crochet and Keunings, 1982b; Mendelson et al., 1982; Tanner, 1982) are carrying out studies to understand the reasons of failure and to improve the method.

Mendelson et al. (1982) studied finite element calculations with Maxwell and second order fluid models and concluded that excessive approximation error in the stress field causes the failure of the calculations for both models. Better approximatioms for the stress field could be obtained by using a refined mesh, but such calculations would be very costly.

Crochet and Keunings (1982b) compared different finite element techniques and studied the effect of mesh refinement. They concluded that the maximum value of $\lambda\dot{\gamma}_w$ allowing convergence is highly dependent on mesh refinement. Tanner (1982) derived some stability criterion expressions and emphasized that mesh refinement affects convergence.

In summary we can say that the numerical simulation of die swell is not of practical use for the time being since the calculations are time consuming and costly and the models cannot be extended to cases where elastic effects are dominant due to convergence problems. However, this approach is novel and studies are continuing to improve it.

Winter and Fischer (1981) studied the melt strain history in extrusion dies and its influence on extrudate swell. The influence of die geometry was demonstrated on three diverging annular dies and one annulus of constant cross section. All the dies had the same exit geometry. An extension of the Lodge-type single integral constitutive equation was used with a time and strain dependent memory function. The kinematics were locally approximated by steady isothermal shear flow and the integral constituitve equation was solved numerically. For the straight annular die the radial and circumferential swells were found to be equal. No comparison with experimental data was given. In a subsequent study Fischer (1981) studied five diverging dies, three of which were the ones used in the previous study (Winter and Fischer, 1981). The same method as in the previous study was employed to evaluate the swell. Only the results from one die were compared with experimental data. The predicted and measured values for thickness swell were in agreement, but the model overpredicted diameter swell. The advantage of this model is that it does not require the long computation times implicit in the use of finite element methods which use a simple material function and a high precision in calculating the flow history of the material. However, there is not enough comparison between model predictions and experimental data to prove the reliabilty of the proposed model.

All of the models discussed above assume isothermal conditions. However, in the actual case, due to the generation of heat by viscous dissipation, the viscosity of the melt is reduced and the flow patterns are more complex than in the isothermal case.

Phuoc and Tanner (1980) investigated the flow of a Newtonian fluid having a temperature dependent viscosity in extrusion problems. A finite element method was used, and it was found that the extrudate expansion up to 70% of the die diameter was obtained due to temperature effects.

In summary, the work reviewed in this chapter shows that no satisfactory theory has been developed so far which can predict swell from basic rheological properties.

CHAPTER 5

EXPERIMENTAL STUDY OF SAG AND SWELL

5.1 Introduction

It was pointed out in Chapter 1 that the central problem in extrusion blow molding is to control the geometry of the parison at the moment of inflation so that the required mechanical properties can be achieved with minimum consumption of the resin. Parison geometry can be described in terms of the length and the distributions of outside diameter and thickness. Two phenonema act to cause a variation with time of the parison cross section from the moment it is formed at the die lips. These are extrudate swell and sag or drawdown. Whereas swell is an unconstrained recoil process, sag is a low-strain-rate extensional flow driven by the force of gravity. Swell is a function of time and sag depends both on time and on position along the length of the parison. Most of the swell occurs in a short period of time as the extrudate moves away from the die, while sag is quite small at the beginning and becomes prominent only after the parison has reached a significant length or has been hanging freely for some time. These two phenomena are coupled and act simultaneously.

Parison behavior depends on system parameters such as

die design, extrusion velocity, temperature and on the resin being processed.

In order to gain a better understanding of swell and sag and to study their relative importance in parison formation, it is necessary to develop experimental techniques and equipment that will allow the uncoupling of these two phenomena. In the present study, the techniques developed by Dealy and Garcia-Rejon (1980) were used to study pure swell and the combined effect of sag and swell separately. Therefore, two different types of experiments were carried out:

1. Pure swell experiments. These experiments were carried out to study the swelling characteristics of the parison in the absence of gravitational forces. The parison was directly extruded into an oil bath which was at the same temperature as the extrusion temperature and had nearly the same density as the melt.

2. Combined effect of sag and swell. In these experiments the combined effect of sag and swell was studied by extruding the parison into an air oven instead of an oil bath. The air oven was at the extrusion temperature.

In the present study, three high density polyethylene resins and four different annular dies were used. Parisons were extruded at different extrusion velocities. All the experiments were carried out under isothermal conditions to eliminate uncertainties as to temperature.

In this chapter, the die geometries and experimental apparatus used will be described. Then the results will be presented and discussed.

5.2 Description of the Dies

Die design is one of the most important parameters that govern parison behavior, since the swelling characteristics of the parison depend largely on die design.

Most of the work done on swell so far has been concentrated on capillary and slit dies and relatively little work has been done on annular dies. In order to gain a better understanding of the effect of die design on parison behavior, four annular die geometries were designed and used in the present study. These are: a straight die, a 20° diverging die, a 20° converging die and a 10° converging die with a tapered gap.

The dies are made of hardened stainless steel and consist of three pieces: an outer cylinder, an inner core and a head piece. This is illustrated in Figure 5.1. The inner core is screwed to the head piece. To have a smooth flow at the entrance region, the head piece is designed to have four orifices through which the melt flows, and the inner core is

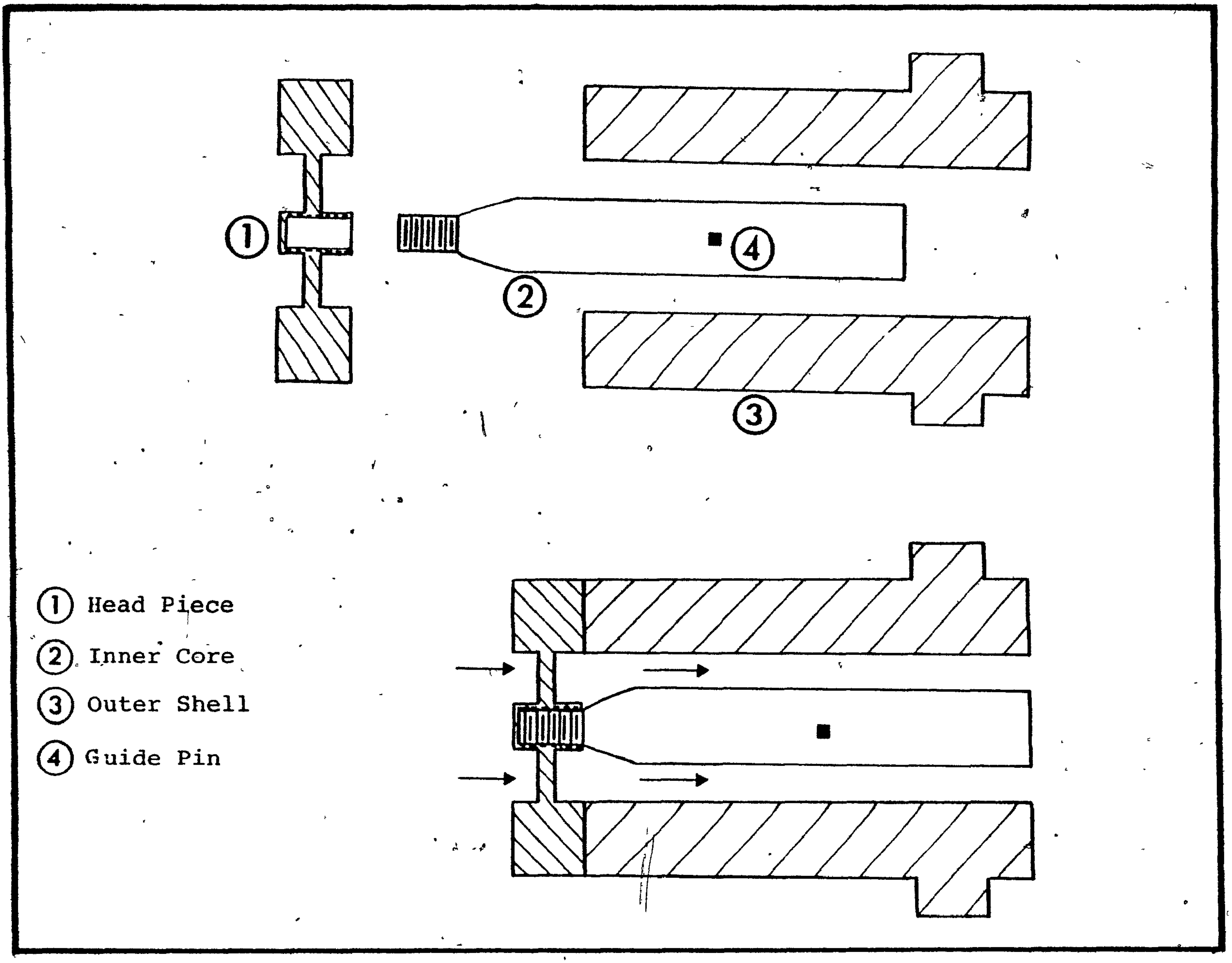

Figure 5.1 Annular Die Components

streamlined at the top. In order to keep the inner and outer pieces concentric, there are three guiding pins on the inner piece. All four dies are sufficiently long (L/H>30) so that the effect of entrance region is eliminated, and the parison behavior is unaffected by the length of the die and by the presence of the guiding pins.

The cross sections of the straight die and the diverging die are sketched in Figure 5.2. The straight die consists of two concentric cylinders with the following dimensions:

Outside diameter = 12.7 mm
Annular gap = 1.5875 mm
Total length = 95.25 mm

The diverging die starts with a smaller inner and outer diameter. Then both the outer and inner pieces diverge with an angle of 20°. The outer and inner walls are always parallel. This die is designed in such a way that, at the exit it has exactly the same geometry, i.e., the same annular gap and outside diameter, as the straight die. Also in the upper section of the die, the die gap is the same as in the straight die. The dimensions of this die are:

Outside diameter in the upper section = 6.35 mm
Annular gap in the upper section = 1.5875 mm
Outside diameter at the exit = 12.7 mm
Annular gap at the exit = 1.5875 mm

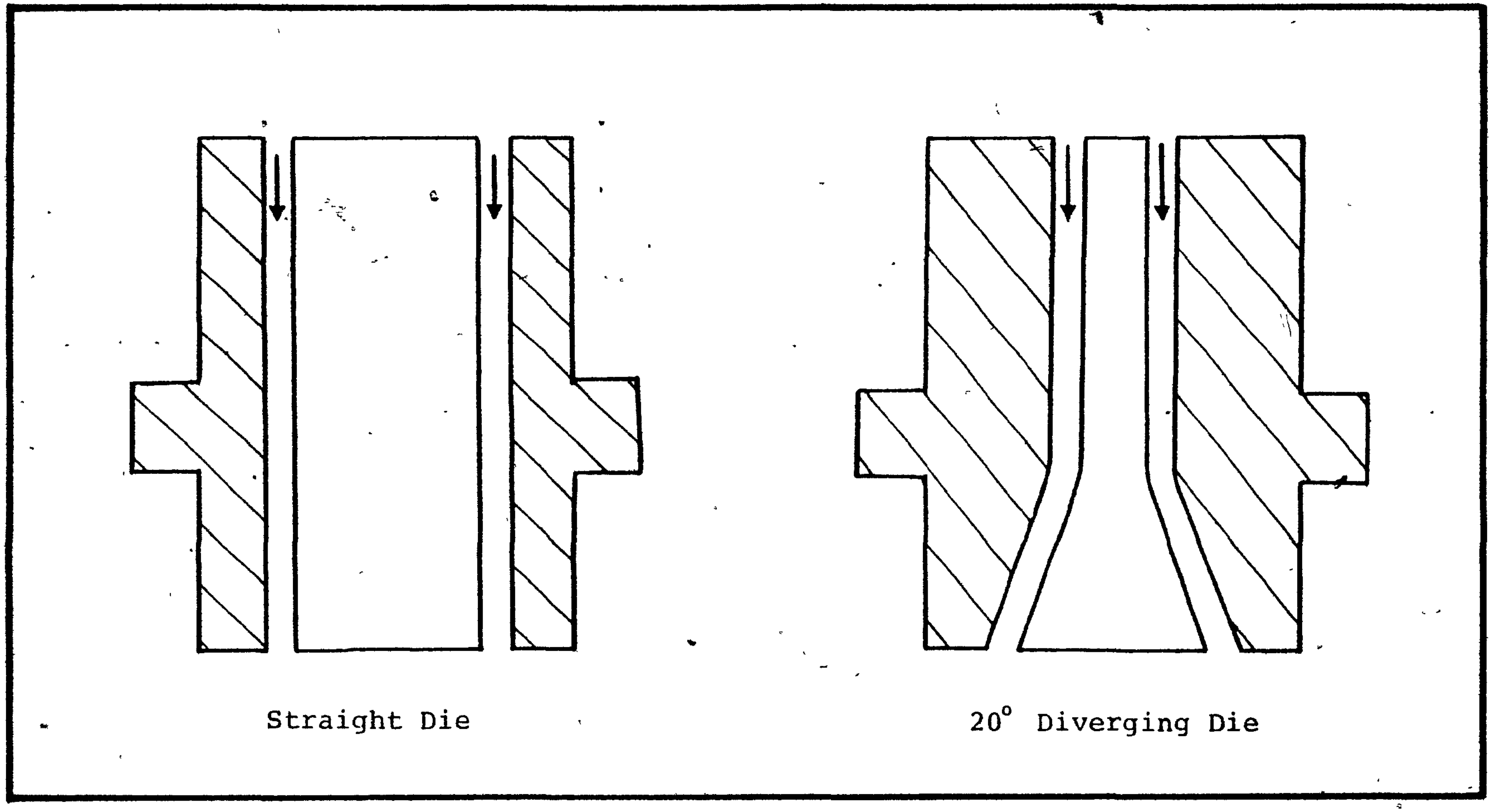

Straight Die

20° Diverging Die

Figure 5.2 Cross-sections of the Straight and the Diverging Die

Total length = 69.850 mm

Length of the diverging section = 8.731 mm

Angle of divergence = 20°

The cross sections of the two converging dies are shown in Figure 5.3. The 20° converging die starts with the same dimensions (outside diameter and the annular gap) as the straight die. Then, both the inner and outer pieces converge with an angle of 20°. As in the previous dies, the inner and outer walls are always parallel. At the exit, this die has a different outer and inner diameter than the other two dies, but the annular gap is the same. The dimensions of the 20° converging die are listed below.

Outside diameter in the upper section = 12.7 mm

Annular gap in the upper section = 1.5875 mm

Outside diameter at the exit = 6.35 mm

Annular gap at the exit = 1.5875 mm

Total length = 69.850 mm

Length of the converging section = 8.731 mm

Angle of convergence = 20°

The 10° converging die was obtained by removing the inner core of the 20° converging die and replacing it with a piece converging with an angle of 10°. So, unlike the other dies used in this study, the inner and outer walls are not parallel along the length of the die. Rather, they are parallel only up to the point of convergence, then the inner

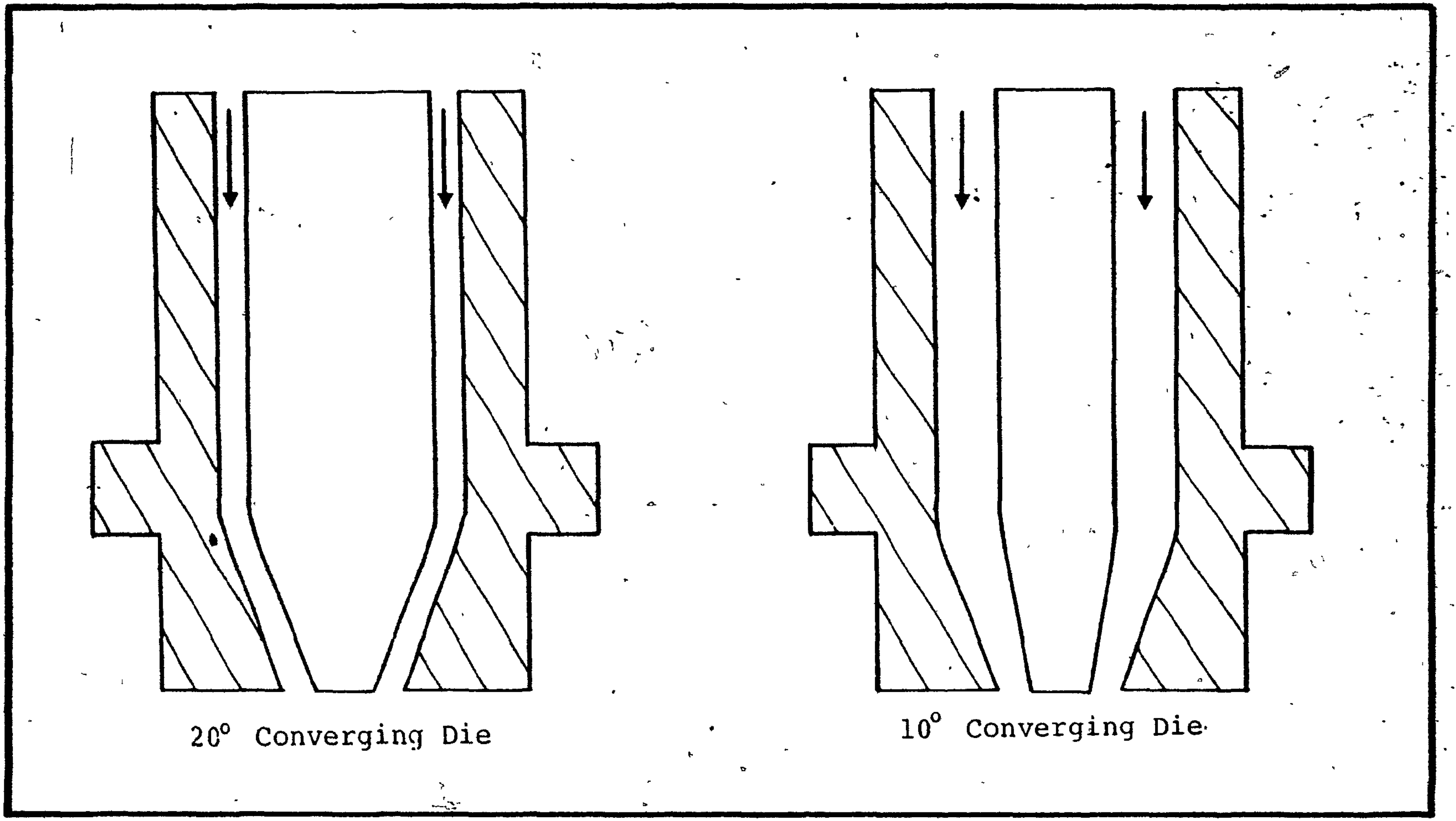

20° Converging Die

10° Converging Die

Figure 5.3 Cross-sections of the two Converging Dies wall converges with an angle of 10° while the outer converges with an angle of 20°. Also, contrary to the other dies, the annular gap in the upper part of the die is not equal to 1.5875 mm. At the exit this die has exactly the same geometry as the 20° converging die. Its dimensions are as follows:

Outside diameter in the upper section = 12.7 mm
Annular gap in the upper section = 3.223 mm
Outside diameter at the exit = 6.35 mm
Annular gap at the exit = 1.5875 mm
Total length = 69.850 mm
Length of the converging section = 8.731 mm
Angle of convergence = Inner wall 10°, Outer wall 20°

In the construction of the dies, the sharp corners in the diverging and converging sections were smoothed and the critical dimensions were manufactured with an accuracy of ± 0.0025 mm.

5.3 Pure Swell Experiments

The aim of pure swell experiments was to study swell in the absence of sag. Experiments were carried out with all three resins for the straight die, diverging die and the 20° converging die. The 10° converging die was used only with Resins 22A and 27. All the experiments were done at a constant temperature of 170 °C and parisons were extruded at six different extrusion velocities.

Two independent swell ratios can be defined in the case of an annular extrudate. We have chosen to present our results in terms of the diameter swell, B_1, and the thickness swell, B_2. Diameter swell is defined as the ratio of the outer diameter of the parison (D_p) to that of the die at the exit (D_o) and the thickness swell is defined as the ratio of the thickness of the parison (h_p) to the annular gap at the die exit (h_o).

$$B_1 = D_p/D_o \quad 5.3.1$$

$$B_2 = h_p/h_o \quad 5.3.2$$

This is also shown in Figure 5.4. Another ratio often used in industry, is the weight swell, B_W, defined as the ratio of the weight of a parison of length L to the weight of the same length of sample having the inner and outer diameters of the die lips. In the case of isothermal extrusion, the weight swell should be equal to the area swell. If the die gap is rather small compared to its radius, the annular die can be approximated as a slit and the area swell will be approximately equal to the product $B_1 B_2$.

$$\text{Area swell} = B_1 B_2 \quad 5.3.3$$

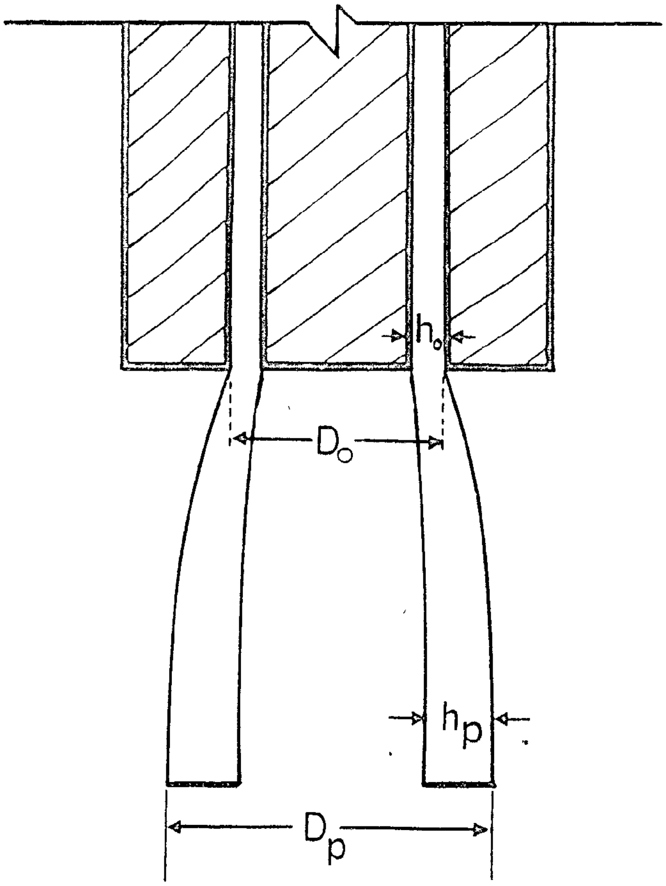

$$\text{Diameter Swell } (B_1) = \frac{D_p}{D_o}$$

$$\text{Thickness Swell } (B_2) = \frac{h_p}{h_o}$$

Figure 5.4 Swell Ratios for an Annular Extrudate

5.3.1 Experimental Apparatus

The experimental apparatus used to measure parison swell consists of the following pieces of equipment:

1. Instron Capillary Rheometer
2. Thermostating chamber
3. Photographic and auxiliary equipment

An Instron Universal Testing Instrument (Floor model, TT-CM-L) was used in conjunction with an Instron capillary rheometer (type MCR) to extrudate the polymer at different crosshead speeds ranging from 0.5 cm/min to 50 cm/min. The Instron capillary rheometer was briefly described in section 2.3.3 and a more detailed description can be found elsewhere (Instron Manual, 1976). A new barrel, having twice the inner diameter of the original Instron barrel, was designed to accomodate the dies described in section 5.2. The new barrel has an inside diameter of 19.05 mm. Other features of the barrel are the same as the original one. The die is inserted in the barrel and held in place by means of a clamping nut. The dies and the clamping nut are designed in such a way that the tip of the die is visible, enabling one to observe the parison as it starts to form at the die lips. This was not possible with the original barrel-die assembly.

The thermostating chamber was originally designed by Utracki et al. (1975) and later used by Dealy and

Garcia-Rejon (1980). It consists of a section of stainless steel pipe with an inner diameter of 15 cm and a length of 25 cm, to which a bottom plate has been welded. An immersion heater (750 W, 115 V) is welded to the bottom of the plate.

One side of the body of the thermostating chamber has a double window mounted in it, through which the parison can be seen. On both sides of the chamber (at 90° from the front window) there are circular windows made of Pyrex glass through which the inside of the chamber is illuminated by 2 halogen lamps of variable intensity (75 W, 12V). These lamps are located in special housings attached to the side windows. Their intensity is controlled by two variable transformers. The chamber is insulated with layers of asbestos paper and an outer layer of heavy asbestos tape painted with heat resistant enamel. The chamber is mounted on rails attached to the base of the Instron testing machine. The chamber can be easily moved forward and backward.

The heating medium in the thermostating bath was Dow Corning's Silicone Fluid (Dow Corning Fluid 200, 200 cs), and a proportional temperature controller (Fenwall 524) was used to adjust the temperature to the desired value. The cover plate of the thermostating chamber was free to rotate and had two holes for pyrex tubes of diameter 50.8 mm into which the polymer was extruded. A metal plate painted black, was attached to the cover plate and acted as a background for photographic purposes. A cross sectional view of the thermostating chamber is given in Figure 5.5. Further details on the design of the chamber can be obtained elsewhere (Garcia-Rejon, 1979).

The test tubes are filled with a mixture of Silicone oil (Dow Corning Fluid 200, 2 cs and 5 cs). Theoretically, the density of the silicone oil mixture should be the same as that of the melt to eliminate gravitational effects. However, it was observed that (Garcia-Rejon, 1979) in order for the polymer to flow smoothly without distortion, the density of the silicone oil mixture should be slightly less than the density of the melt. In the present study, the density of the oil mixture was adjusted using a trial and error procedure and observing the bouyancy of a piece of polymer melt in mixtures of different compositions. The composition of the mixture was approximately 40% 2 cs and 60% 5 cs silicon oil. The temperature inside the glass tubes was monitored by a type J thermocouple. The temperature was read directly with a digital thermometer (Fluke 2100A). The temperature gradient between the top and the bottom of the tube was less than 1 °C.

A 35 mm SLR camera (Nikon F) was used to take the pictures of the parison. The camera was equipped with a motor drive and it was mounted on a tripod so that the depth of field for each shot was the same. A 50 mm macro lens was

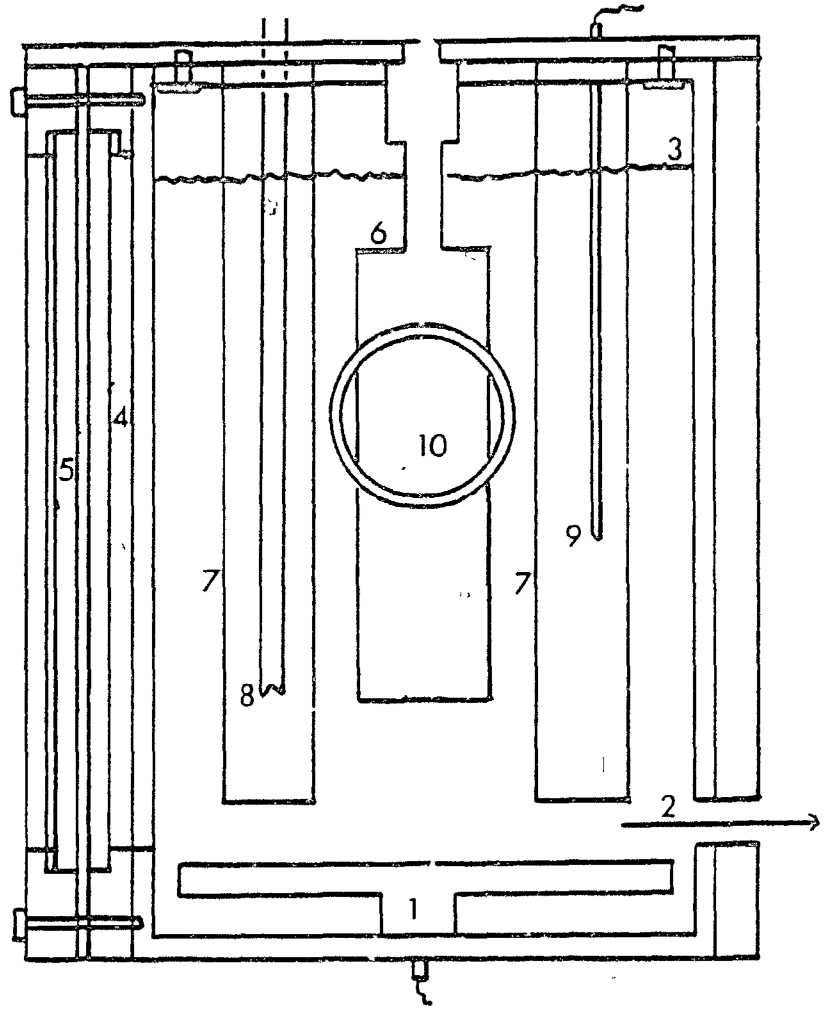

1. Immersion Heater	6. Screen
2. Liquid Outlet	7. Pyrex Tubes
3. Liquid Level	8. Extrudate
4. Vycor	9. Thermocouple
5. Pyrex Plates	10. Illumination Window

Figure 5.5 Cross-sectional View of the Thermostating Chamber

used so that the camera could be placed very close to the thermostating chamber. Thus the dimensions of the parison could be determined more accurately.

5.3.2 Experimental Technique

In pure swell experiments, the diameter and thickness of the parison were measured. Since swell is a function of time, material elements extruded first will swell more. Thus the dimensions of the parison will not be uniform along its length. Also the leading end portion of the parison has a different shape than the rest of the parison. This is because the extrusion starts from rest and the material initially near the die exit experiences a different strain history than the rest of the material in the parison. Therefore the swell depends on where the measurement is made along the length of the parison. To identify a position for data measurement, the parison was marked with carbon black particles ejected from a syringe. This was important at the lowest extrusion velocities. For higher extrusion velocities, due to the short times involved, the parison was uniform (excluding the end portion), and it was not necessary to put a mark on the parison.

Also, at low extrusion speeds the end of the parison was cut off by a hot wire cutter after steady state was obtained. The hot wire cutter consists of a casing with two rods, between which a thin wire is streched. The wire is heated by the application of voltage across the rods. The system cuts through the parison with minimum disturbance. At higher extrusion velocities, the end portion could not be cut off due to time limitations. In such cases, this portion of the parison was ignored in taking the measurements.

The experimental procedure can be summarized as follows:

At the beginning of each experiment, the thermostating chamber and the barrel-die assembly was heated to the desired temperature. Once the temperature was stable at the desired level, the extrusion was started. When the force reading reached steady state, the parison was cut with the hot wire cutter. Then the parison was marked with the carbon black particles and at the same time, t was set equal to zero. Immediately the chamber was slid forward to its preset position so that the extrudate flowed directly into the glass tubes. To check the consistency of this method, different marks were put on the same parison and the results obtained from these points were compared. Good agreement was found between these results.

Photographs started to be taken at predetermined time intervals at the moment when the parison was seen through the window of the thermostating chamber. Extrusion was stopped after a predetermined mass had been extruded. At the beginning, photographs were taken at short time intervals. They continued to be taken, at longer intervals, until the dimensions of the parison did not change with time. The parison extruded in the oil was transparent so that both the outer diameter and thickness could be measured. At the end of each run, the picture of a standard ruler inserted in the oil filled test tube of the thermostating chamber was taken for calibration purposes. To verify the thickness measurements, pictures of a standard placed inside the parison in the oil filled test tubes were taken and compared with the pictures of the same standard in the oil filled test tubes. The two methods gave the same results.

The negative of the developed film (Ilford HP5, 400 ASA) was analyzed using a Reichert microscope with an accuracy of ± 0.0012 mm to obtain the diameter and thickness of the parison as functions of time. Diameter and thickness swell values were than calculated using equations 5.3.1 and 5.3.2.

The front window of the thermostating chamber does not extend all the way up to the die outlet. Therefore, some time passes before the parison can be seen inside the test tubes. This does not pose a problem in the case of high extrusion velocities where extrusion is fast, but in the case of low extrusion velocities data cannot be obtained at short times. To obtain short time data, pictures of the parison extruded directly into air were taken for a period of 5 seconds. In this time interval the effects of gravity and nonisothermal conditions are assumed to be negligible. Only diameter swell values can be obtained from these experiments, however, since the parison is not transparent when extruded into air.

5.3.3 Results and Discussion

The time dependent thickness and diameter swell values obtained from pure swell experiments for each die geometry, resin and extrusion velocity are given in Tables A3.1-33 in Appendix A3. It was mentioned previously that the experiments were done at 170 °C. The straight die, the diverging die and the 20° converging die were employed with all the three resins and the 10° converging die was used with only Resins 22A and 27. Six different extrusion rates were used with each die-resin combination. Using the shear rate at the wall as a measure of extrusion rate has been the general custom. Due to the difficulties associated with calculating the shear rate at the wall in the complex geometries used in this study, we used volumetric flow rate as a measure of extrusion rate.

The time dependency of diameter and thickness swell can be studied by plotting the data in Tables A3.1-33. Such graphs for Resin 27 extruded from the 10° converging die are shown in Figures 5.6 and 5.7 where diameter and thickness swell values are plotted as functions of time, volumetric flow rate being the parameter. Figure 5.6 shows that nearly 60-80% of the diameter swell occurs in a relatively short period of time after the parison is formed. The swelling then continues at a decelerating rate until a constant value is reached at around 7-8 minutes. This constant value of swell is termed the "equilibrium diameter swell" and denotes a completely recovered parison. Similar observations were made for the time dependency of thickness swell . Most of the thickness swell occurs at a relatively short time after the parison exits from the die, and a constant value, termed the "equilibrium thickness swell" is reached after 5-7 minutes have elapsed. The same observations were made for all the resins and die geometries used in this study.

Garcia-Rejon (1979) also reports similar behavior for the HDPE and PP resins extruded from a straight annular die. He considered the swell mechanism to be composed of an instantaneous and a secondary slow recovery region and proposed the following emprical relation:

$$B_i(t) = B_{i\infty}(1-e^{-t/\zeta_1}) + B_{io}e^{-t/\zeta_1} \qquad 5.3.4$$

where $B_{i\infty}$ and B_{io} are the swells at equilibrium and zero time respectively and the quantity ζ_1 is a characteristic time.

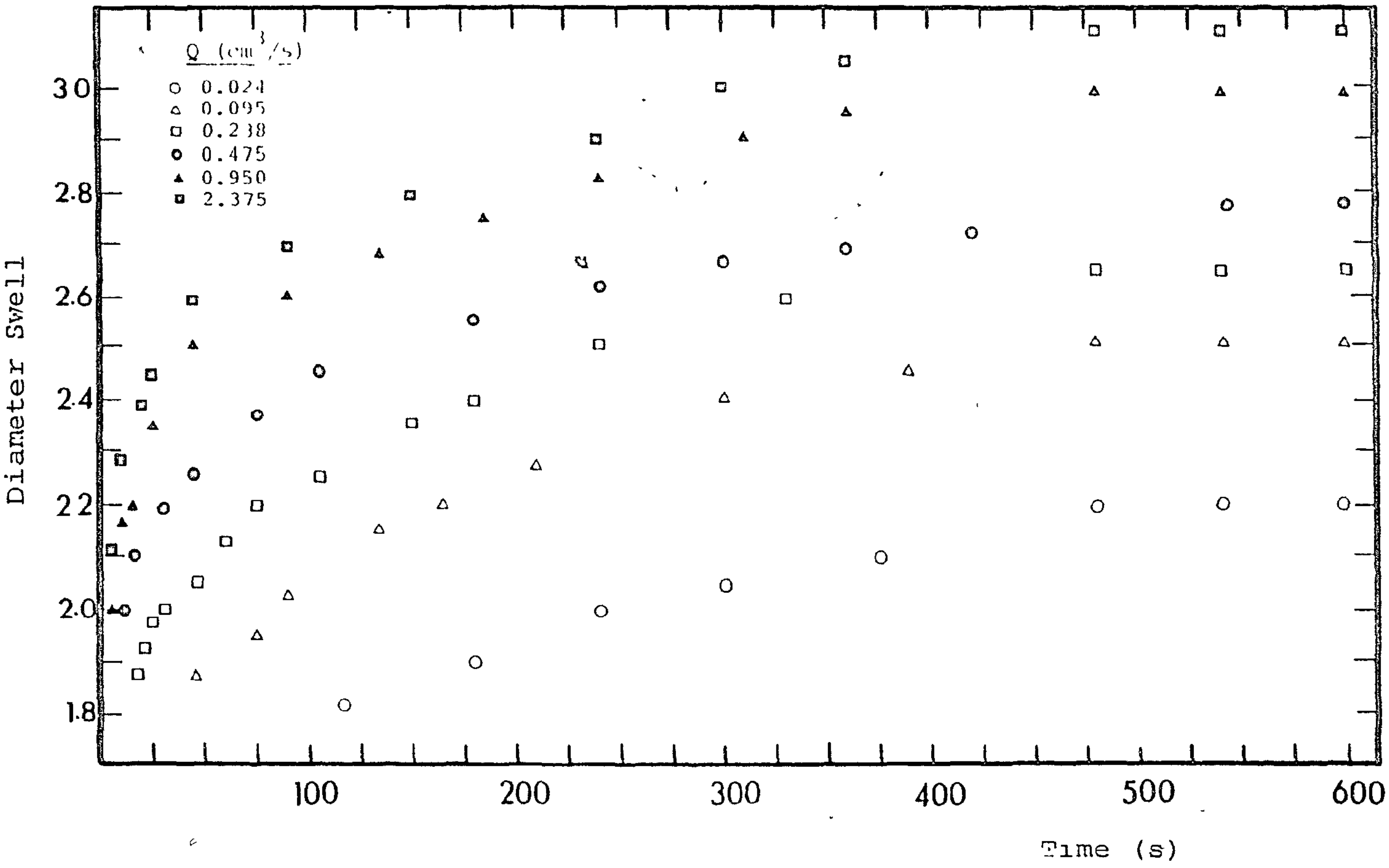

<u>Figure 5.6</u> Diameter Swell as a Function of Time (Resin 27, 10° Converging Die)

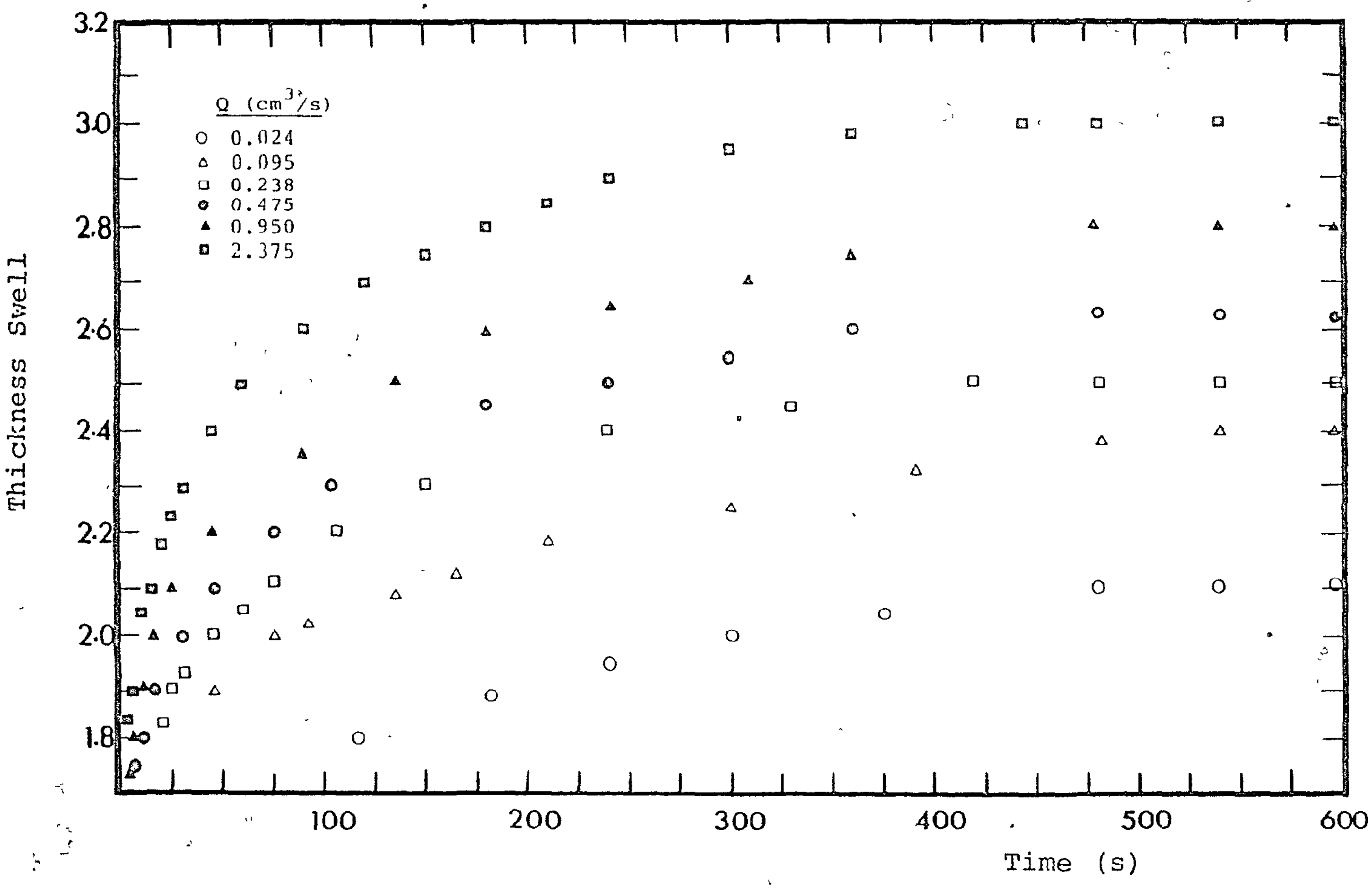

Figure 5.7 Thickness Swell as a Function of Time (Resin 27, 10° Converging Die)

The subscript i can take values of 1 or 2 to denote diameter or thickness swell. This equation was found to fit data reasonably well over the entire time interval, but gave slightly higher values at very short times. Equation 5.3.4 was also applied to the present experimental results and fits the data quite well except in the first few seconds where slightly higher values are predicted. The values of $B_{i\infty}$, B_{io} and ζ_i obtained for some of the data are given in Tables 6.1 and 6.2 of Chapter 6.

The time dependency of post-extrusion swell has also been studied by Cotten (1979) using a rubber compound and a capillary die. A laser beam was used to record the swell. He concluded that almost half of the ultimate swelling occurs in less than 0.2 seconds which is followed by a much slower relaxation to reach the final equilibrium value. The following emprical relation was proposed for the slow recovery region.

$$B = B_\infty(1-kt^{-n}) \qquad 5.3.5$$

where B_∞ is the equilibrium swell and k and n are emprical constants. This equation is similar to the first term of the equation proposed by Garcia-Rejon (equation 5.3.4).

In the present study, no data were obtained at times smaller than 1 second, but it was observed that 60-80% of swell occurs within the first few seconds.

The reproducibility of the experimental results was checked using Resin 29 and the 20° converging die at a volumetric flow rate of 0.950 cm^3/s. Six seperate experiments were done under these conditions, and diameter and thickness swell values were obtained as functions of time. The average and the standard deviation of the data are calculated and are given in Tables 5.1 and 5.2. The reproducibility was deemed to be acceptable.

As was mentioned earlier, diameter and thickness swell values for lower extrusion speeds could not be obtained at short times due to the design of the isothermal oil bath. The number of missing data depended on the extrusion speed. To obtain the short-time data, parisons were extruded directly into air and were monitored for 5 seconds. During this period, nonisothermal effects and drawdown were assumed to be negligible. At higher extrusion rates, data could also be obtained from the isothermal oil bath experiments enabling one to check the consistency of the two methods. This is shown in Figure 5.8, where the diameter swell obtained by extruding directly into air is plotted as a function of time in the short time range for various extrusion velocities. The available data obtained from the isothermal oil bath experiments are also plotted on the same graph. Inspection of this figure show that data obtained by the two methods are

TABLE 5.1 Mean Values and Standard Deviation for Measurements of Diameter Swell (Resin 27, 20° Converging Die, $Q=0.950\ cm^3/s$)

Time (s)	$^*B_1$	Std. Dev.
2	1.82	0.0196
5	1.97	0.0256
7	2.02	0.0176
10	2.12	0.0261
30	2.32	0.0204
60	2.45	0.0147
90	2.51	0.0237
120	2.57	0.0194
150	2.62	0.0160
225	2.71	0.0172
300	2.75	0.0049
360	2.77	0.0052
480	2.81	0.0172
540	2.81	0.0172
600	2.81	0.0172

---

* mean of 6 replicate measurements

TABLE 5.2 Mean Values and Standard Deviation for Meausurements of Thickness Swell (Resin 27, 20° Converging Die, $Q=0.950\ cm^3/s$)

Time (s)	$^*B_2$	Std. Dev.
2	1.22	0.0163
5	1.29	0.0175
7	1.31	0.0207
10	1.34	0.0197
30	1.44	0.0194
60	1.55	0.0163
90	1.63	0.0138
120	1.67	0.0167
150	1.72	0.0223
225	1.79	0.0176
300	1.85	0.0109
360	1.89	0.0049
420	1.92	0.0075
480	1.96	0.0155
540	1.96	0.0155
600	1.96	0.0155

---

* mean of 6 replicate measurements

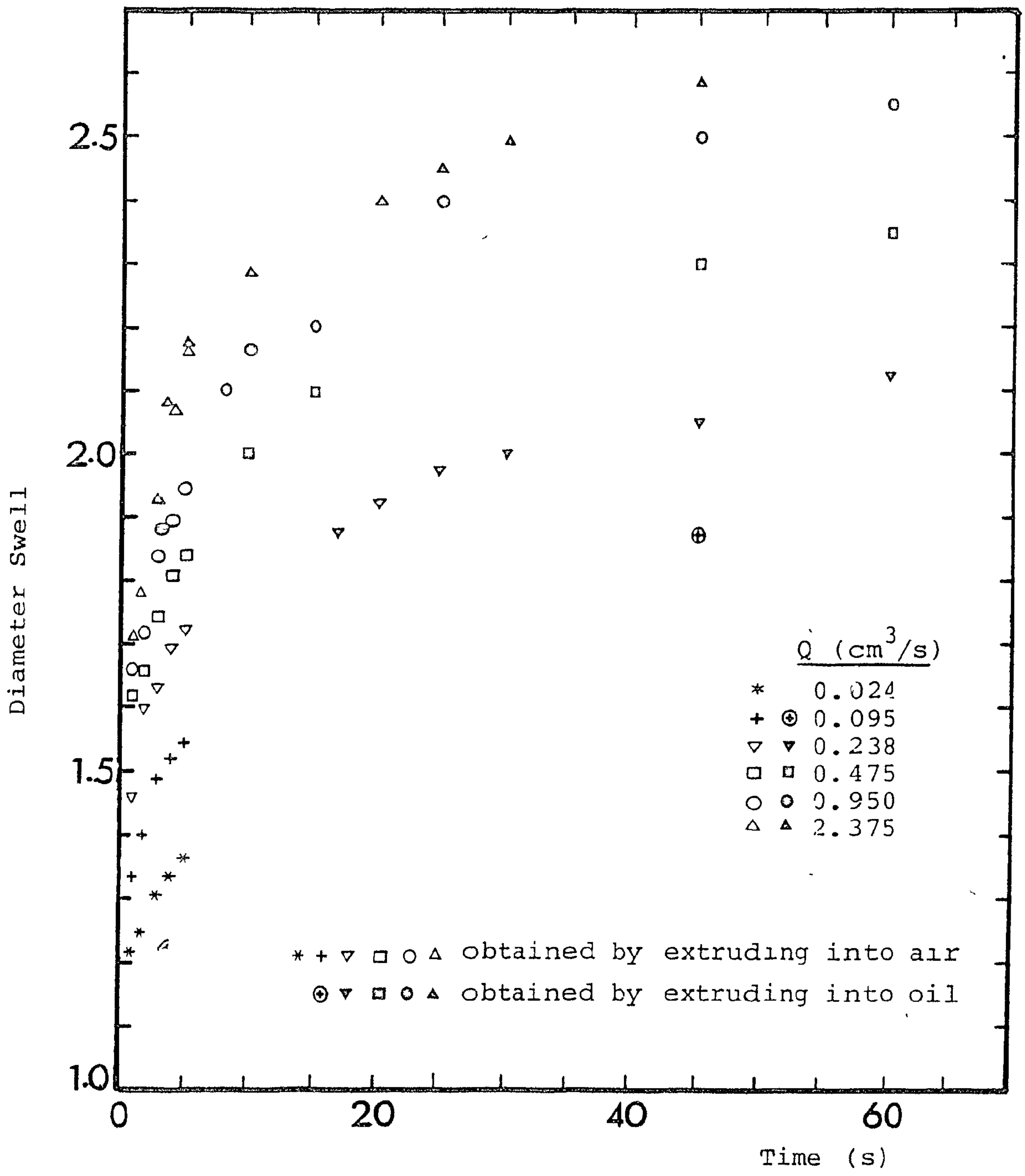

Figure 5. 8 Diameter Swell in the Short Time Region
(Resin 27, 10° Converging Die)

in good agreement. In the cases where very short time data could only be taken by direct extrusion method, the data obtained by this method and data obtained at higher times from regular experiments follow a smooth curve. Thus, we can say that by directly extruding into air, short time data could be taken satisfactorily. However, since the parisons extruded into air were not transparent, thickness swell could not be obtained by this method. Thus short time thickness swell data are available only for those resins extruded at the two highest extrusion velocities.

Inspection of the transient swell results permits some general conclusions to be drawn. It is observed that the exact relation between swell and time depends on the resin and die geometry. In general, diameter swell increases more rapidly in the straight die and in the diverging die than in the two converging dies. Also, in some cases the same equilibrium swell value can be attained but the transient swell functions may be quite different. For example Resins 22A and 29 show the same equilibrium diameter swell values when extruded from the straight die at volumetric flow rates of 0.95 cm^3/s and 2.375 cm^3/s (Tables A3.3 and A3.9) but their transient diameter swell functions are quite different. In other cases, both the transient and equilibrium swell values are the same. This was observed for Resin 27 where practically the same diameter swell function was obtained from the 10° and 20° converging dies at volumetric flow rates of 0.095 cm^3/s and 0.95 cm^3/s (Tables A3.22, A3.31 and A3.24, A3.33).

It is apparent that in order to compeletely characterize the swelling behavior of a resin, both equilibrium and transient data must be available. The extrusion of the parison and the subsequent clamping and blowing in the blow molding process all takes place in a short period of time, so that the material does not have time to swell to its equilibrium value. Therefore, in the blow molding process, it is the transient swell which is of relevance. Equilibrium swell data are useful to study the effects of various parameters such as die geometry, extrusion rate, temperature and so on.

Effect of Die Design

From the structural point of view, die swell can be considered to occur as a result of a disorientation of macromolecules which have been oriented at the die entrance and within the die by the elongational and/or shear fields.

The effect of die geometry on equilibrium diameter and thickness swell for each resin used is shown in Figures 5.9 to 5.14, where equilibrium diameter and thickness swell are plotted as functions of volumetric flow rate. Each data point in these figures represents the constant swell value

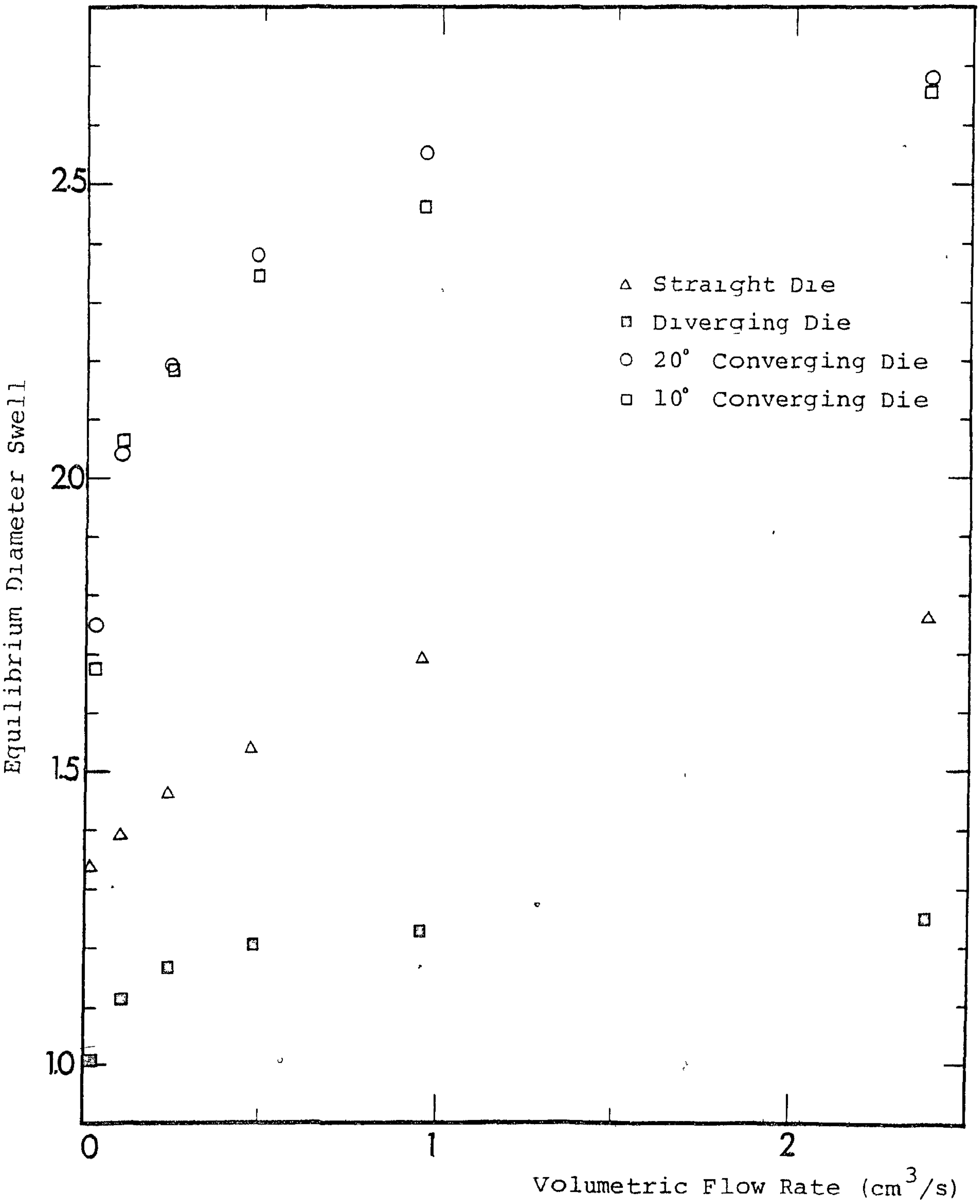

Figure 5.9 Effect of Die Design on Diameter Swell
(Resin 22A)

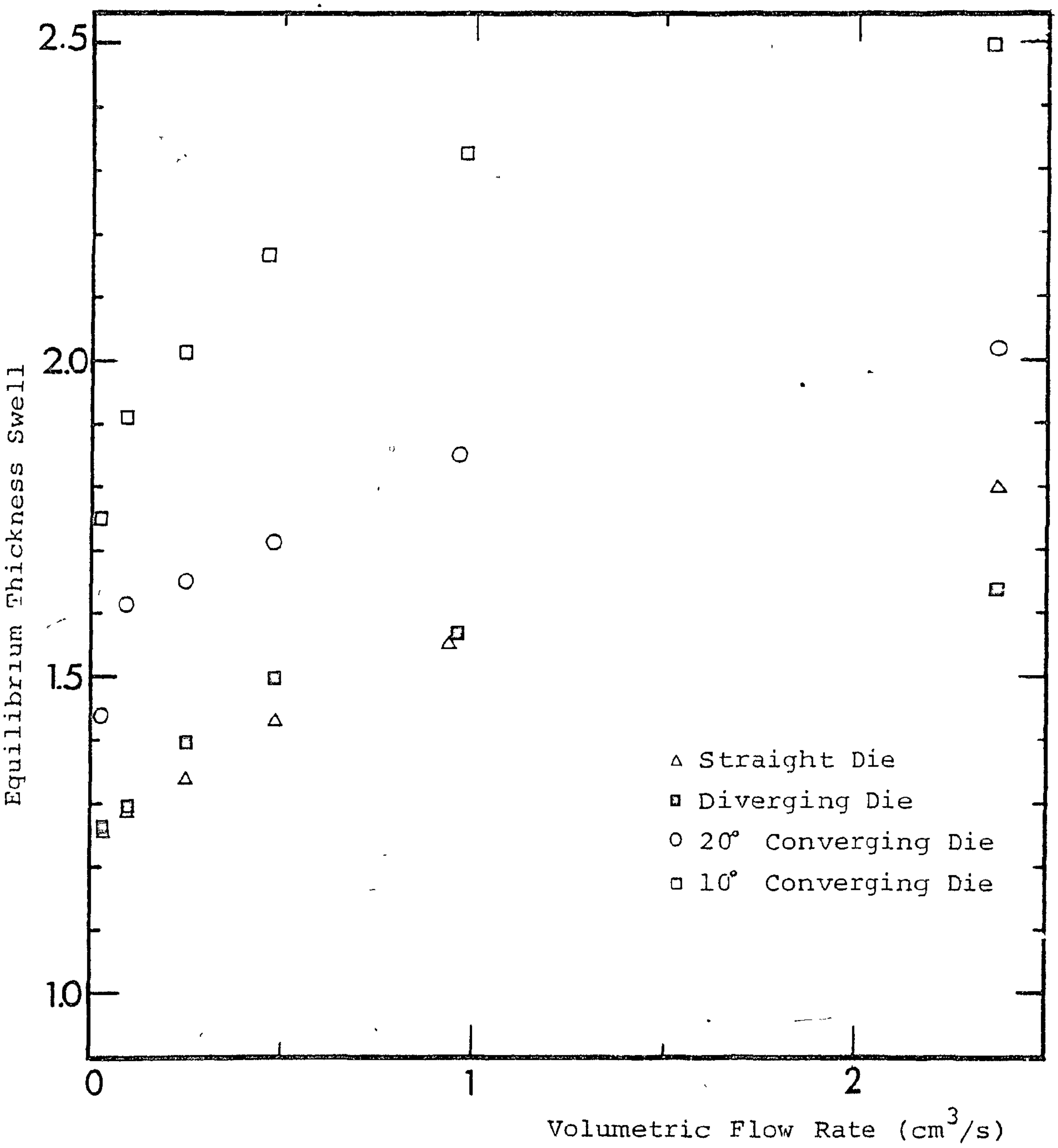

Figure 5.10 Effect of Die Design on Thickness Swell (Resin 22A)

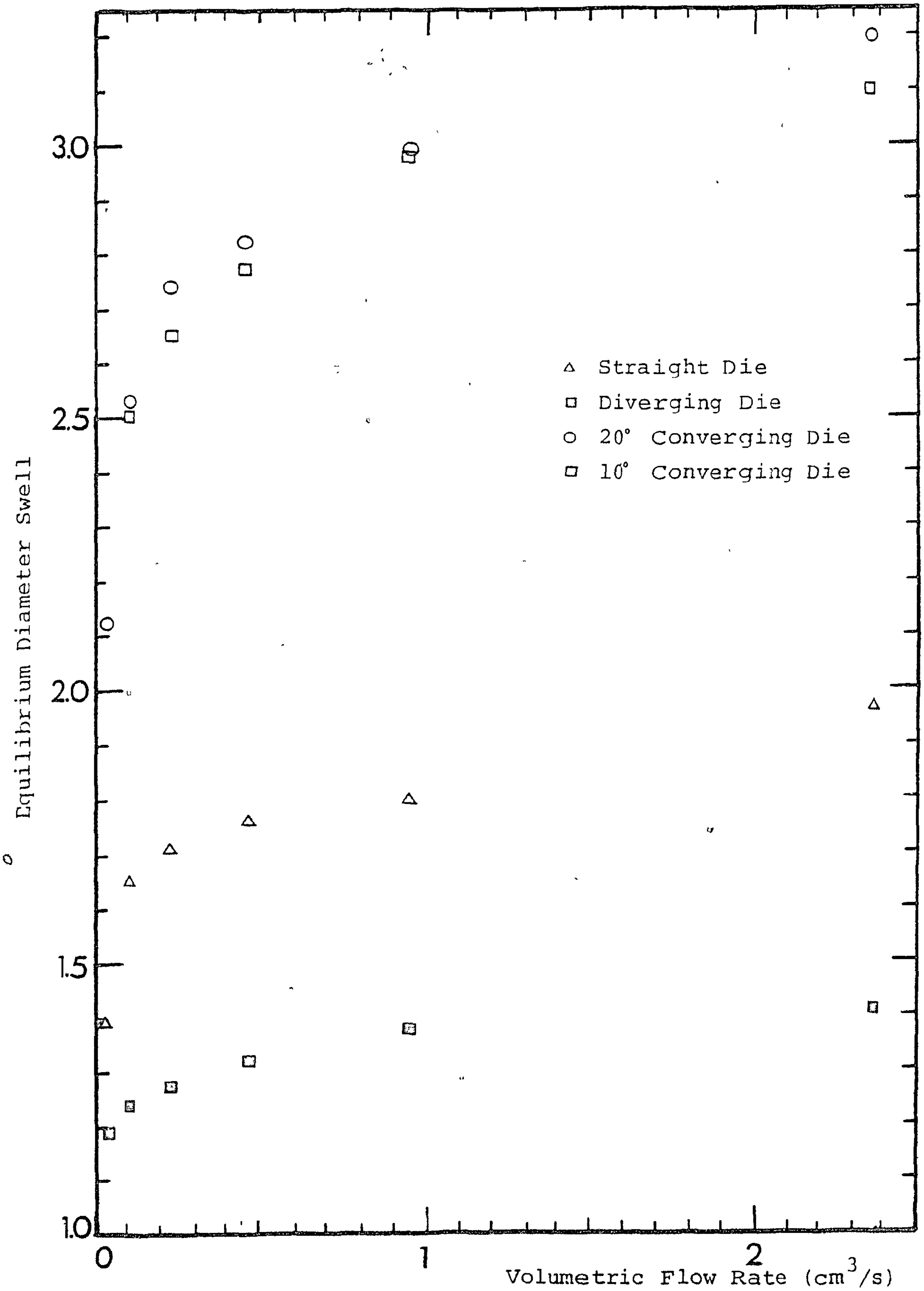

Figure 5.11 Effect of Die Design on Diameter Swell(Resin 27)

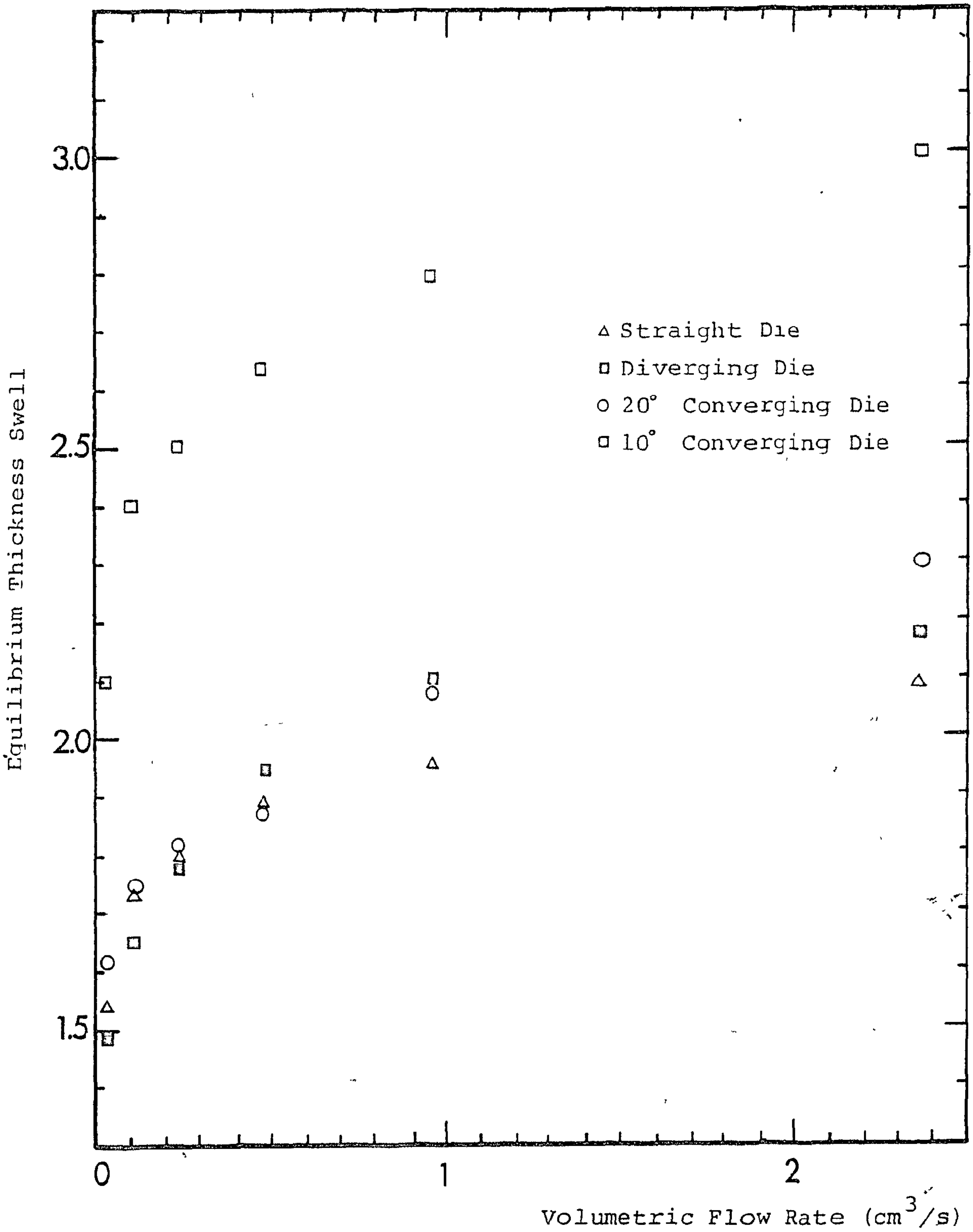

<u>Figure 5.12</u> Effect of Die Design on Thickness Swell
(Resin 27)

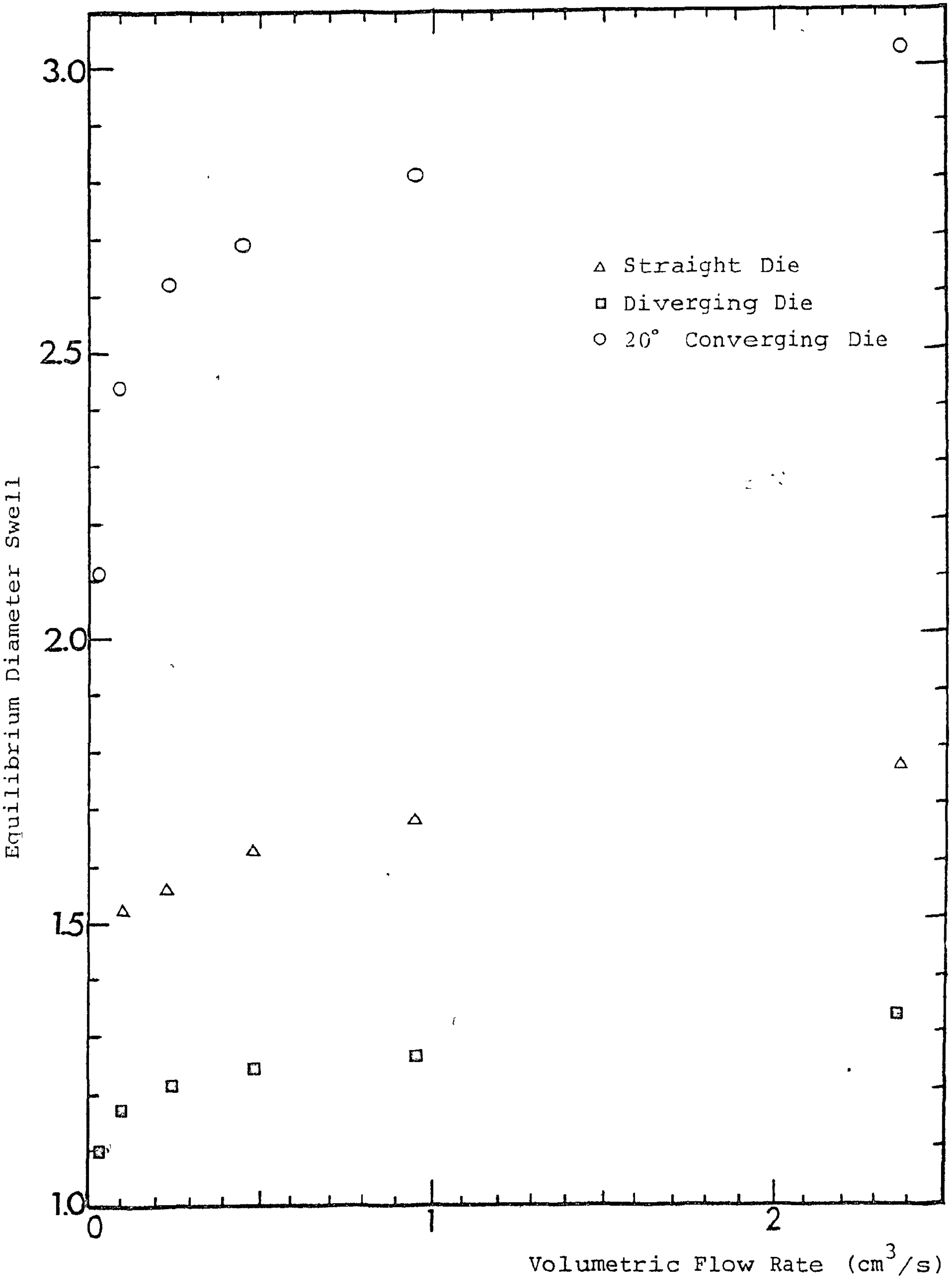

Figure 5.13 Effect of Die Design on Diameter Swell
(Resin 29)

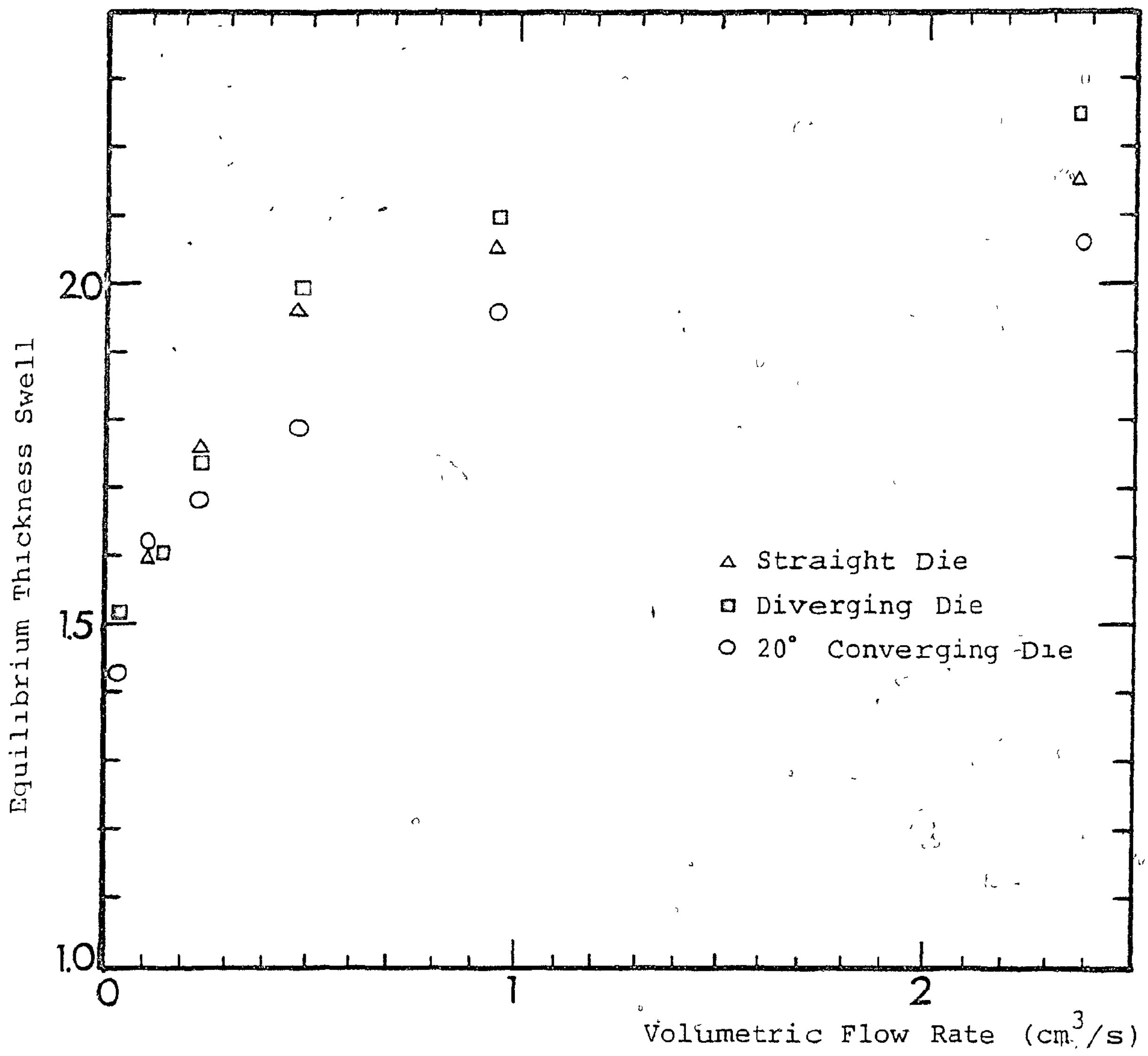

Figure 5.14 Effect of Die Design on Thickness Swell (Resin 29)

obtained from a single experimental run.

The results indicate that for all the resins used, the diverging die gave the lowest equilibrium diameter swell values. Higher diameter swell values were obtained with the straight die than with the diverging die, but the highest diameter swell values were obtained with the 20° converging die. The percent increase in equilibrium diameter swell in going from the diverging die to the straight die and from the straight die to the 20° converging die depends on the resin and extrusion rate, but it can be said that an average increase of 30% is observed between the diverging and the straight die and an average increase of 50-60% is observed between the straight die and the 20° converging die. The results concerning the effect of die geometry on diameter swell are qualitatively in agreement with the results of Wilson et al. (1970). They reported the increase in swell in changing from a diverging die to a straight die or a converging die to be 6% and 30% respectively for the resins and die geometries used in their study (see section 3.2.1)

Experiments with the 10° converging die were carried out with the two resins, Resins 22A and 27. For both of these resins the diameter swell values obtained from the 10° converging die were found to be very similar to the ones obtained from the 20° converging die. As described in section 5.2, the two converging dies had the same outer shell, and the 10° converging die was obtained by replacing the mandrel of the 20° converging die with one having the same dimensions at the exit but converging with an angle of 10°. The results indicate that changing only the mandrel in this manner does not have a strong effect on the diameter swell.

The effect of die design on equilibrium thickness swell is shown in Figures 5.10, 5.12 and 5.14. For Resin 27 and 29, the equilibrium thickness swell values for the straight die, the diverging die and the 20° converging die were found to be quite similar. The extrusion rate dependence of equilibrium thickness swell was different for different dies, but the differences for these three dies were relatively small compared to the differences in diameter swell values. For Resin 22A, the diverging die and the straight die were very similar, and the 20° converging die gave slightly higher values. A considerable change in equilibrium thickness swell values was obtained with the 10° converging die. For the two resins studied with this die (Resins 22A and 27) a significant increase was observed in thickness swell. The 10° converging die has a larger annular gap (3.223 mm) at the entrance than the other dies, and in the converging section the inner and outer walls are not parallel; the outer wall converges with an angle of 20° while the inner wall converges with an angle of 10°. Thus the thickness is reduced to

1.5875 mm at the die exit. This was the only die in which the walls were not parallel and in which the gap decreased along some portion of the die.

The effect of die geometry on transient swell is the same as the effect of die geometry on equilibrium swell (Tables A3.1-33) The diverging die always gave the lowest diameter swell values. For all the resins at the lower extrusion velocities, practically no diameter swell was observed with this die (Tables A3.10-18). The two converging dies gave similar diameter swell values, which were significantly higher than those obtained with the other dies. The thickness swell values from the 10° converging die were substantially higher over the whole time range.

It is apparent from the above discussion that die geometry has a strong influence on the swelling characteristics of the polymers. Different die geometries create different flow fields which tend to orient the molecules of the polymer melt in certain directions. Since swell is a reaction to the orientation imposed during the flow in the die, wherein the molecules tend to regain their random configuration, it follows that polymer melts extruded from different die geometries will show different swelling behavior. To develop a quantitative relation between die swell and die design by consideration of molecular orientation is a very difficult task, since it involves the flow of a viscoelastic fluid in a complex geometry, and such a study is beyond the scope of the present work. As was noted in section 4.2, the attempts to predict die swell from annular dies have been limited to low shear rates due to convergence problems associated with the numerical techniques. Even at such low shear rates these attempts have been mostly unsuccessful. It was mentioned in section 4.2 that Crochet and Keunings (1981) tried to predict diameter and thickness swell resulting from the straight die, the diverging die and the 20° converging die used in the present study. Their predictions are not in agreement with the present experimental results. They predict a higher diameter swell value for the diverging die than the converging die, whereas the reverse was observed experimentally.

If the relation between molecular orientation and die design could be understood, then it would be easier to make a qualitative correlation between die geometry and swell. Recent work by Goettler et al. (1979) shows the effect of die design on orientation. Their work describes a process for extruding short fiber reinforced rubber hose through special die geometries that produce the proper fiber orientation for hose reinforcement. For this purpose, they designed four annular dies. It is observed that the presence of fibers, even nonreinforcing fillers, supresses swell. Therefore in the work by Goettler et al. (1979) the fiber orientation imposed in the die is retained in the parison. The dies used in their study and the resulting fiber orientations are shown in Figure 5.15. In the so callad "conventional die" the combination of the shear forces with the overall reduction in cross sectional area occuring between the head of the extruder and and the die orifice cause the fibers to become aligned parallel to the axis of the extrudate. In the "expanding mandrel die", the channel thickness is constant. When the material is flowing over the expanding section, it is streched circumferentially, resulting in a predominantly hoop orientation. In the extreme case, all the fibers will be oriented in the circumferential direction.

In the obstructed flow die, after flowing over the dam the material expands radially to fill the channel cross section. The fibers consequently turn on end into a position lying essentially across the wall of the hose and in the extreme case the resulting fiber orientation will be as shown in Figure 5.15. The "combination die" is a hybrid design combining the types of flow expansions in the above two dies, and leading to a three-dimensioanal fiber distribution.

It should be emphasized that the fiber orientations shown in Figure 5.15 represent the extreme cases. Actually the degree of fiber orientation depends on various factors such as the response characteristics of the fibers to the flow and the ratio of the area of the outlet annulus of the

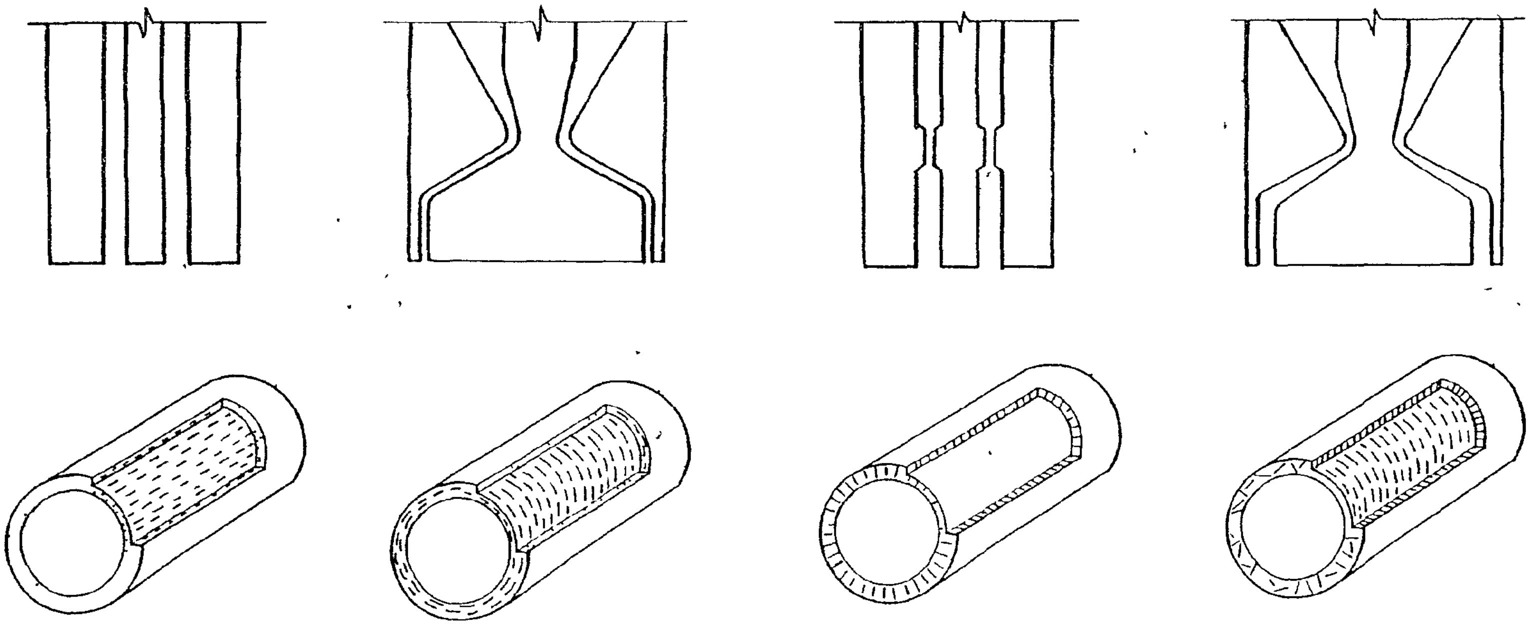

Conventional Die

Expanding Mandrel Die

Obstructed Flow Die

Combination Die

Figure 5.15 Die Geometries and the Resulting Fiber Orientations Obtained by Goettler et al.(1979) die to the minimum area at the point of constriction.

In the present case, the parison swells upon exiting the die, and swell occurs as a reaction to the molecular orientation in which the molecules tend to regain their thermodynamically preferred state, i.e., random configuration. The 20° diverging die of this study resembles the expanding mandrel die used by Goettler et al. (1979). Thus the diverging die is expected to cause a circumferential orientation of polymer molecules within the die. Once the polymer exits the die, to regain their random configuration the molecules will tend to orient mostly in the other two directions, namely the axial and radial directions. Thus a lower diameter swell is expected in this case. Of course, the amount of swell will be determined by the degree and extent of the circumferential orientation achieved in the die. Our experimental results confirm this, since the lowest diameter swell is obtained with the diverging die. In the straight die the molecules will tend to orient in the axial direction thus causing a higher swell than the diverging die. The converging dies will cause further axial orientation since the cross sectional area is reduced constantly along the converging section, and a greater diameter swell is expected. The experimental results confirm this hypothesis.

The 10° converging die gave a distinctively different swell behavior than the other dies. This die was the only one in which the channel thickness changed significantly. Apparently, a decreasing channel thickness enhances thickness swell, since substantially higher thickness swell values were obtained with this die. In the obstructed flow die of Goettler et al. (1979) contrary to the 10° converging die, the channel thickness was <u>increased</u>, and the polymer molecules were oriented in the radial direction. Upon exiting this die, the only directions the molecules can go for random configuration are the circumferential and axial directions. By this argument a lower thickness swell might be expected. However, we have no experimental results to confirm this argument.

Although the above discussion shed some light on our understanding of the effects of die geometry on swell, more experimental work with different die geometries will be neeeded before a general correlation can be developed.

Effect of Resin

The effect of the resin on diameter swell is shown in Figures 5.16, 5.18, 5.20 and 5.22 where equilibrium diameter swell is plotted as a function of volumetric flow rate. The results indicate that with all the die geometries used, Resin 22A gave the lowest diameter swell and Resin 27 the highest. Resin 29 gave intermediate values.

The behavior of different resins in terms of thickness

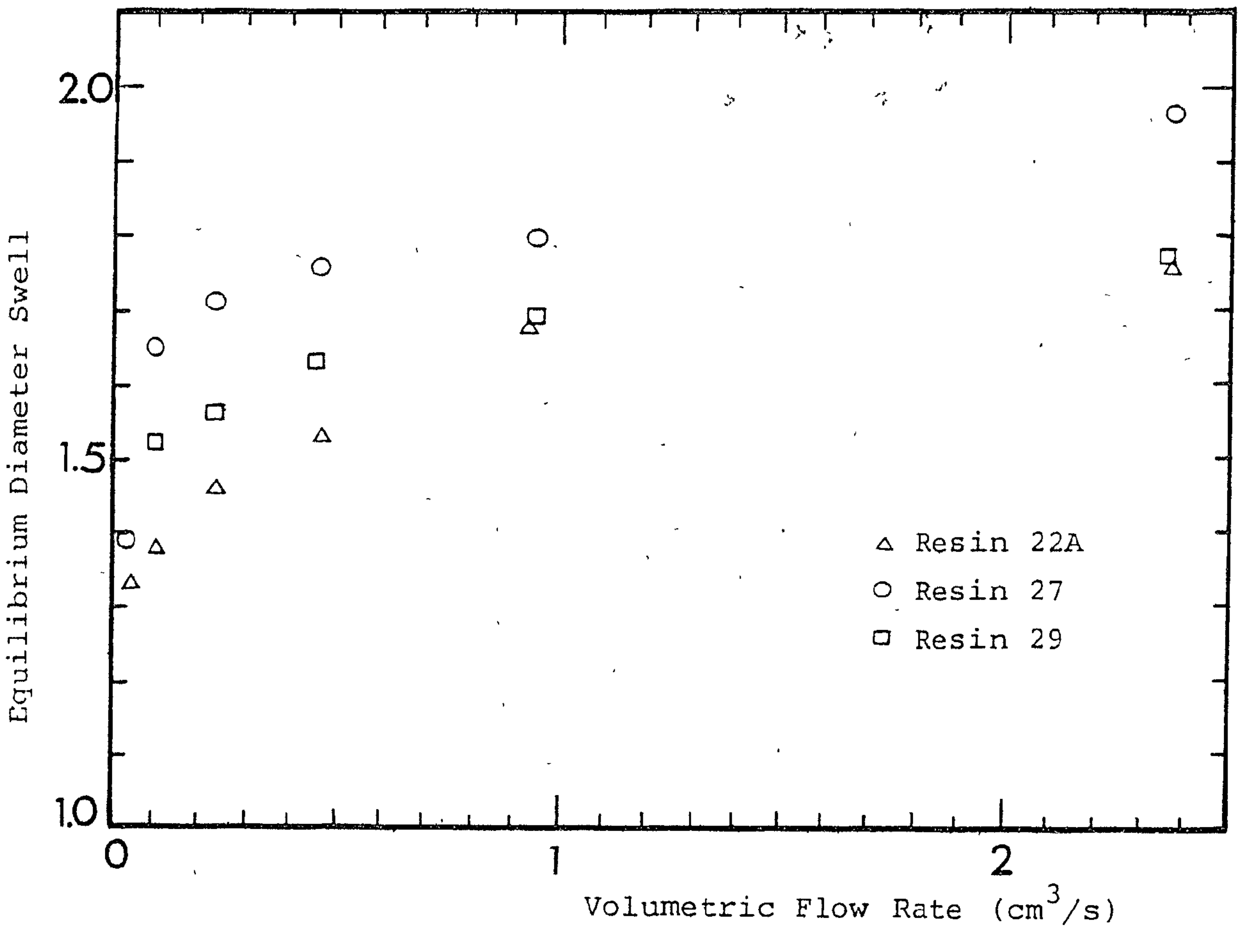

Figure 5.16 Effect of the Resin on Diameter Swell
(Straight Die)

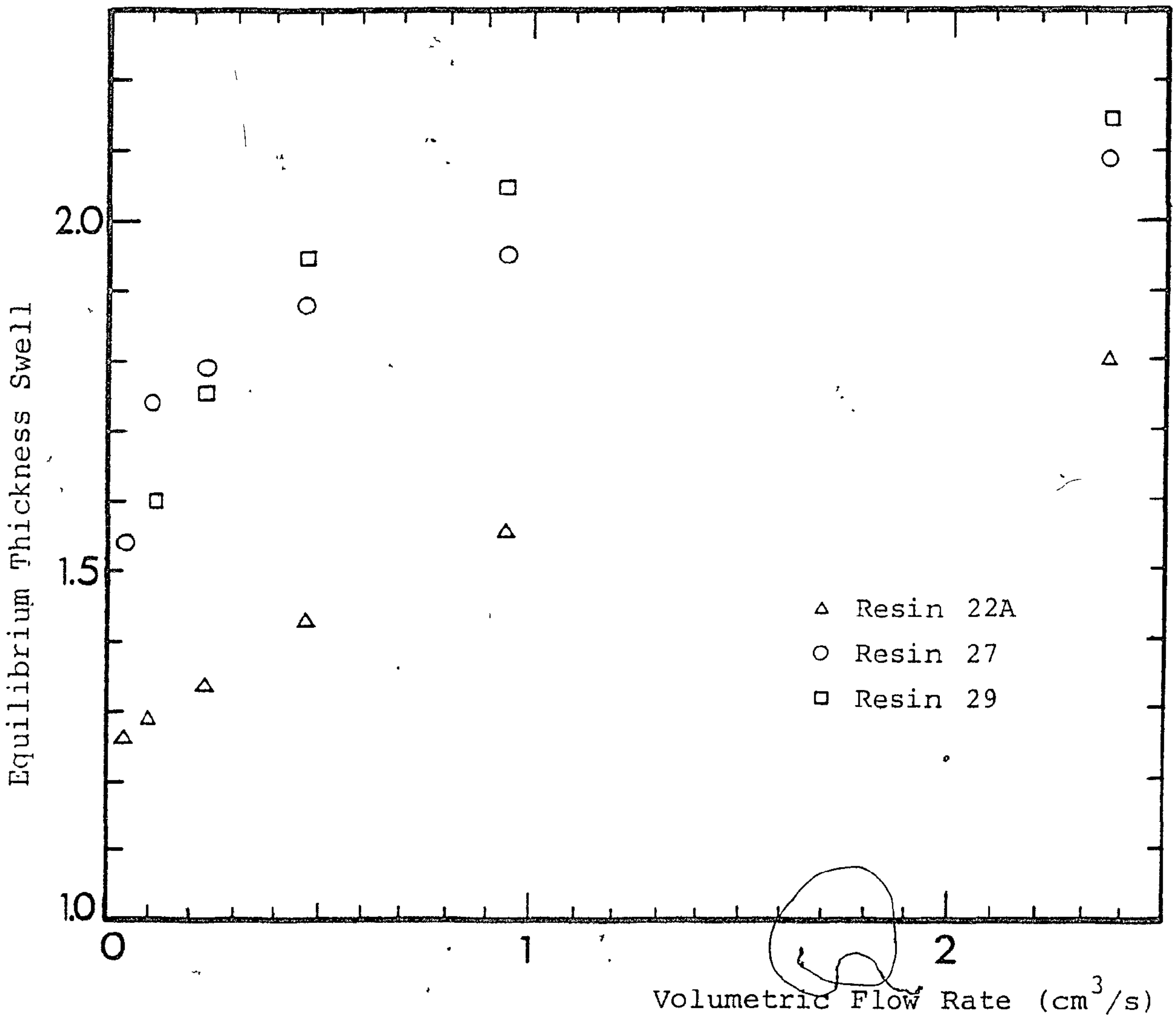

Figure 5.17 Effect of the Resin on Thickness Swell (Straight Die)

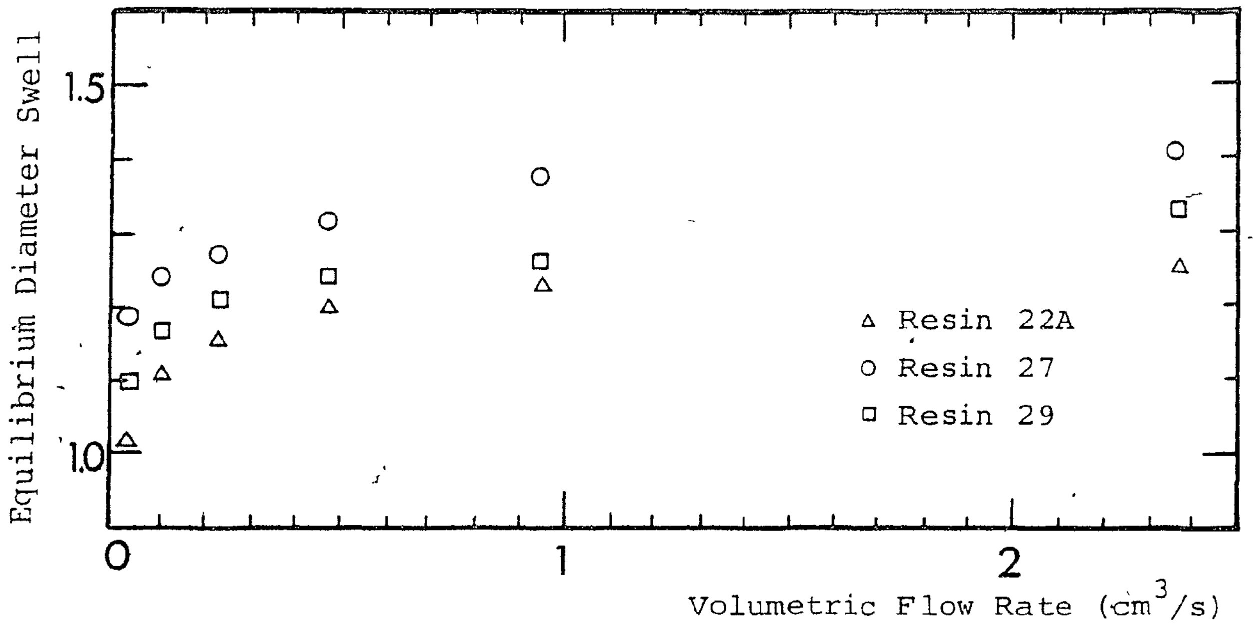

Figure 5.18 Effect of the Resin on Diameter Swell (Diverging Die)

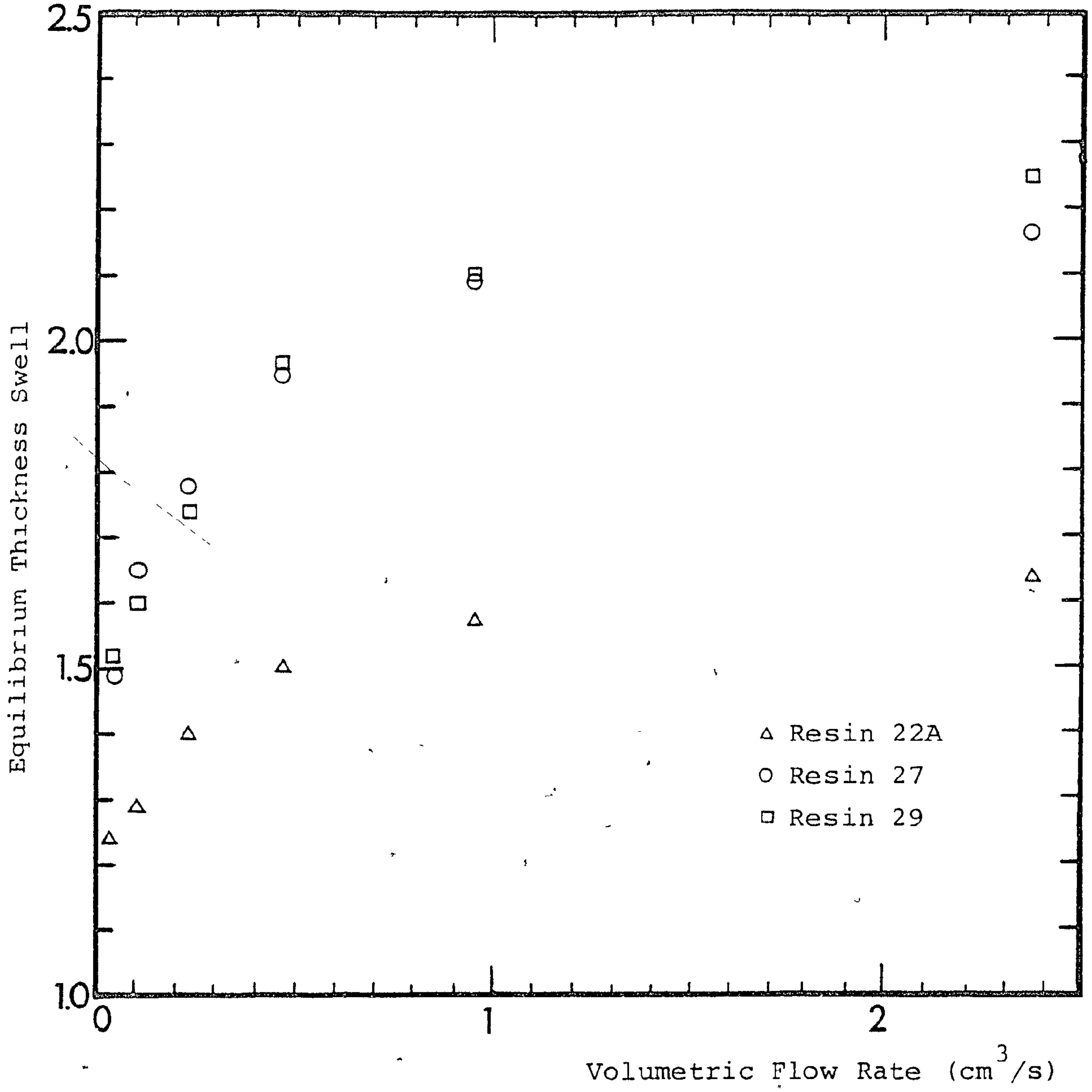

Figure 5.19 Effect of the Resin on Thickness Swell (Diverging Die)

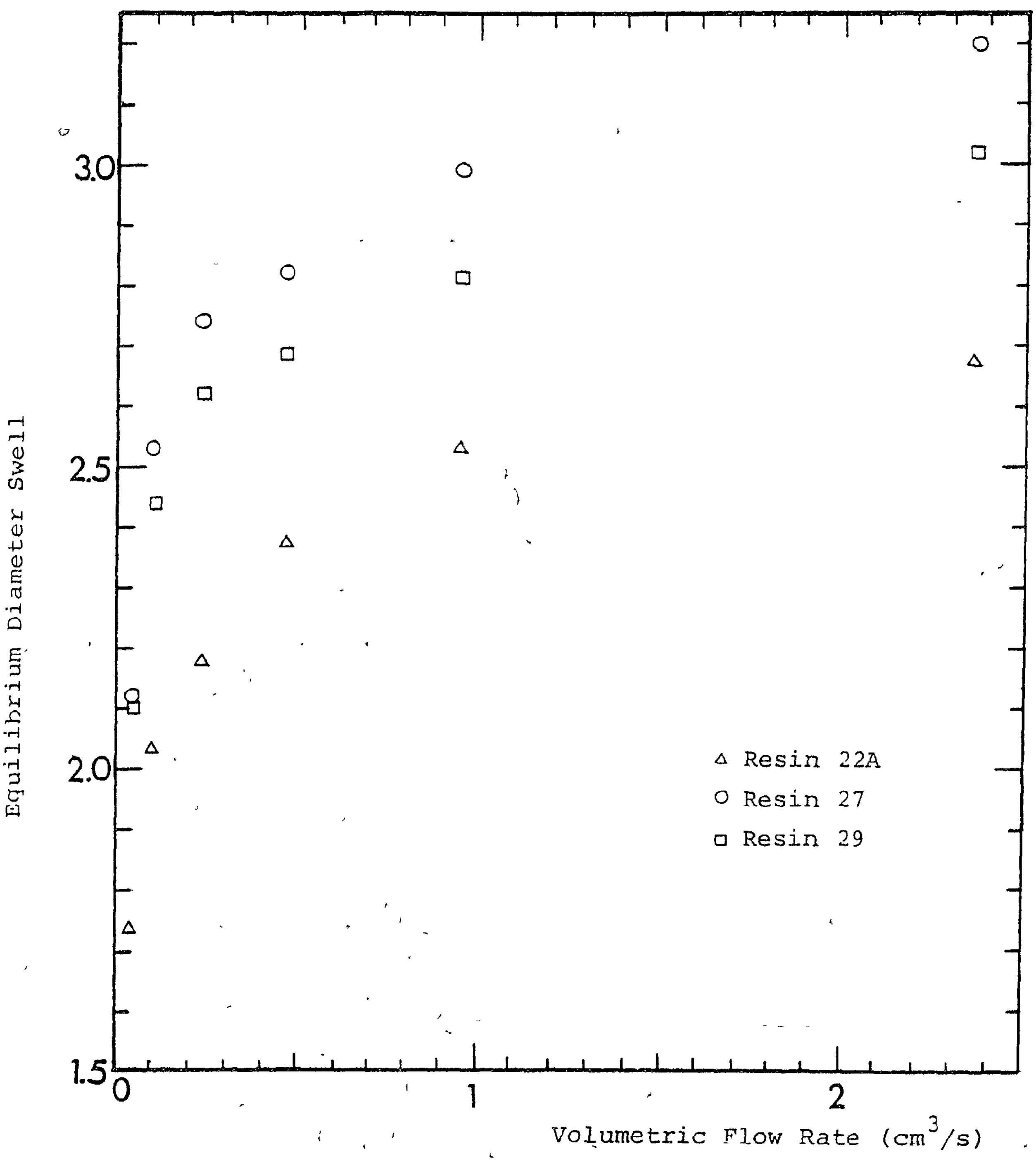

Figure 5.20 Effect of the Resin on Diameter Swell
(20° Converging Die)

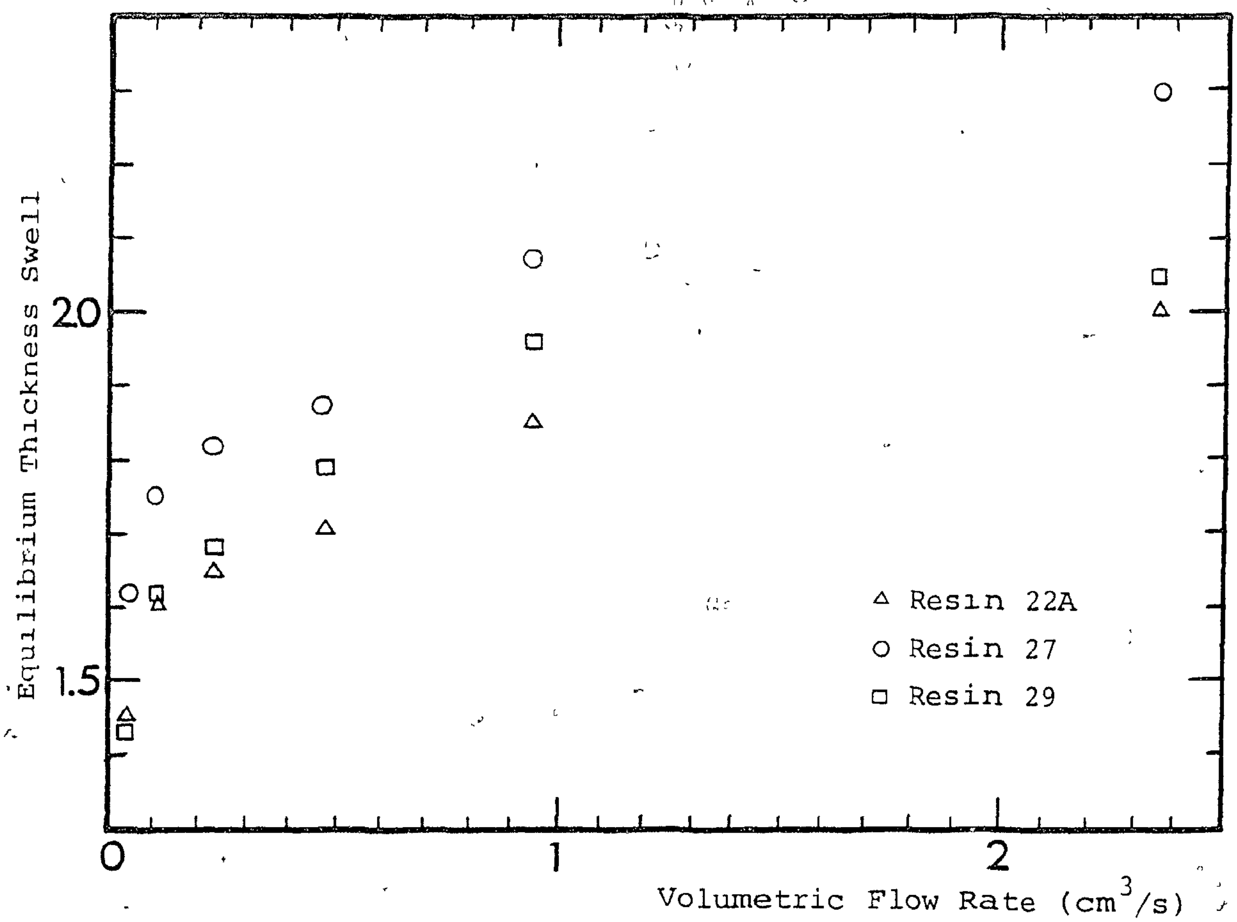

Figure 5.21 Effect of the Resin on Thickness Swell (20° Converging Die)

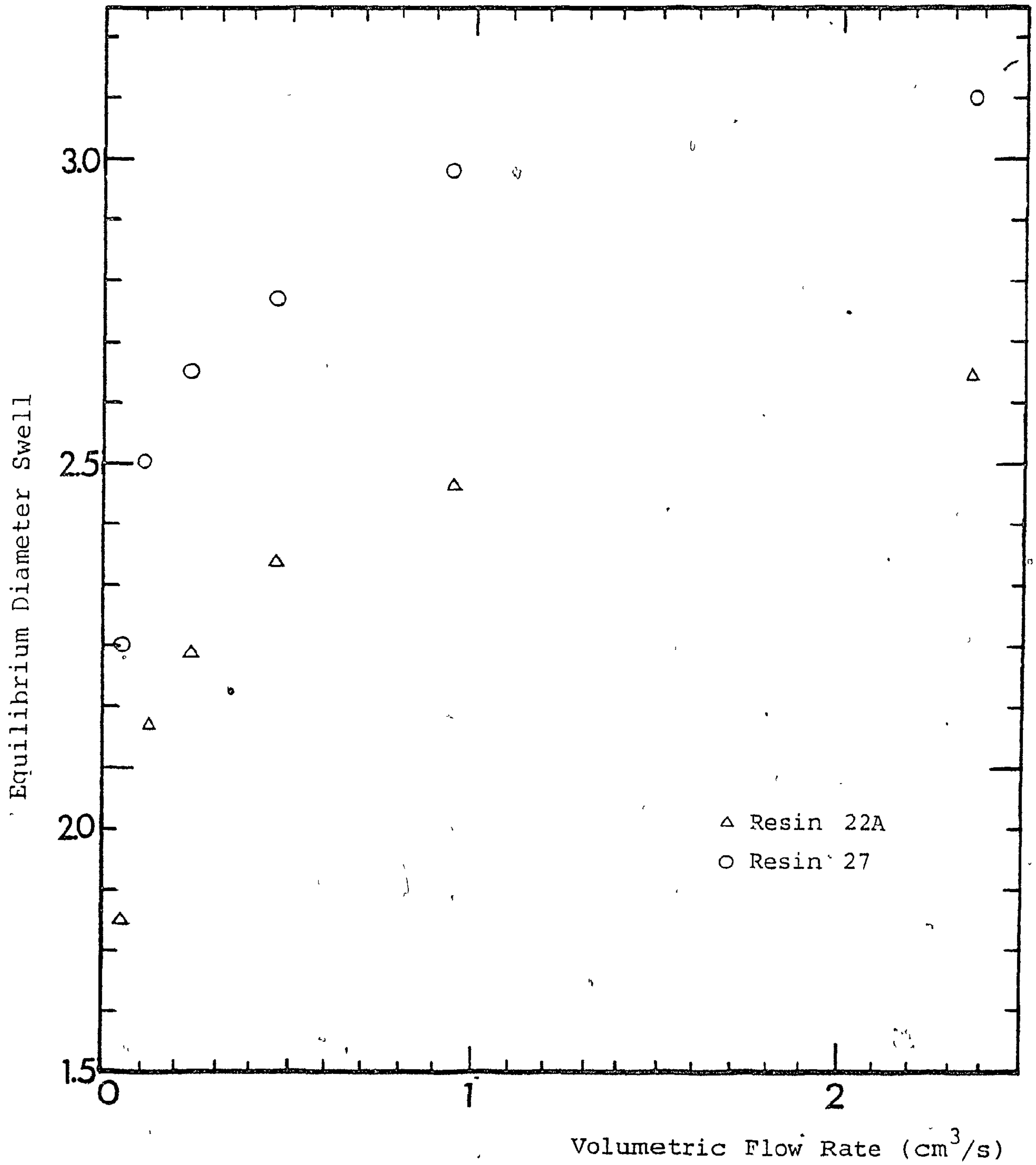

Figure 5.22 Effect of the Resin on Diameter Swell
(10° Converging Die)

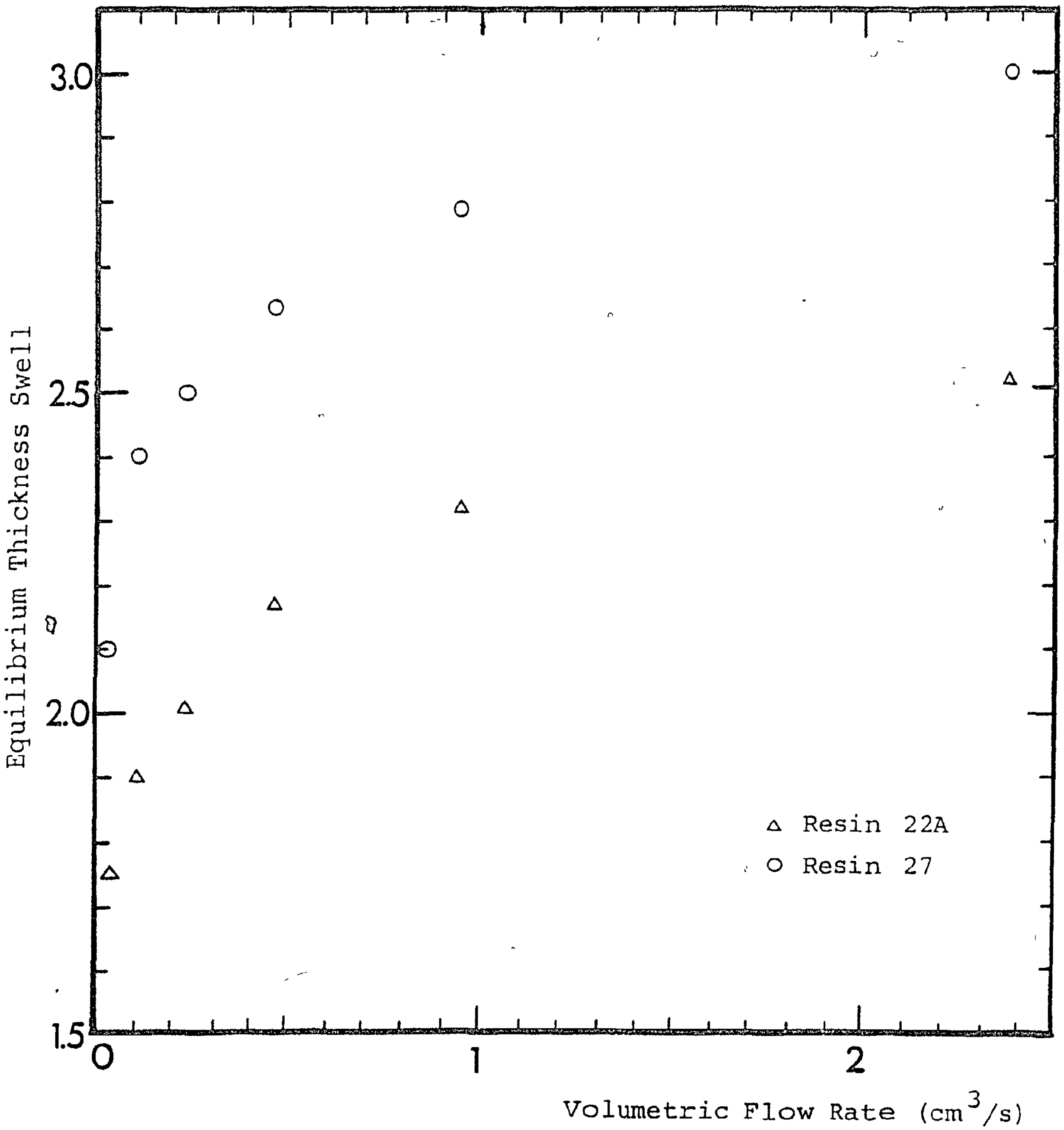

Figure 5.23 Effect of the Resin on Thickness Swell
(10° Converging Die)

swell is shown in Figures 5.17, 5.19, 5.21 and 5.23 where equilibrium thickness swell is plotted as a function of volumetric flow rate. As in the case of the diameter swell, Resin 22A gave the lowest thickness swell values among the three resins. For the diverging and straight die, Resins 27 and 29 gave similar values while for the 20° converging die the highest values were obtained with Resin 27.

The ranking of the resins in terms of the magnitude of diameter swell was found to be the same for all the die geometries and extrusion velocities used in this study. In the case of thickness swell, die design seemed to affect the ranking of the two resins (Resin 27 and 29) slightly.

The results indicate that Resin 22A has the lowest diameter and thickness swell for all the dies and extrusion rates. This resin has the highest weight average molecular weight and the polydispersity index of the three resins. In the literature contradictory results are given as to the effect of weight average molecular weight and molecular weight distribution on swell. This was reviewed in section 3.3. The present results are in agreement with the results of Mendelson and Finger (1975). They observed that capillary die swell for HDPE decreased with increasing $\bar{M}_w$ and MWD.

Effect of extrusion velocity

Previous work carried on swell indicate that as extrusion rate increases swell increases. Our experimental results are in agreement with this general observation. Using shear rate at the wall as a measure of extrusion rate has been the general custom. However, due to the difficulties associated with calculating the shear rate at the wall in the complex die geometries used in the present study, we used volumetric flow rate as a measure of extrusion rate.

Both the transient and equilibrium swell values obtained in this study are increasing functions of volumetric flow rate. This can be seen in Figures 5.6, 5.7, 5.9-5.14 and 5.16-5.23. These figures indicate that the exact relation between swell and extrusion velocity depends on the resin and the die geometry.

Effect of temperature

It is generally believed that the higher the temperature the lower the swelling, all other variables remaining the same. By considering that at constant shear rate the viscosity decreases with increasing temperature, an explanation can be suggested for the temperature effect on extrudate swell. Simply stated, this is that the lower the viscosity the lower the flow resistance of the material and consequently lower the stress and associated elastic strain that results from flow within the die.

In the present study, experiments were usually carried out at 170 °C . However, to see the effect of temperature on die swell Resin 27 was also extruded at 150 °C and 190 °C through the diverging die. The equilibrium diameter and thickness swell values at these three temperatures (150 °C, 170 °C, 190 °C) are listed in Table 5.3. These results indicate that under the present experimental conditions, die swell is not a strong function of temperature. This may be due to viscous heating which is inevitable in the processing of high viscosity polymers. At lower temperatures, the viscosity is increased causing a higher swell. However this can be counterbalanced by the enhanced viscous heating owing to higher viscosities. To calculate quantitatively the viscous heating of a viscoelastic material flowing in a die of complex geometry is a difficult task and it is beyond the scope of the present work. Similar results regarding the effect of temperature are reported by various researchers (Dutta and Ryan, 1982).

TABLE 5.3 Effect of Temperature on Swell

(Resin 27, Diverging Die)

Q (cm^3/s)	B_1		
	T = 150 °C	T = 170 °C	T = 190°C
0.095	1.24	1.24	1.21
0.475	1.38	1.32	1.32
2.375	1.55	1.41	1.40

Q (cm^3/s)	B_2		
	T = 150 °C	T = 170 °C	T = 190°C
0.095	1.69	1.65	1.70
0.475	1.91	1.94	1.93
2.375	2.35	2.17	2.13

Relation between diameter and thickness swell

For Resins 27 and 29 the equilibrium thickness swell was greater than the equilibrium diameter swell for all extrusion rates when the straight die was employed. This was also true for Resin 22A at the highest extrusion rate. For other extrusion rates the reverse was the case. With the diverging die all resins gave higher equilibrium thickness swell values than diameter swell. In the case of the two converging dies, equilibrium diameter swell was always greater than equilibrium thickness swell. The relation between diameter and thickness swells has been studied by several researchers. As was mentioned in section 3.2.1, Henze and Wu (1973) attempted to relate diameter swell ratio, B_1, to the weight swell ratio, B_W. The following relation was proposed:

$$B_1 = B_W^a \qquad 5.3.6$$

The exponent "a" in this equation is an indication of the anisotropy of deformation. In the isotropic case, when the deformation in the radial and circumferential directions is the same, $B_1 = B_2$, and "a" is equal to 0.5. For the 30° diverging die used by Henze and Wu (1973) the value of "a" was found to be 0.25, indicating that the swelling was anisotropic with this die.

Garcia-Rejon (1979) used a similar equation to that proposed by Henze and Wu (1973) to relate the diameter and thickness swell:

$$B_1 = A\, B_w^a = A\, (B_1 B_2)^a \qquad 5.3.7$$

where the second equality is obtained using equation 5.3.3 in which the annular die is approximated as a slit. With the straight annular die used in that study regression analysis gave for the HDPE resins:

$$B_w = 0.66 B_1^{2.56} \qquad 5.3.8$$

This result indicates anisotropic swelling behavior, but Garcia-Rejon's results were closer to the isotropic behavior than the results obtained with the 30° diverging die by Henze and Wu (1973).

Figures 5.24-5.27 are plots of diameter swell versus weight swell obtained in the present study for different die geometries. Each point in these figures corresponds to a specific volumetric flow rate. The weight swell values were obtained from the following relation which is valid for isothermal extrusion and for the cases where the slit approximation is applicable.

$$B_W = B_A = B_1 B_2 \qquad 5.3.9$$

Bernhardt (1959) suggests that for values of $D_o/D_i<3$, the slit approximation is a reasonable one. For the straight and diverging dies, at the exit $D_o/D_i = 1.33$, and for the two converging dies the ratio of D_o/D_i at the exit is equal to 2. Also, all the experiments were carried out under isothermal conditions, therefore the use of equation 5.3.9 is justified.

The solid lines in Figures 5.24-5.27 denote the isotropic case. It can be seen that the straight die and the 10° converging die are closer to the isotropic case than the diverging and the 20° converging die. The dotted line in Figure 5.25 represents the data obtained from the 30° diverging die of Henze and Wu (1973). The data obtained from the 20° diverging die of this study fall close to this line.

Garcia-Rejon (1979) reported that all the data obtained from three different HDPE's fell on a single curve when B_1 was plotted versus B_W. In the present work, the behavior of the three resins were similar but not identical.

The values of parameters A and a of equation 5.3.7 were calculated for each resin and die geometry by regression analysis and are listed in Table 5.4. The isotropic case is represented by A = 1 and a = 0.5.

One of the resins used in the present study, Resin 27 was also used by Garcia-Rejon (1979). As was described in

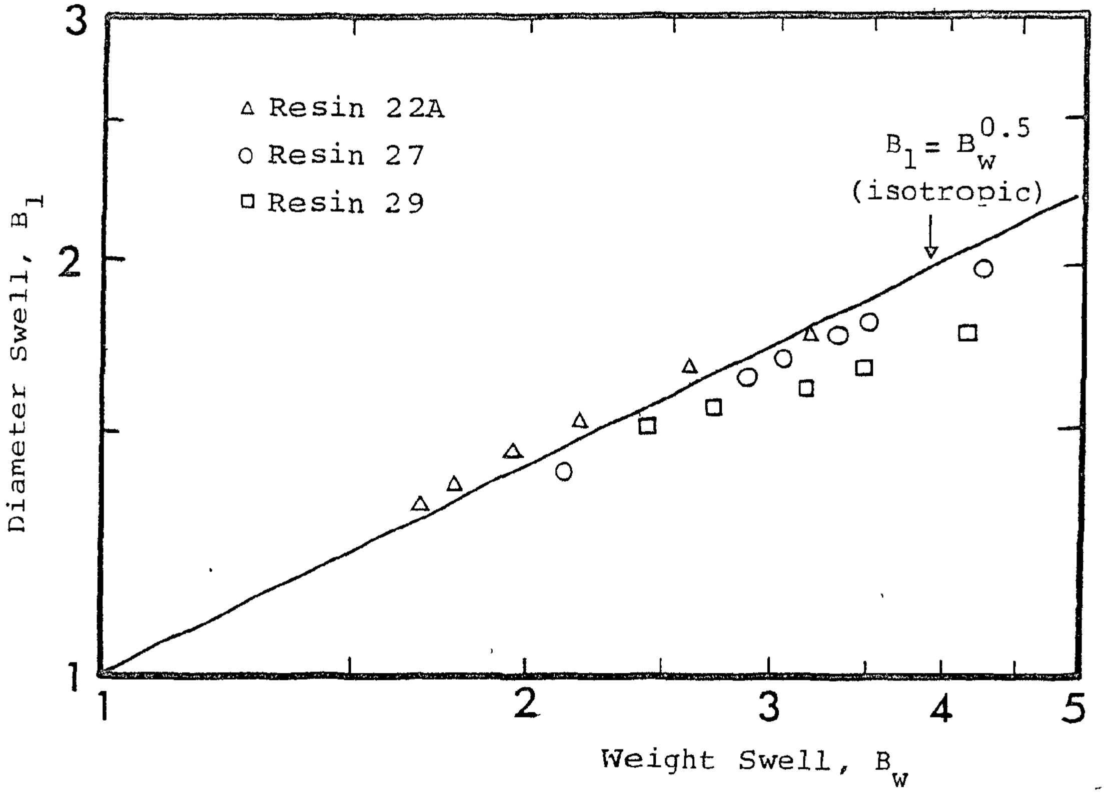

Figure 5.24 Comparison Between Diameter and Weight Swells (Straight Die)

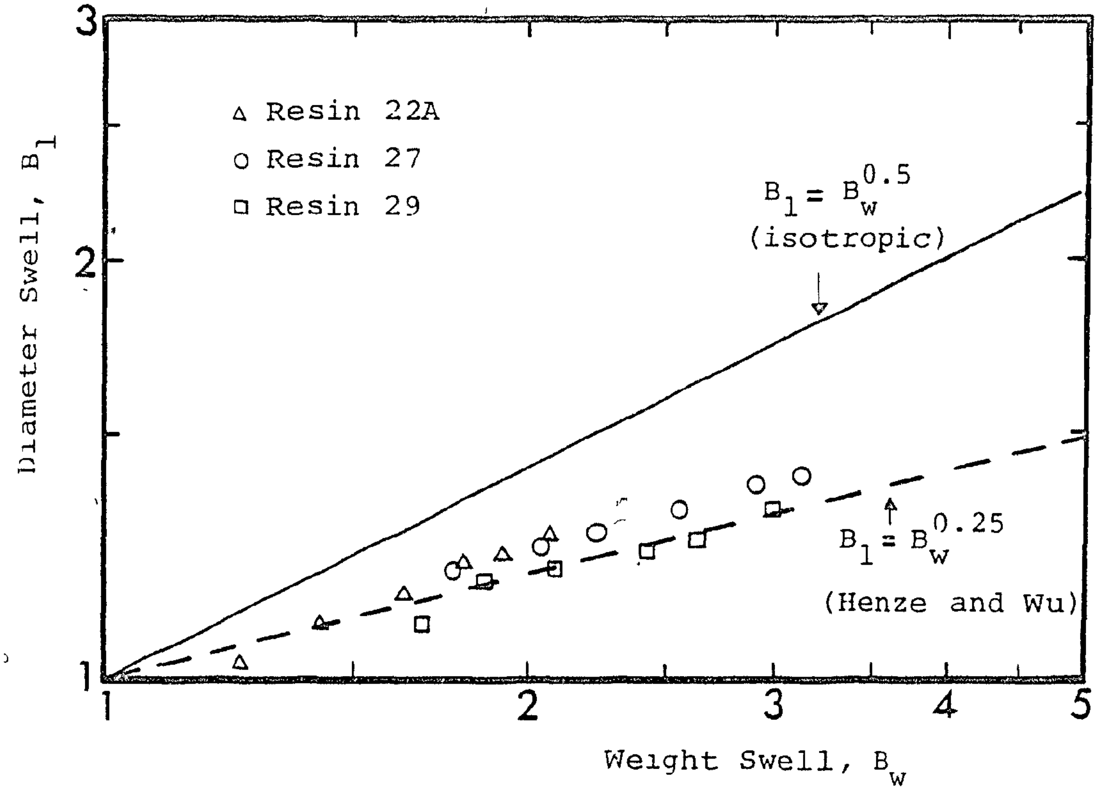

Figure 5.25 Comparison Between Diameter and Weight Swells (Diverging Die)

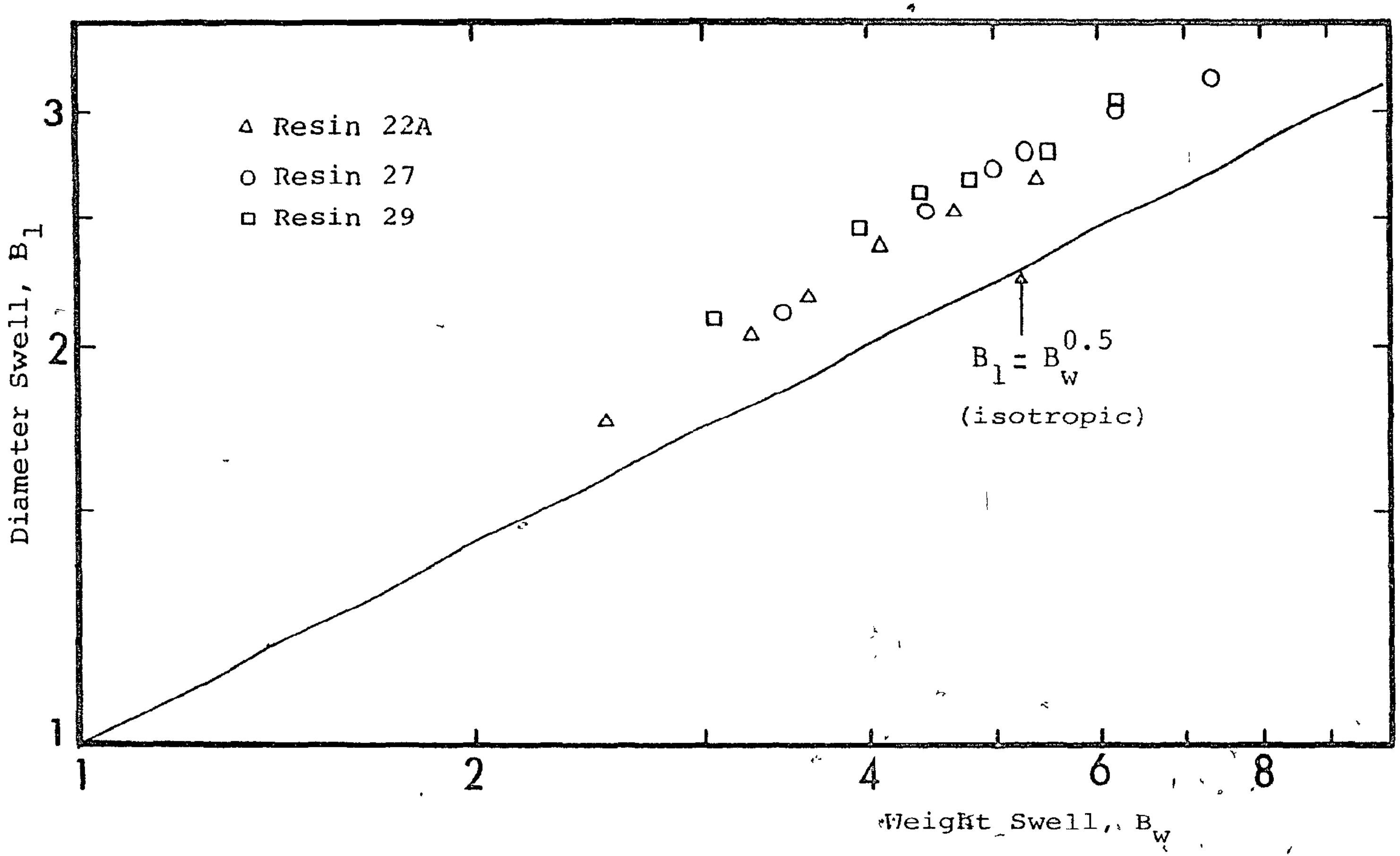

Figure 5.26 Comparison Between Diameter and Weight Swells (20° Converging Die)

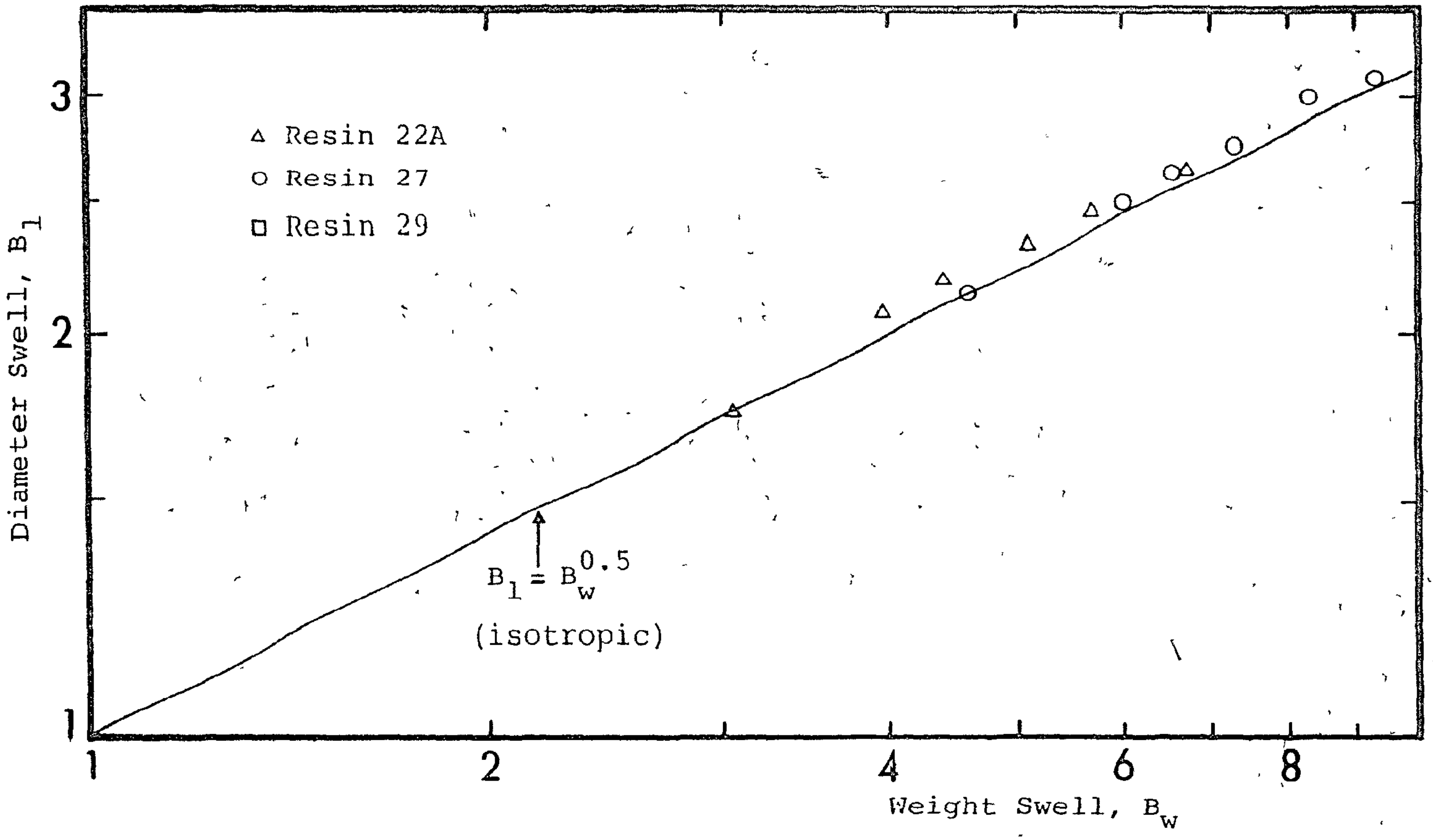

Figure 5.27 Comparison Between Diameter and Weight Swells (10° Converging Die)

section 3.2.1, he used the same method as in the present study to study the swell of extrudate from a straight annular die. The straight die used by Garcia-Rejon has dimensions different from those of the straight die used in this study, but the ratio of the outer diameter to the inner diameter is the same for both dies. In the case of capillary dies, it has been found experimentally that once the capillary is long enough (L/D>30) so that the entrance effects are eliminated, swell becomes independent of the dimensions of the die and depends on the shear rate in the die.

The shear rate at the wall for the straight die was calculated assuming that the annulus can be approximated as a slit. The shear rate at the wall is given by the following relations:

$$\dot{\gamma}_W = ((2+b)/3)\dot{\gamma}_A \tag{5.3.10}$$

$$\dot{\gamma}_A = 6Q/\pi(R_o+R_i)(R_o-R_i)^2 \tag{5.3.11}$$

$$b = d\log \dot{\gamma}_A / d\log \tau_W \tag{5.3.12}$$

Since the annular gap in the present die was less than Garcia-Rejon's die, data obtained in the present study correspond to lower extrusion rates. Figure 5.28 shows the equilibrium area swell $(B_1B_2)_\infty$ values obtained from the

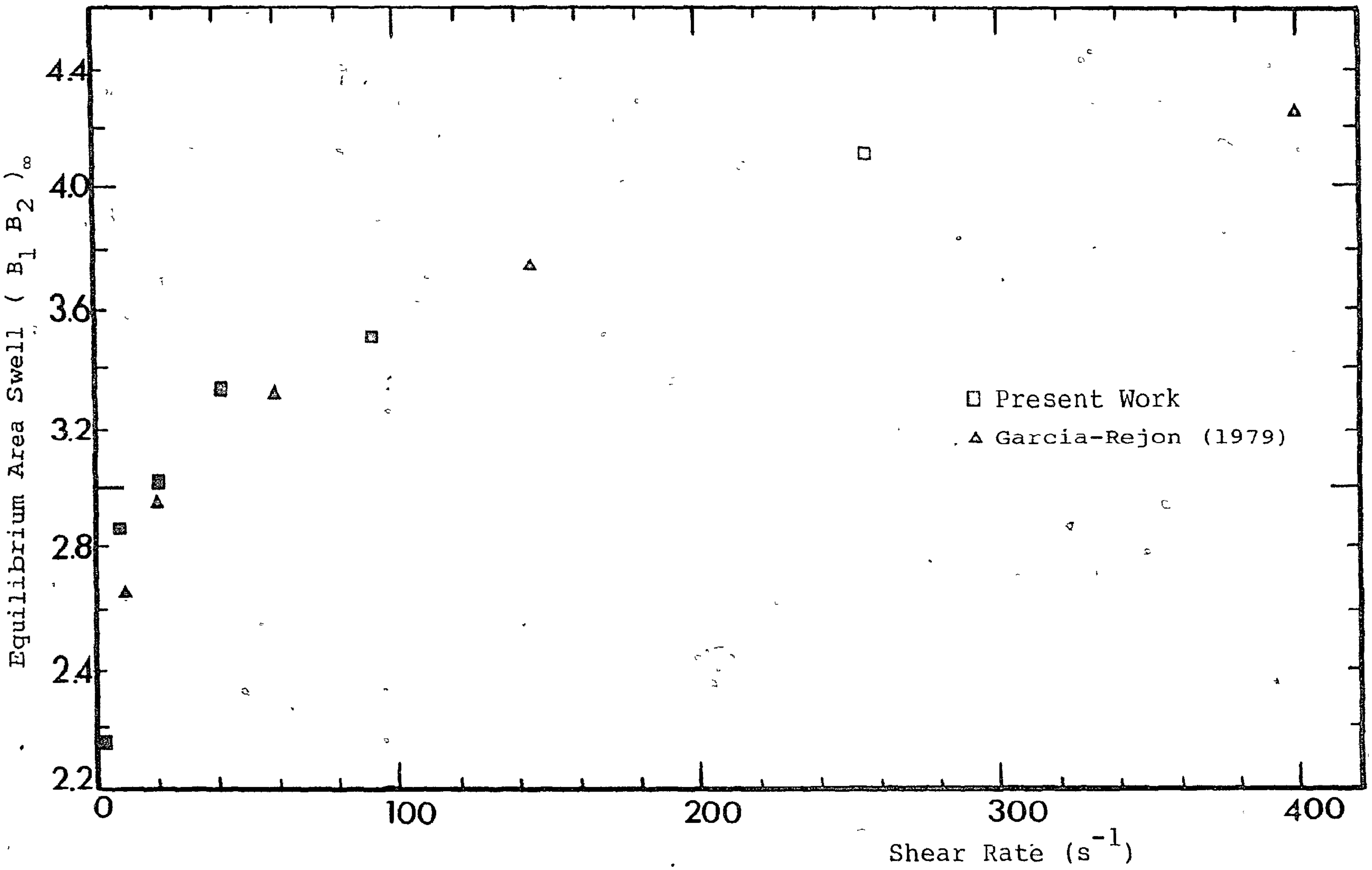

Figure 5.28 Comparison of Area Swell Obtained from two Geometrically Similar Straight Annular Dies

TABLE 5.4 Parameters "a" and "A" of Equation 5.3.7

	Straigth	20° Diverging	20° Converging	10° Converging
Resin 22A	a = 0.44	a = 0.40	a = 0.58	a = 0.52
	A = 1.07	A = 0.95	A = 1.03	A = 1.00
Resin 27	a = 0.52	a = 0.31	a = 0.53	a = 0.50
	A = 0.94	A = 0.99	A = 1.13	A = 1.02
Resin 29	a = 0.29	a = 0.29	a = 0.48	–
	A = 1.17	A = 0.96	A = 1.25	–

present work and from the work of Garcia-Rejon as functions of wall shear rate. The curves from the two studies are quite similar, although individual diameter and thickness swell values were different.

In summary knowledge of transient and equilibrium swell is necessary to characterize the swelling properties of a resin. Also, the diameter swell and thickness swell act quite independently from each other, and their interrelation depends on the die design and the resin used.

5.4 Combined effects of sag and swell

In these experiments the combined effect of sag and swell was studied under isothermal conditions using the experimental technique developed by Dealy and Garcia-Rejon (1980). This type of experiment resembles more closely the parison formation stage in the actual blow molding process.

5.4.1 Experimental Apparatus

The same experimental set up that was used in the pure swell experiments was employed in the sag and swell experiments with the exception of the thermostating chamber which was replaced by an isothermal air oven.

The oven is shown in Figure 5.29. It has a rectangular shape (25*30*20 cm^3) with exterior walls made of wood and

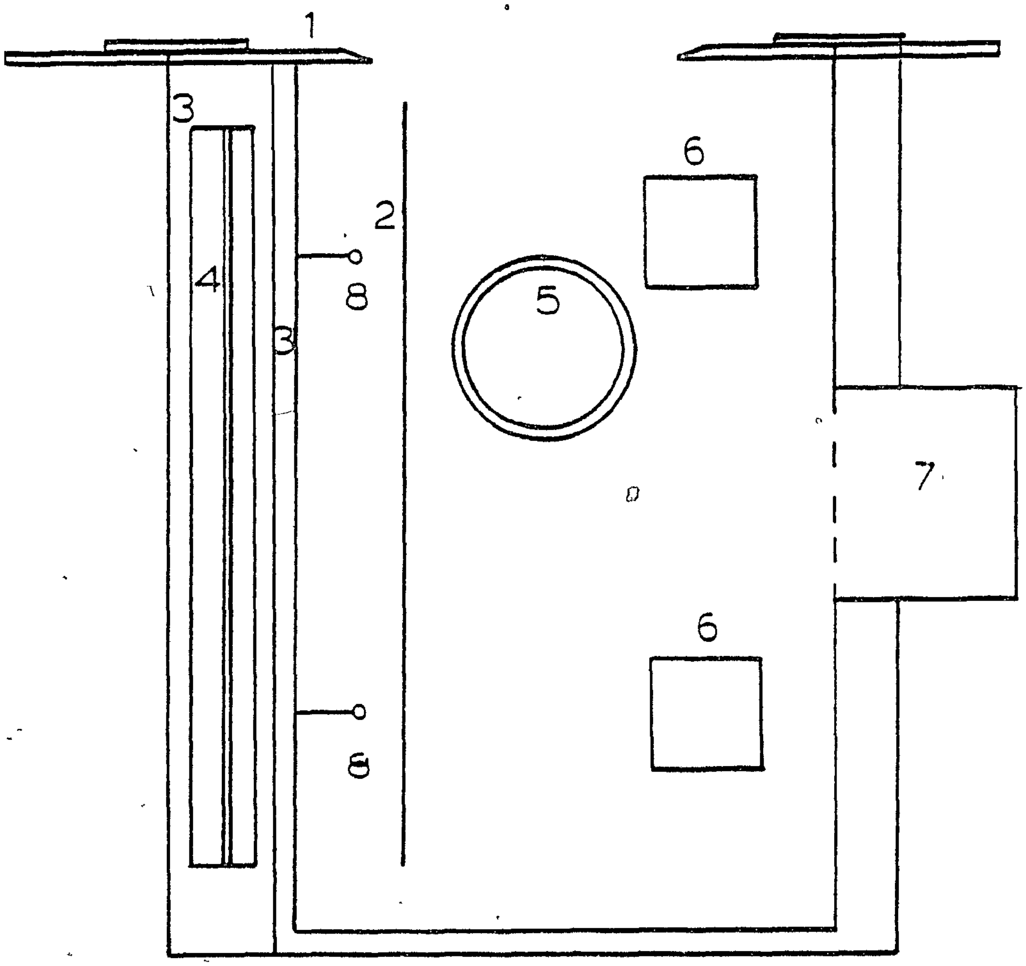

1. Insulated Cover
2. Ruler
3. Asbestos
4. Pyrex plates
5. Illumination Window
6. Heater
7. Fan
8. Thermocouple

Figure 5.29 Cross-sectional View of the Isothermal Air Oven interior walls made of asbestos sheet. The oven has a front window made of pyrex glass. Two lateral circular windows located at right angles to the front one provide the openings for the lamps that illuminate the inside of the oven. Variable intensity halogen lamps (75 W, 12 V) were used. A coil heater (660 W) wrapped around a ceramic core is used to heat the system. It is located at the back of the oven and is connected to a proportional temperature controller (Fenwall 524). A small fan at the back of the oven enhances convection to maintain a uniform temperature. Three thermocouples monitor the temperature at three points along the centerline of the oven. The top of the oven has a circular opening and a pair of sliding doors. This circular opening fits the external diameter of the barrel in such a way that the tip of the die can be seen through the front window. The air oven is mounted on a platform which can be raised or lowered to be placed in the position for the experiment. The whole assembly is mounted on rails attached to the base of the Instron testing machine to permit a forward and backward movement. Further details about the air oven can be found elsewhere (Garcia-Rejon, 1979).

5.4.2 Experimental Technique

The experimental procedure can be summarized as follows:

The tip of the die was cleaned and the air oven was raised so that the barrel could be placed in the circular opening at the top of the oven. The oven was then heated to the extrusion temperature, and after the temperature became stable extrusion was started. A predetermined amount of material was extruded. A graduated metal ruler was placed in the oven in the same plane as the parison for calibration purposes. The experimental arrangement was such that the tip of the die could be seen through the front window. The pictures of the parison were taken from the start of extrusion (time zero) until the parison collapsed under its own weight. The photographs were taken at shorter time intervals in the extrusion stage and at longer intervals in the post-extrusion stage. A stop watch was employed to record the time. After developing the photographs it was possible to obtain the length of the parison directly from the negatives with a resolution of ±0.8 mm because of the presence in the field of view of the graduated metal ruler.

5.4.3 Experimental Results and Discussion

The experiments were carried out using Resin 27 and three of the dies. These were the straight die, the diverging die and the 20° converging die. The parisons were extruded at several extrusion rates, and all the experiments were done at 170 °C. The extrusion of each parison started from rest. This simulates the intermittent extrusion blow molding process rather than the continuous process. To study the effect of parison weight on sag, two different weights of parisons were extruded from the straight die. All the data obtained in this type of experiments are given in Tables A4.1-A4.6 in Appendix A4.

A typical set of data is shown in Figure 5.30 where the length of the parison is plotted as a function of time. The data are presented in two sections due to the difference of time scales appropriate for the extrusion and post-extrusion stages. The first section represents the extrusion stage in which the length of the parison increases with time. The second section starts with the end of extrusion and continues into the post extrusion stage. The data indicate that just after the extrusion there is a period in which swell dominates over sag and the length of the parison decreases with time. Then gravitational effects start to dominate, and the length of the parison increases. After some time the parison starts necking at the tip of the die and eventually

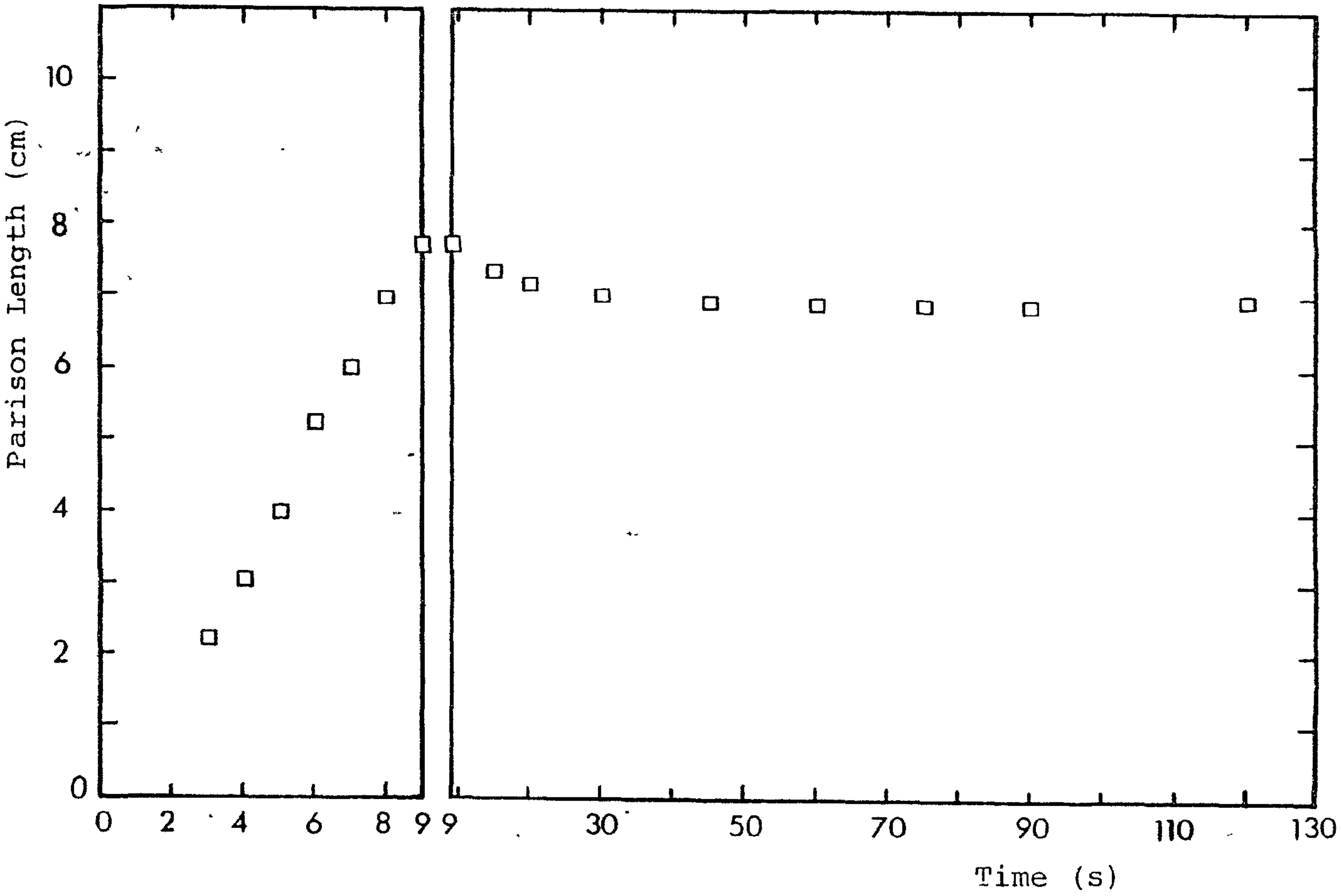

Figure 5.30 Parison Length as a Function of Time (Resin 27, Straight Die, m = 6.8 g, Q = 0.950 cm^3/s)

collapses under its own weight. The experimental results showed that once the parison starts necking the reproducibility of the data becomes very poor. Therefore, the length versus time data are presented only up to the onset of necking. The onset of necking was found to depend on the die geometry and extrusion rate.

The statistical analysis of the data, obtained by 4 replicate measurements under the same conditions, is given in Table 5.5.

In the blow molding process, of course, inflation occurs very quickly after extrusion so that data at long periods after extrusion do not correspond directly to a part of the commercial process. However, in the production of large containers, significant sag occurs during the formation of the parison. Since our experimental parisons were quite short, significant sag effects could only be studied by extending experiments to long times.

Figures 5.31 and 5.32 show the effect of different weights of parison on swell and sag. The sag effect is expected to become more dominant with increasing parison weight due to the increase of elongational stress. However, for the two different parison weights used in this study, the results indicate that the length versus time curves can be brought closely by normalizing on the basis of mass. The effect of the weight of the parison became more dominant at

TABLE 5.5 Mean Values and Standard Deviation for Measurements of Parison Length (Resin 27, Straight Die, $Q=0.950\ cm^3/s$ $m=6.8\ g$)

Time (s)	L (cm)	Std.Dev.
3	2.21	0.140
4	3.03	0.130
5	4.02	0.180
6	5.19	0.180
7	5.98	0.180
8	6.96	0.170
9	7.72	0.120
15	7.35	0.120
20	7.22	0.160
30	7.01	0.120
45	6.91	0.075
60	6.88	0.095
75	6.88	0.095
90	6.88	0.095
120	6.96	0.043

---

* mean value of 4 replicate measurements

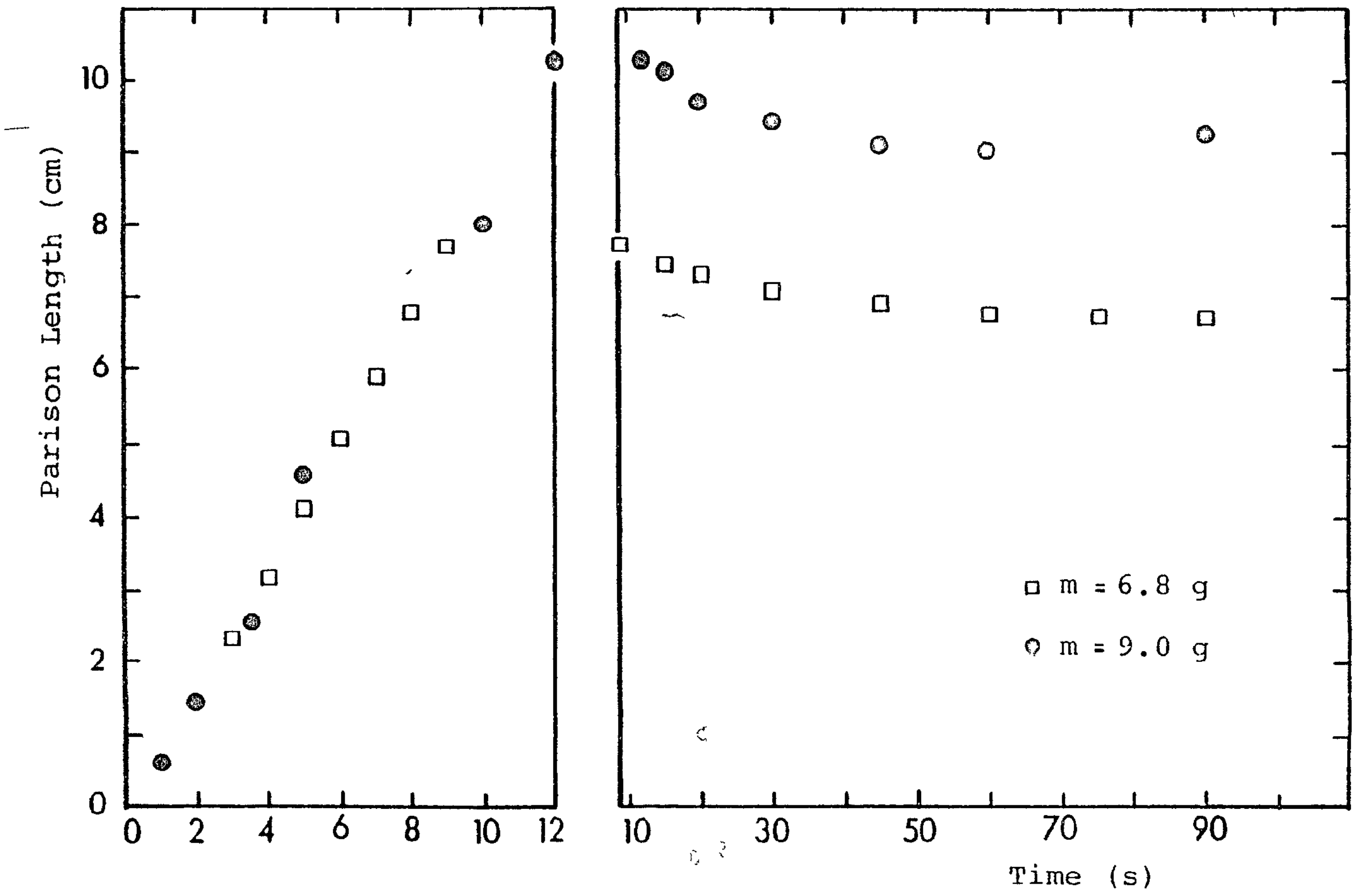

Figure 5.31 Effect of Parison Weight on the Length of the Parison (Resin 27, Straight Die, Q = 0.95 cm^3/s)

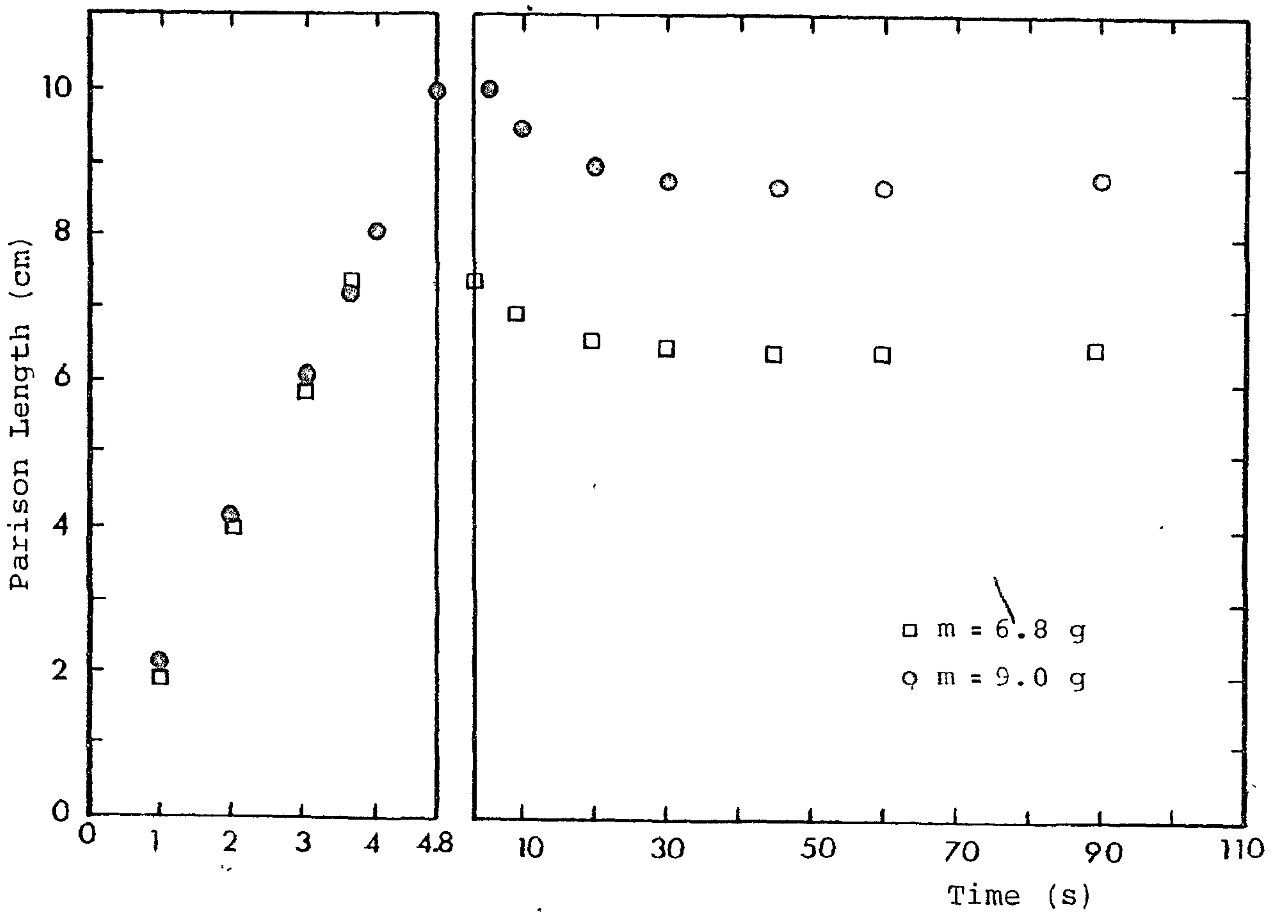

Figure 5.32 Effect of Parison Weight on the Length of the Parison (Resin 27, Straight Die, $Q = 2.375\ cm^3/s$)

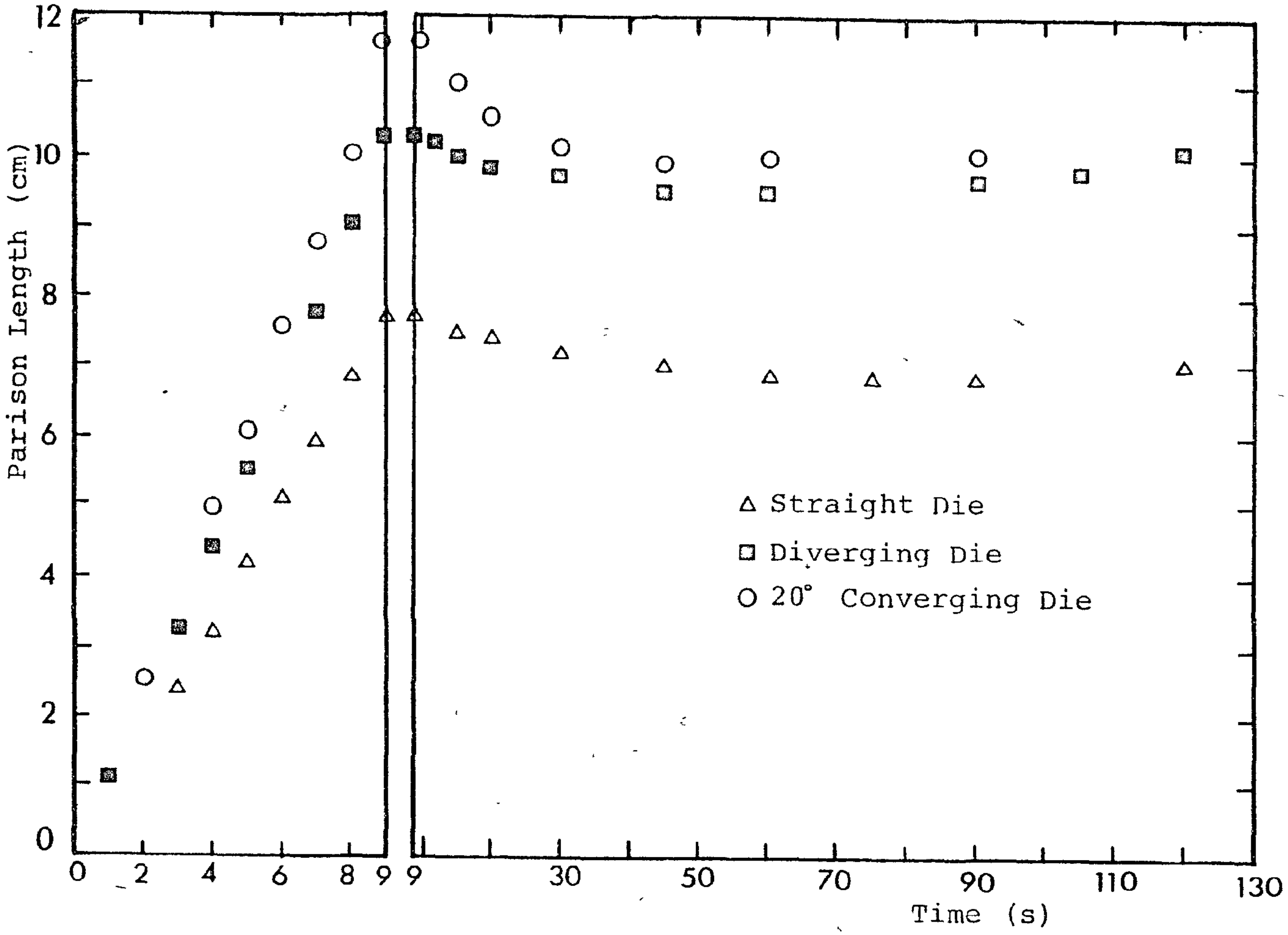

Figure 5.33 Effect of Die Geometry on Parison Length
(Resin 27, m = 6.8 g, Q = 0.950 cm^3/s)

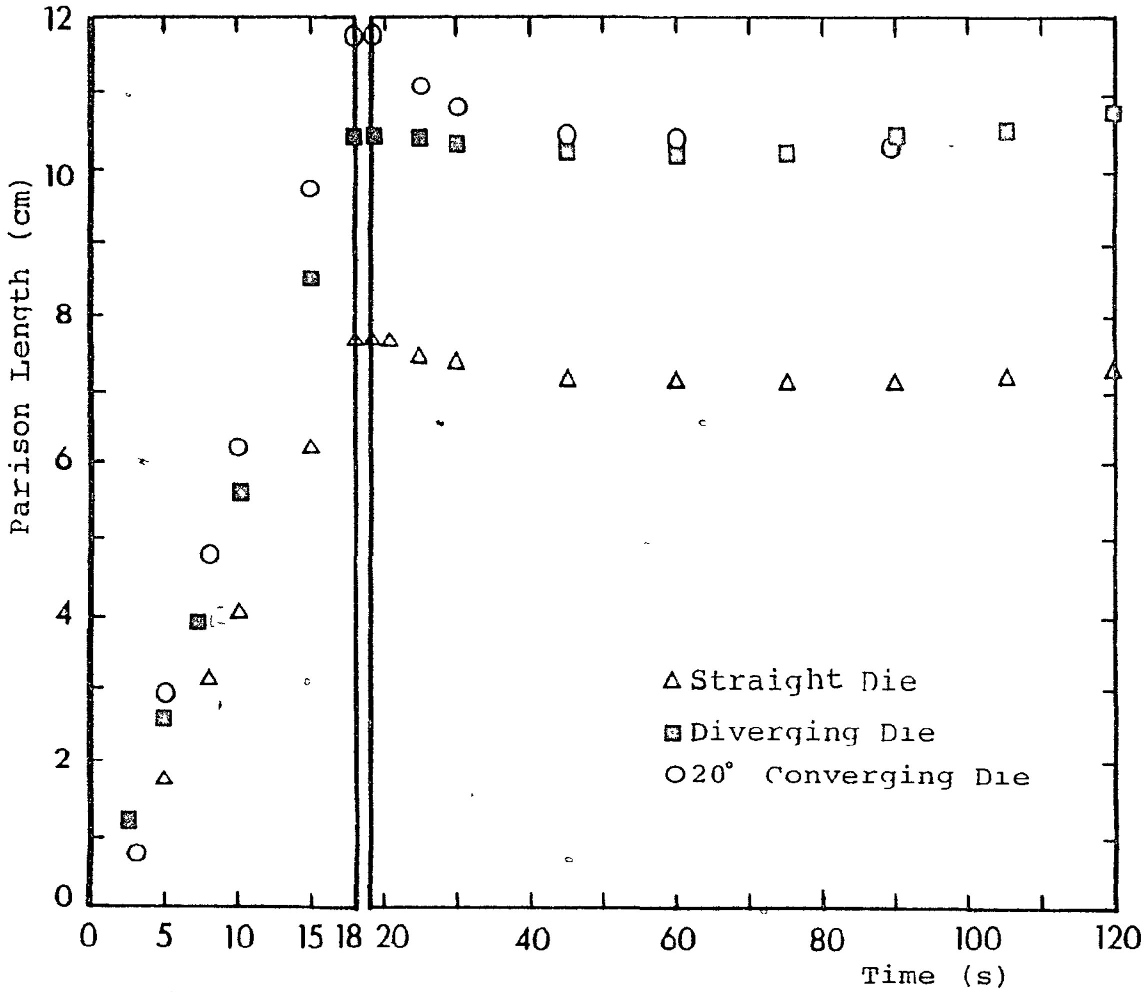

Figure 5.34 Effect of Die Geometry on Parison Length (Resin 27, $m = 6.8$ g, $Q = 0.475$ cm^3/s)

longer times in the post extrusion stage and necking started at an earlier time with the heavier parison.

The effect of die geometry on swell and sag is shown in Figures 5.33 and 5.34. The same amount of material was extruded from each die. The diverging die gave longer parisons than the straight die and the decrease in the length of the parison was smaller in the diverging die. This was the expected result since the pure swell experiments showed that the swell from the diverging die was less than that from the straight die. The 20° converging die gave the longest parisons since the same weight of material was extruded and the cross sectional area of this die is smaller than the other two dies. The decrease in the length of the parison in the post extrusion stage is the highest in the 20° converging die. This is the die that produced the highest swell in the pure swell experiments. The time for the onset of necking was shortest with the 20° converging die.

In summary, we can say that the parison length versus time data indicate the combined effect of sag and swell on parison behavior. A simple lumped parameter model to predict the length of the parison was also developed in this study. This will be presented in the following chapter.

In the present work, some experiments were also done using a commercial extrusion blow molding machine (Impco, Ingersoll-Rand B13) of Union Carbide of Canada Limited.

These experiments were carried out to see the effect of the resin on the final product produced using the same processing conditions. A converging die was used. The processing temperature was 205 °C. The die gap and the processing conditions were determined by a standard resin used by Union Carbide Limited. Resins 22A, 27 and 29 were then used to produce bottles under these conditions. The properties of the bottles obtained from different resins were different. Bottles obtained from one resin had acceptable thickness distribution and surface properties whereas bottles obtained from another resin had very thin walls and had streaks on the surface indicating flow instabilities. This is shown in Figure 5.34. The operating conditions are given below:

Die gap: 0.66 mm
Blow time: 10 s
Cycle time: 19 s
Screw speed: 125 rpm
Screw back pressure: 0.52 MPa
Blow air pressure: 0.55 MPa

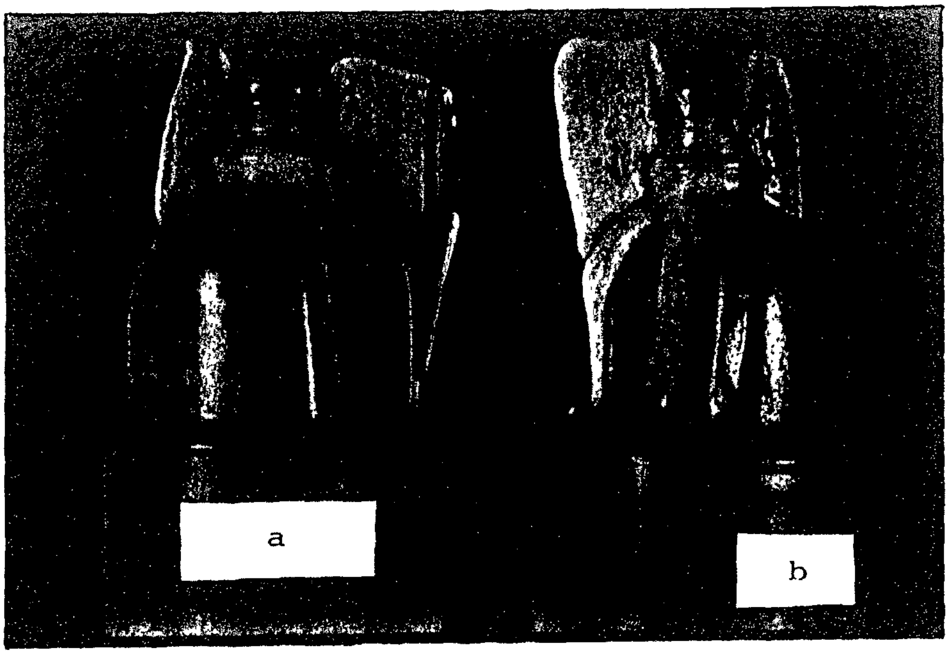

Figure 5.35 Bottles Obtained from two Different Resins under the Same Processing Conditions.

a. Acceptable thickness distribution and surface properties

b. Poor thickness distribution and surface irregularities.

CHAPTER 6

PREDICTION OF PARISON DIMENSIONS

6.1 Introduction

In the present study, a simple lumped parameter model to predict the parison dimensions is developed.

The most crucial stage in the extrusion blow molding is the parison formation stage. The parison dimensions prior to mold closing play a central role in controlling the inflation process and thus influence the quality and the thickness distribution of the final product.

The parison dimensions are determined by two distinct phenomena: swell and sag. Swell depends on time and sag depends both on time and position along the length of the parison. As a result, different material elements in the parison sag and swell differently. For example, material elements extruded first will have the highest swell since they are exposed for longer times and almost no sag since there are almost no other material elements hanging beneath them. The opposite happens for the elements extruded last. Furthermore, swell and sag occur simultaneously. These render the exact analysis of the problem very difficult.

The goal of the present approach is to develop a model which needs only a few parameters that can be easily obtained and which is mathematically simple enough so that the computations can be carried out on a small computer.

This chapter is devoted to the description of the model. First, previous studies on predicting parison dimensions are reviewed in section 6.2. The derivation of the model and the methods used in calculations are described in section 6.3. Finally, in section 6.4, results are presented and discussed.

6.2 Literature review

Attempts at developing a quantitative analysis of the parison behavior prior to mold closing have been relatively few owing to the enormous complexity of the problem.

Cogswell et al. (1971) developed the first overall analysis of the blow molding process. Their work was particularly involved with the parison formation stage. They assumed the parison to be composed of sections identified by the time at which they were extruded. The time dependency of swell was neglected and it was assumed that each segment swells instantaneously as it emerges from the die. Thus the initial cross-sectional area of a section included all the potential swelling. Then this swollen segment started to sag, and this was taken to be both time and position dependent. Cogswell's (1970) equation was used to obtain the swell data (see section 4.1). The sag phenomenon was analyzed in terms of the variation of strain with time. The total strain was taken to be the sum of elastic and viscous components. The values of the cross-sectional area, radius and length of parison were calculated and compared with a single set of experimental data obtained by cine-photography and an extruded parison. The predictions were found to be satisfactory. However, there is not enough experimental evidence to back this model and no explanation is given on how to obtain the rheological properties that are required in the model.

Henze and Wu (1973) also attempted to model the parison behavior. Their experimental data were obtained employing a parison pinch-off mold. A 30° diverging die was used. Parisons with different weights and different mold close delay times were obtained. A mathematical model for weight ratio was presented that included parameters describing the swell and drawdown phenomena. These parameters are rate constants for swell and sag and initial and ultimate weight ratios at zero loading. These were evaluated by curve fitting experimental weight ratio data. Then they tried to correlate the parameters thus obtained with each other and with the rheological properties of the resin. It was proposed that once these parameters were obtained, weight ratio for each segment of parison could be calculated. Using an emprical relation between weight swell and diameter swell proposed in the same study, the diameter swell can also be obtained. It was also proposed that an iterative procedure be used to predict the dimensions of the entire parison. However, there is not enough evidence to validate this theory, since the model equation and parameters obtained from curve fitting have never been compared with different experimental data.

Ajroldi (1978) in his analysis assumed sag and swell to be additive. He applied his analysis to individual parison segments and assumed that the stress acting on each section is in the linear viscoelastic range and that it does not change too much in time due to the variations in the cross-section. In this way, sag can be described in terms of creep compliance. Swell was taken to be the recovery due to tensile deformation. For parison elements having the same length, the following equation was obtained:

$$\ln w_i(t) = \ln w_r(t) - gl\rho J(t)(\Sigma\, w_i(t))/w_i(t) \qquad 6.2.1$$

where $w_i(t)$ is the weight of the i'th segment, $w_r(t)$ is the mass that segment would have in the absence of gravity, g is the gravity constant, l is the length of the pillow, ρ is the density, J(t) is the creep compliance and $\Sigma\, w_i(t)$ is the total weight of other segments hanging below. The $w_i(t)$ data were obtained by means of a parison pinch-off mold for different mold close delay times. Using these data and equation 6.2.1, $\ln w_i(t)$ was plotted against $(\Sigma\, w_i(t))/w_i(t)$, to obtain area swell and creep compliance values from the intercept and slope. The area swell thus obtained was compared with area swell values obtained from Cogswell's (1970) equation (see section 4.1). The agreement was poor. The creep compliance values were compared with the values obtained from relaxation moduli. Different values were obtained, although they were of the same order of magnitude.

Kamal et al. (1981) used an equation similar to that proposed by Ajroldi (1978) in reverse, i.e., they used experimentally obtained swell data and creep compliance data to predict the approximate dimensions of the parison. For parison elements having the same weight, equation 6.2.1 becomes:

$$\ln A_s'(t) = \ln A'(t) - gJ(t)\,(\Sigma\, w_i'(t))/A_s'(t) \qquad 6.2.2$$

where A_s' is the cross-sectional area of an element and $A'(t)$ is the cross-sectional area in the absence of drawdown. The values of creep compliance reported by Plazek et al. (1979) for different HDPE resins were used. The swell data were obtained from pinch-off experiments and cinematographic techniques and the effect of sag on the swell data was neglected. The model prediction was compared with a single set of experimental data and found to be satisfactory. The swell data used in this study were questionable since a constant value was assumed to be reached at about 2 seconds whereas it is known that swell continues to increase for much longer periods of time (Dealy and Garcia-Rejon, 1980; Kalyon, 1980).

Garcia-Rejon (1979) also proposed a model to predict the length of the parison. In his approach the parison was considered as a whole rather than being considered to be made up of individual elements. The extrusion and post-extrusion stages were treated seperately. During the extrusion stage sag was neglected. The effect of drawdown was considered in the post extrusion stage, where it was assumed to be equivalent to stress growth in uniaxial extension, with the initial length taken to be the length at the moment extrusion ended. The stress due to the weight of the parison was taken to be concentrated at the top of the parison. The effects of sag and swell were considered to be additive. The following equations were thus obtained:

$$L_p(t) = \alpha v_e t/B_1(t)B_2(t) \quad ; \; t \leqslant t_e \qquad 6.2.3$$

$$L_p(t) = \frac{\alpha v_e t_e}{B_1(t)B_2(t)} + L_p(t_e)\left\{\frac{1}{1-\rho g L_p(t_e)\int_{t_e}^{t} dt/\eta_T^{+}(t)} - 1\right\} \qquad 6.2.4$$

where α is a geometric parameter, v_e is the extrusion velocity, $B_1(t)B_2(t)$ is the area swell function, t_e is the extrusion time, $L_p(t)$ is the length of the parison at the end of extrusion, and $\eta_T^+(t)$ is the stress growth function in uniaxial extension. Experimentally obtained stress growth function for a strain rate of 0.0067 s^{-1} were used. Experimental area swell data was used in the model equations. The model predictions were compared with experimental data for different resins at various extrusion velocities. Satisfactory results were obtained for some cases. The present model is an extension of that of Garcia-Rejon.

Dutta and Ryan (1982) also attempted to develop a model capable of predicting parison dimensions. They modelled sag and swell phenomena separately. The pure swell behavior was modelled using exponential functions with experimentally determined constants. To model pure drawdown, corotational Maxwell model was employed. These two seperate effects were then linearly combined to obtain the actual parison dimensions. Dutta and Ryan (1982) compared the model predictions with experimental data obtained by employing pinch-off mold technique in conjunction with photography. The quantitative agreement between model predictions and experimental results were found to be poor.

6.3 Model Development

6.3.1 Mathematical Derivation

The parison formation stage is a very complex phenomenon. Both sag and swell not only depend on time, but also on deformation history. Furthermore, neither are the deformations involved sufficiently small nor the deformation rates sufficiently low so that the process can be described in terms of linear viscoelasticity. It is evident that a rigorous analysis of parison development represents a formidable problem. Such an analysis would require a difficult and questionable choice among the various nonlinear viscoelastic theories and would involve time consuming computations involving finite difference or finite element techniques. In the present study, in order to avoid elaborate numerical computation a simple lumped parameter model has been developed, which can be solved using a microcomputer.

In the present model, the parison is considered to be made up of uniform elements each having the same mass being that amount of resin extruded in a fixed time interval, Δt. This is shown schematically in Figure 6.1. This approach of considering the parison to be made up of individual elements allows us to account for the position dependency of swell and time and position dependency of sag.

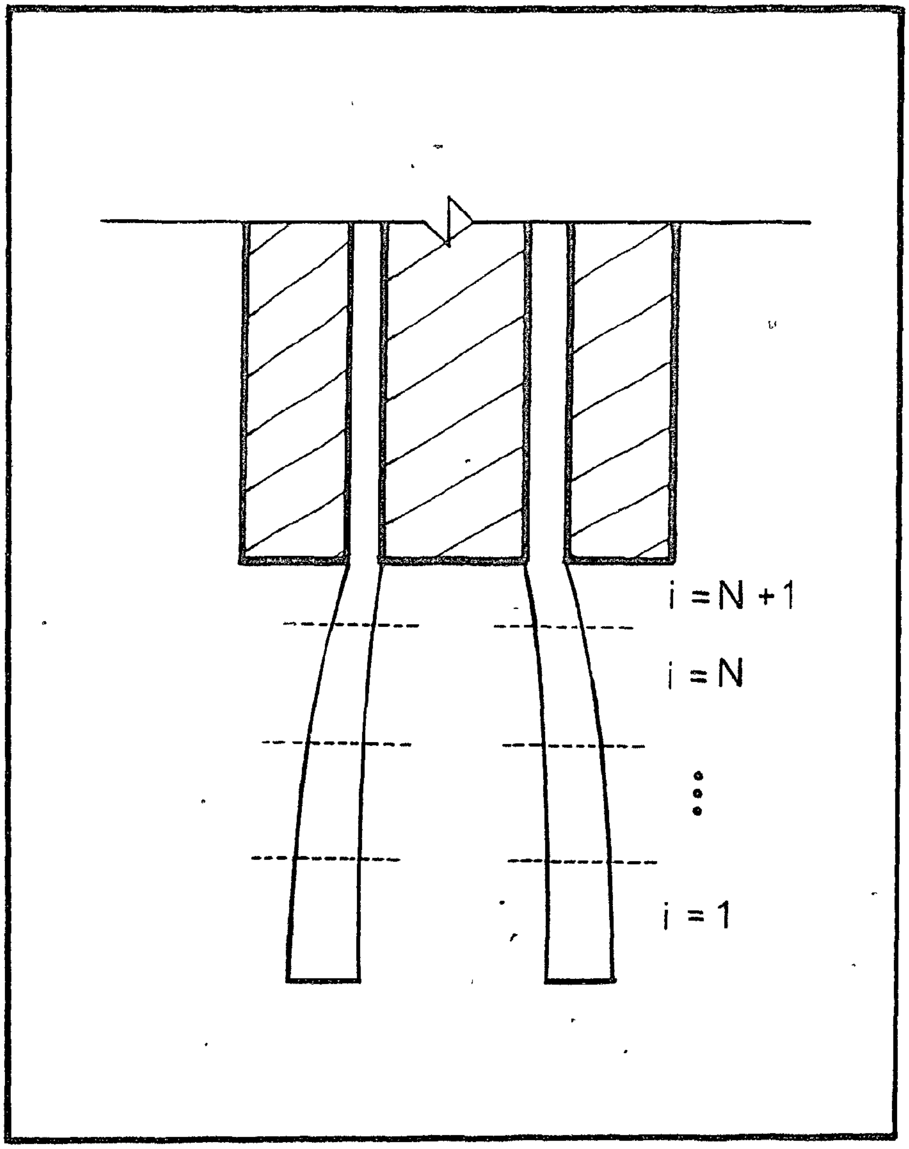

Figure 6.1 Schematic Diagram of Parison Elements

The time interval, Δt, is selected in such a way that an integral number of elements is obtained at the end of extrusion. Thus, for times equal to or greater than extrusion time, the total number of elements that are formed, N, is given by the following equation:

$$N = t_e/\Delta t \qquad ; \; t \geq t_e \qquad 6.3.1$$

For times smaller than the extrusion time, N denotes the number of elements that are fully extruded and it is given by the next integer below $t/\Delta t$. The element that is being currently extruded is denoted by N+1.

We begin our analysis with a single mass balance between the barrel and the parison:

$$\dot{M} = \dot{M}_b \, . \qquad 6.3.2$$

where $\dot{M}_b$ and $\dot{M}$ are the mass flow rate in the barrel and the mass flow rate of the parison respectively. The experiments were carried out under isothermal conditions so that the temperature in the barrel was the same as the temperature of the parison and if we assume the effect of pressure on the density of the polymer to be negligible equation 6.3.2 becomes:

$$Q = Q_b \qquad 6.3.3$$

or

$$Q = A_b v_e \qquad 6.3.4$$

where Q is the volumetric flow rate of the parison, Q_b is the volumetric flow rate in the barrel, A_b is the cross-sectional area of the barrel, and v_e is the extrusion velocity in the barrel.

In order to justify the assumption concerning the effect of pressure on density, the density of the parison and the density of the melt in the die were calculated using equations developed for HDPE by LeVan (1972). It is found that even for the highest extrusion rate used, the difference for the two values is 1.6%. Therefore, the effect of pressure on density can be neglected.

Next we assume that within an element the cross-section is uniform. This assumption is obviously invalid in the case of the element which is at the die exit. Thus equation 6.3.4 becomes:

$$\pi(R_{op}^2(t) - R_{ip}^2(t))\,dL_i(t) = \pi R_b^2 v_e\,dt \qquad 6.3.5$$

In the above equation $R_{op}(t)$, $R_{ip}(t)$ and R_b are the outer and inner radii of the of the parison and radius of the barrel respectively and $dL_i(t)$ is the differential length of parison formed during the time interval dt. If both sides of equation 6.3.5 are divided by the quantity $(R_{od}^2-R_{id}^2)$, the following expression is obtained:

$$dL_i(t) = \frac{v_d\ dt}{\{(R_{op}^2(t)-R_{ip}^2(t))/(R_{od}^2-R_{id}^2)\}} \qquad 6.3.6$$

where R_{od} and R_{id} denote the outer and inner radii at the die exit and v_d $(= R_b^2 v_e/(R_{od}^2-R_{id}^2))$ is the velocity at the die exit.

The quantities $R_{op}(t)$ and $R_{ip}(t)$ are determined by the combined effect of sag and swell and if their values are known or can be predicted, the length of the parison can be obtained from equation 6.3.6. Evidently if there were no sag and no swell, the parison would retain the dimensions at the die exit so that the denominator of equation 6.3.6 would be unity and the differential parison length would be:

$$dL_i(t) = v_d dt \qquad 6.3.7$$

Equation 6.3.6 can be applied to each parison element. To develop the model, the extrusion and post-extrusion stages of an element are considered seperately.

To find the length of an element that is being currently extruded, it is assumed that an element does not sag during its extrusion. Thus the terms $R_{op}(t)$ and $R_{ip}(t)$ depend only on swell, and they can be calculated using the following relations:

$$R_{op}(t) = R_{od}B_1(t) \qquad 6.3.8a$$

$$R_{ip}(t) = R_{od}B_1(t)-(R_{od}-R_{id})B_2(t) \qquad 6.3.8b$$

$B_1(t)$ and $B_2(t)$ are the diameter and thickness swell ratios as before and the above equations can be substituted into equation 6.3.6 to obtain the length of the element that is currently being extruded. If the slit approximation can be made, the denominator of equation 6.3.6 becomes equal to the area swell ratio $B_1(t)B_2(t)$, and the equation becomes:

$$L_i(t) = L_{N+1}(t) = \int_{N\Delta t}^{t} \frac{v_d \, dt'}{B_1(t')B_2(t')} \qquad 6.3.9$$

Noting that nearly 70% of the total swell occurs very quickly, we simplify equation 6.3.9 by using constant average values of B_1 and B_2 evaluated at $\Delta t/2$. Thus:

$$L_{N+1}(t) = \frac{v_d(t-N\Delta t)}{B_1(\Delta t/2)B_2(\Delta t/2)} \qquad 6.3.10$$

The calculations are carried with the experimentally obtained diameter and thickness swell values, since so far there exists no reliable correlation between the rheological properties of the resin and the swell functions. The experimental diameter and thickness swell data are fitted with the following equations proposed by Garcia-Rejon (1979):

$$B_1(t) = B_{1\infty}-(B_{1\infty}-B_{1o})\ e^{-t/\zeta_1} \qquad 6.3.11a$$

$$B_2(t) = B_{2\infty}-(B_{2\infty}-B_{2o})\ e^{-t/\zeta_2} \qquad 6.3.11b$$

where ζ_1, ζ_2 are the characteristic times for diameter and thickness swell, $B_{1\infty}$ and $B_{2\infty}$ are the equilibrium diameter and thickness swell values and B_{1o} and B_{2o} are the diameter and thickness swell values respectively corresponding to zero time. These functions are capable of fitting the rapid initial swelling and the equilibrium value at longer times. The equations gave a very good fit with the experimental data. However, at very short times, i.e., less than 5 seconds the equations gave slightly higher values than those observed experimentally. The data are fitted for the time range used in the calculations, and the constants in these equations are given in Tables 6.1 and 6.2.

To find the length of an element that is already extruded we consider both swell and sag. To model the

TABLE 6.1 Parameters of Equation 6.3.11a for Resin 27

Q (cm^3/s)	B_{1o}	$B_{1\infty}$	ζ_1 (1/s)
Straight Die			
0.095	1.25	1.66	132
0.238	1.29	1.70	109
0.475	1.33	1.74	57
0.950	1.35	1.76	69
2.375	1.38	1.94	103
Diverging Die			
0.475	1.02	1.31	160
0.950	1.05	1.38	162
20° Converging Die			
0.475	1.92	2.81	110
0.950	2.10	2.70	45

TABLE 6.2 Parameters of Equation 6.3.11b for Resin 27

Q (cm^3/s)	B_{2o}	$B_{2\infty}$	ζ_2 (1/s)
Straight Die			
0.095	1.17	1.84	268
0.238	1,24	1.86	218
0.475	1.43	1.92	211
0.950	1.48	1.97	129
2.375	1.56	2.10	154
Diverging Die			
0.475	1.40	1.97	150
0.950	1.47	2.15	185
20° Converging Die			
0.475	1.29	1.92	143
0.950	1.31	1.81	55

process we assume that sag and swell are uncoupled and occur independently of each other. For each element, the time elapsed since its formation is different and is given by the following formula:

$$t_i = t - i\Delta t \qquad 6.3.12$$

where t_i denotes the time during which an element is subjected to the effects of drawdown.

To model sag it is assumed that sag is the uniaxial extension of a hypothetical unswollen element. To this end we define z_i to be the length of this hypothetical element. The time dependent extensional strain rate, $\dot{\varepsilon}_i(t_i)$, is thus given by the following definition:

$$\dot{\varepsilon}_i(t_i) = (1/z_i)(dz_i/dt_i) \qquad 6.3.13$$

Note that in the case of no sag z_i is given by equation 6.3.7 and thus the initial value of z_i is:

$$z_i = v_d \, \Delta t \qquad ; \; t_i = 0 \qquad 6.3.14$$

The length of a fully extruded element can thus be obtained by anology with equation 6.3.10.

$$L_i(t) = \frac{z_i(t_i)}{B_1(t_i+\Delta t/2)B_2(t_i+\Delta t/2)} \qquad 6.3.15$$

The average net stretching stress due to gravity in the unswollen element can be obtained by dividing the total weight hanging beneath the element by its cross-sectional area. Each element has the same weight, which can be determined from a mass balance between the element and the barrel, so that:

$$\tau_{zz}-\tau_{rr} = \tau_i = \rho A_b v_e \, \Delta t \, g(i-1)/A_i' \qquad 6.3.16$$

where τ_i is the stress, g is the gravity constant and A_i' is the area of the hypothetical unswollen element. A_i' can also be found from continuity. Assuming constant density:

$$z_i A_i' = v_e A_b \Delta t \qquad 6.3.17$$

Combining equations 6.3.16 and 6.3.17, the stress is found to be:

$$\tau_i = \rho g(i-1) z_i \qquad 6.3.18$$

Finally for the relation between stress and strain several possibilities were considered. In some of the previous work done on modelling parison behavior, the phenomenon of sag was assumed to be related to creep compliance (Ajroldi, 1973; Kamal et al., 1981). However, the inherent assumption in this approach, that the stress is constant, is not valid since the cross-sectional area of the parison is changing with time. Also, creep compliance data are difficult to obtain in the laboratory. Garcia-Rejon (1979) assumed sag to be equivalent to stress growth in uniaxial extension. He considered several choices: using a constant elongational viscosity, using a stress growth function, $\eta_T^+(t)$ predicted by linear viscoelastic theory, using $\eta_T^+(t,\dot{\varepsilon})$ as predicted by a non-linear model like the one of Acierno et al. (1976), and using the experimentally determined stress growth function at a specific strain rate. Experimentally obtained stress growth data at a constant strain rate of 0.0067 s^{-1} gave the best predictions.

In the present work, the possibility of using stress growth function as the relation between stress and strain rate was also examined. The strain rate was taken to be position dependent along the length of the parison but was constant for each element. The strain rates involved were found to be in the order of magnitude of 10^{-3}. Lodge's Rubber-like liquid model (Lodge, 1974) was used to evaluate the values of the stress growth function, and an average value of strain rate was found by trial and error for each element. Then, instead of using the stress growth function, the possibility of using a constitutive equation in uniaxial extension was considered. The strain rate was taken to be both position and time dependent and was integrated over the past history. Lodge's rubber-like liquid model (Lodge, 1974) was used as the constitutive equation. The results indicate that using this method gave better predictions of parison length compared to those obtained by using the stress growth function. Therefore, this method was preferred. The predictions of these two models will be compared in section 6.4.

Lodge's Rubber-like liquid model was selected as the constitutive equation since it is a fairly simple model which does not need elaborate computations yet it satisfies the principle of material objectivity. Although the model has some limitations and deficiencies, it is found to be a good model for transient elongational flows at low extension rates and at short times (Bird et al., 1979; Chang and Lodge, 1972; Lodge, 1974). Since commercial processing involves rather short times from the start of extrusion to inflation and since the strain rates associated with sag are low, Lodge's rubber-like liquid model suffices for our purposes.

The general form of Lodge's rubber-like liquid model is (Lodge, 1974; Bird et al., 1979):

$$\tau = \int_{-\infty}^{t} M(t-t')\underline{H}^{-1}dt' \qquad 6.3.19$$

with

$$M\ (t-t') = \sum_k \frac{G_{ok}}{\lambda_{ok}}\ \exp(-(t-t')/\lambda_{ok}) \qquad 6.3.20$$

where t' denotes the past times, $M(t-t')$ is the memory function, $\underline{H}^{-1}$ is the Finger tensor, and G_{ok} and λ_{ok} are the relaxation modulus and the relaxation time respectively. Applying this model to the present case where the parison elements are subjected to a time dependent strain rate, $\dot{\varepsilon}_i(t_i)$, for $t_i \geq 0$, the following equation is obtained:

$$\tau_i = \left(\Sigma G_{ok} e^{-t_i/\lambda_{ok}}\right)\left(\frac{z_i^2(t_i)}{z_i^2(0)} - \frac{z_i(0)}{z_i(t_i)}\right)$$
$$- \int_0^{t_i} \left(\Sigma \frac{G_{ok}}{\lambda_{ok}}\ e^{-(t_i-t')/\lambda_{ok}}\right)\left(\frac{z_i(t')}{z_i(t_i)} - \frac{z_i^2(t_i)}{z_i^2(t')}\right)dt' \qquad 6.3.21$$

where $z_i(0)$, $z_i(t_i)$, $z_i(t_i')$ are the values of z_i at time zero, at time t_i and at some past time t_i' respectively. The derivation of equation 6.3.21 is given in detail in Appendix A5.

Equations 6.3.18 and 6.3.21 can be used to obtain the value of z_i for each element at the desired time. The value of z_i thus obtained is then substituted in equation 6.3.15 to obtain the length of the element. Finally the actual length of the parison at any time t is obtained by summing up these individual contributions. Thus, the length of the parison for times smaller than extrusion time is given by the following equation:

$$L(t) = \frac{v_d(t-N\Delta t)}{B_1(\Delta t/2)B_2(\Delta t/2)} + \sum_{i=1}^{N} L_i(t) \quad ; \quad t \leqslant t_e \qquad 6.3.22a$$

For times greater than the extrusion time, we have:

$$L(t) = \sum_{i=1}^{N} L_i(t) \quad ; \quad t > t_e \qquad 6.3.22b$$

In the experiments in which the combined effects of sag and swell were studied, it was observed that when the length of the parison was plotted as a function of time the values did not pass through the origin. Rather, a zero length is observed for a time which is larger than zero. This phenomena, which is not uncommon in intermittent extrusion, is due to the compression of the melt before enough pressure has been built up to make it flow. This causes a time lag, and the real extrusion time is less than the calculated one.

The value of the time lag, t_c, can be obtained by extrapolating experimental L(t) data to L=0. The value of t_c increases with decreasing extrusion velocity and amounts to about 3-13% of the extrusion time for the lowest and highest extrusion velocities used. So the time, t, appearing in the model equations should be corrected for this effect. Accordingly equations 6.3.22 become:

$$L(t^*) = \frac{v_d(t-N\Delta t)}{B_1(\Delta t/2)B_2(\Delta t/2)} + \sum_{i=1}^{N} L_i(t) \quad ; \; t \leqslant t_e \qquad 6.3.23a$$

$$L(t^*) = \sum_{i=1}^{N} L_i(t) \qquad ; \quad t > t_e \qquad 6.3.23b$$

where t^* is given by

$$t^* = t + t_c \qquad 6.3.24$$

The model performance is described in terms of the length of the parison, since it is the most easily measured quantity. However, the ultimate aim of such a model is to predict the cross-sectional area and thickness distribution as well as the length. The present model can be extended to satisfy these demands. The cross-sectional area of an element can be obtained through a mass balance:

$$A_i = v_d A_d \, \Delta t / L_i(t) \qquad 6.3.25$$

To determine the approximate distribution of diameter and thickness swell in the parison, it can be assumed that the ratio of swell ratios for the parison is equal to that for the parison extruded into oil:

$$\frac{B_{1i}}{B_{2i}} = \frac{B_1(t_i)}{B_2(t_i)} \qquad 6.3.26$$

Equation 6.3.25 assumes that the area swell does not change along the element length. However there is a small section at the tip of the parison which has different dimensions than the rest of the extrudate. This is caused by the fact that, since the extrusion stars from rest, the material near to the die exit will experience little shear and thus does not have the same strain history as the rest of the material in the parison. Fortunately, this portion is only a small fraction of the parison length and it becomes the discarded tail flash of the bottle in the process. Also just at the tip of the die; the cross-sectional area is not constant along the length of the element, because of the difference of dimensions between the die exit and the parison. However, this portion also is not significant in the actual process.

The basic assumptions made in the derivation of the model can be summarized as follows:

1. The parison is assumed to be made up of individual elements, each having the same mass and each extruded in the same time interval, Δt. The cross-sectional area is taken to be uniform within an element.

2. It is assumed that an element does not sag while it is being extruded.

3. Sag and swell are assumed to be uncoupled.

4. Sag is assumed to be the uniaxial extension of a hypothetical unswollen element.

6.3.2 Model calculations

In order to be able to calculate the length of the parison, the swell functions and the hypothetical length, $z_i(t_i)$ must be evaluated.

It was mentioned in the previous section that experimentally obtained swell functions are used with the model equations. The experimental diameter and thickness swell data are fitted using equations 6.3.11 (see Tables 6.1 and 6.2).

To obtain the value of $z_i(t_i)$, equations 6.3.18 and 6.3.21 must be solved simultaneously. A trial and error procedure is used for this purpose. First an initial estimate of $z_i(t_i)$ is made and the value of the stress τ_i is obtained from equation 6.3.21. This value is then used to calculate $z_i(t_i)$ through equation 6.3.18. This procedure is repeated until the difference between the trial value and calculated value is very small. The calculations are carried out using Wegstein's method for convergence (Franks, 1972). This method is based on a projection technique whereby the next trial value is determined from the projection of the latest two trial values. The convergence is achieved rapidly.

Discrete relaxation spectrum data obtained from the storage modulus (see section 2.4.3) are used in equation 6.3.21. These values are given in Table 2.2. Equation 6.3.21 is integrated numerically since the function $z_i(t_i)$ is not known a priori. A composite integration formula is used whereby the integration interval $(t_i - 0)$ is subdivided into smaller intervals of $\Delta\theta$ and the trapezium rule is applied to each small interval (Carnahan et al., 1969). The small time interval for integration $\Delta\theta$, is taken to be an integer fraction of Δt for convinience. Selection of $\Delta\theta$ affects the final results. Too large a $\Delta\theta$ gives a less accurate result whereas too small a $\Delta\theta$ increases computation time. However, there is an optimum value of stepsize in a numerical integration beyond which the results obtained become less sensitive to the selection of the stepsize. For the present model, the optimum value for $\Delta\theta$ is obtained by trying several values.

A small computer (PET Commodore 2001) was used to solve model equations. The computer program (in Basic) is given in Appendix A6. The procedure used in the calculations is outlined below:

1. The time increments Δt and $\Delta\theta$ are selected.

2. For any time t^*, the actual time t is evaluated using equation 6.3.24.

3. The number of elements that are fully extruded (N) is calculated.

4. For each element i (i= 1,...,N)

   a. t_i is calculated from equation 6.3.12

   b. $z_i(t_i)$ is obtained from equations 6.3.18 and 6.3.21

   c. Diameter and thickness swell values are obtained from equations 6.3.11a and 6.3.11b.

   d. The length of the element, $L_i(t)$ is calculated using equation 6.3.15.

5. If $t \leqslant t_e$, the length of the element that is currently being extruded is calculated from equation 6.3.10.

6. The actual length of the parison is obtained from equation 6.3.23.

7. Steps 3-6 are repeated for a new time t^*.

Since equation 6.3.21 requires the knowledge of the value of $z_i(t_i)$ at past times, it is best to start the calculations with t^* being equal to $(t_c + \Delta\theta)$ and increase the time with an increment equal to $\Delta\theta$.

6.4 Results and Discussion

The results obtained from the model equations are now compared with the experimental data. The model predictions and experimental data are tabulated in Tables A4.1-A4.6 in Appendix A4 and plotted in Figures 6.2-6.13.

Figures 6.2-6.9 show both the experimental and predicted parison lengths for the straight die. Results are presented for two parison weights and four extrusion velocities for each parison weight. The experimental data and model predictions are found to be in good agreement, especially in the extrusion stage and at short times in the post-extrusion stage. These are the important time scales in a commercial blow molding operation. However, at longer times in the post-extrusion stage, the model predictions are higher than the experimental data indicating that the model predicts a larger and faster swell than is observed. The model performance at longer times is better for lower extrusion rates.

The performance of the model for the diverging die is shown in Figures 6.10 and 6.11 for two extrusion rates. As

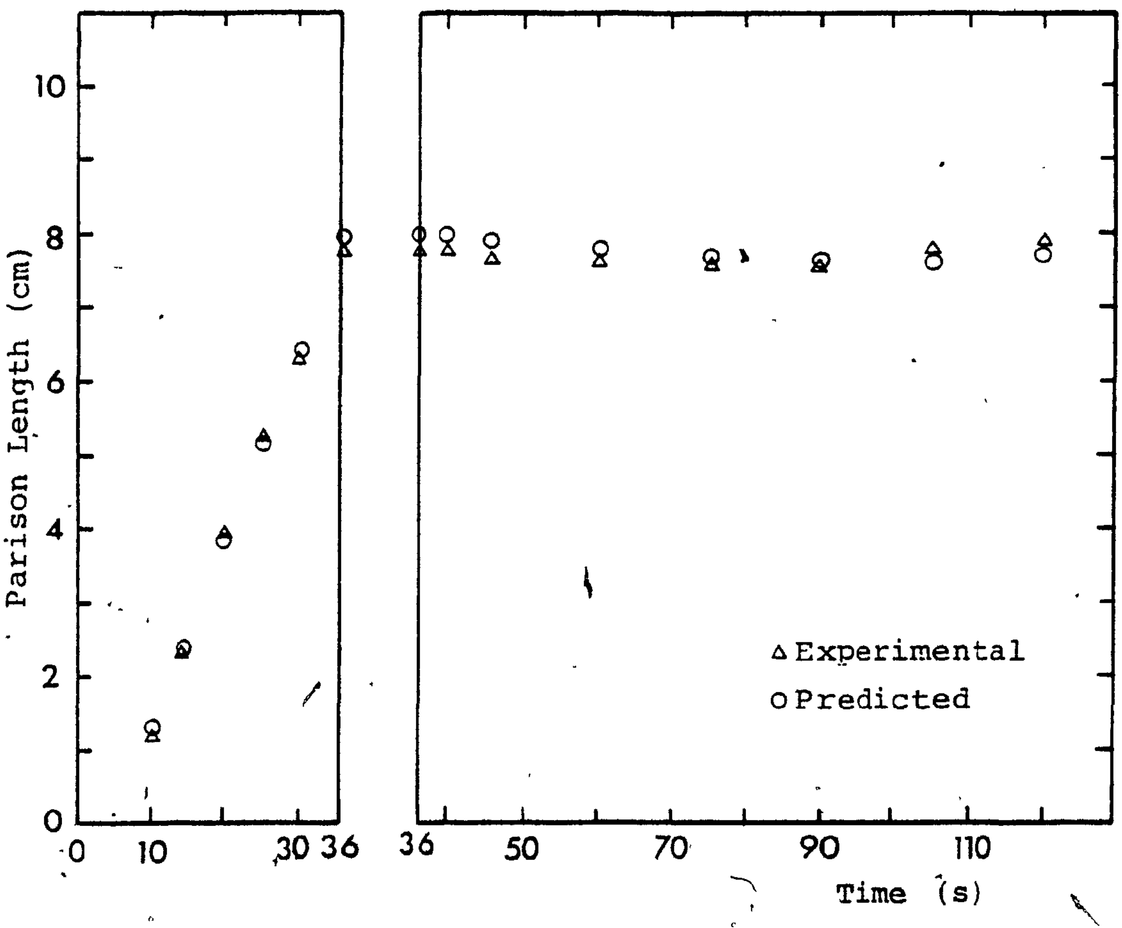

Figure 6.2 Comparison of Experimental and Predicted Values of Parison Length (Resin 27, Straight Die, m = 6.8 g, Q = 0.238 cm^3/s)

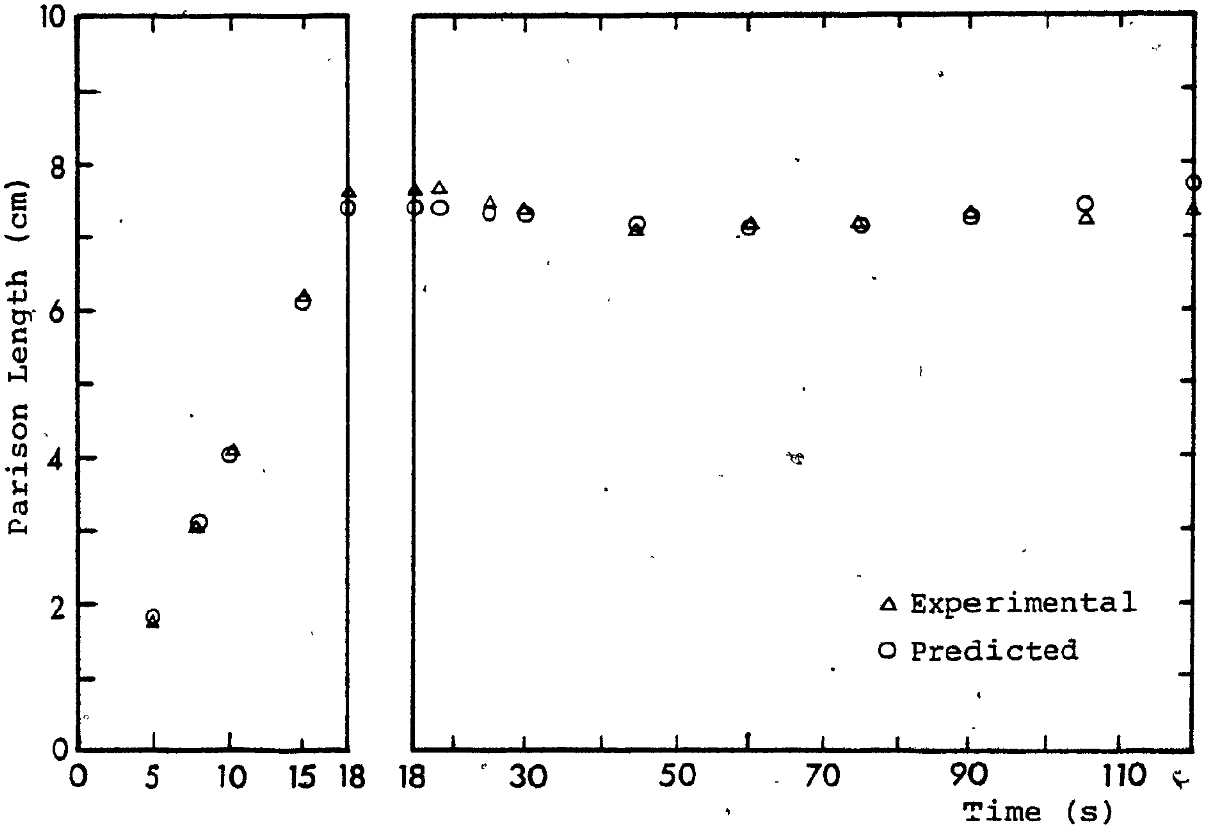

Figure 6.3 Comparison of Experimental and Predicted Values of Parison Length (Resin 27 Straight Die, m = 6.8 g, Q = 0.475 cm^3/s)

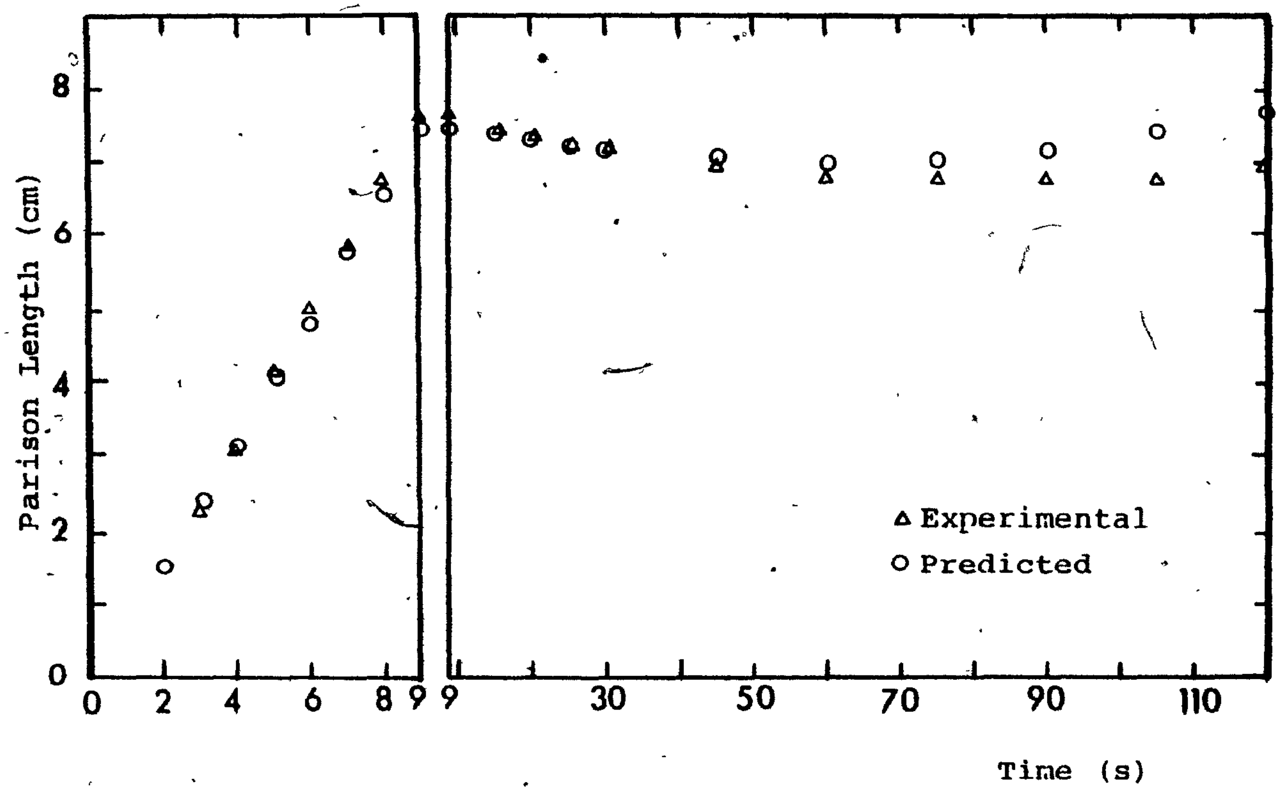

Figure 6.4 Comparison of Experimental and Predicted Values of Parison Length (Resin 27, Straight Die, $m = 6.8$ g $Q = 0.950$ cm^3/s)

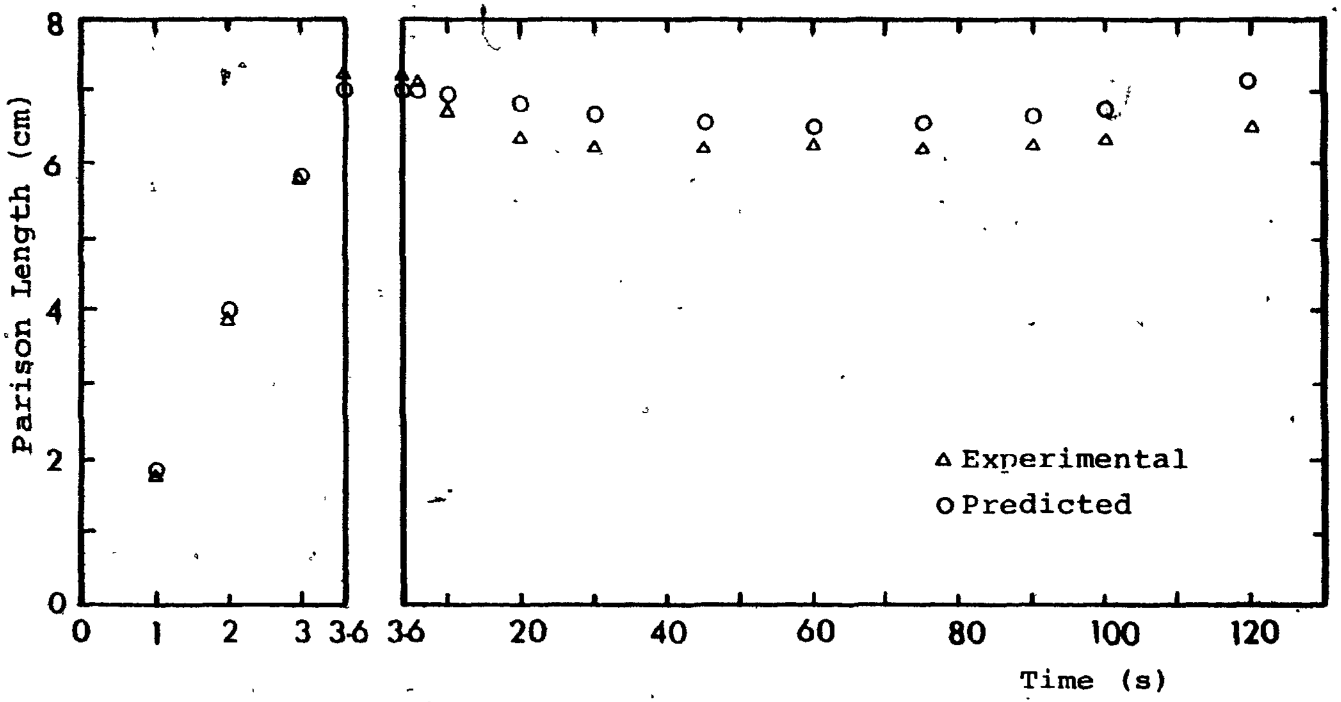

Figure 6.5 Comparison of Experimental and Predicted Values of Parison Length (Resin 27, Straight Die, m = 6.8 g $Q = 2.375\ cm^3/s$)

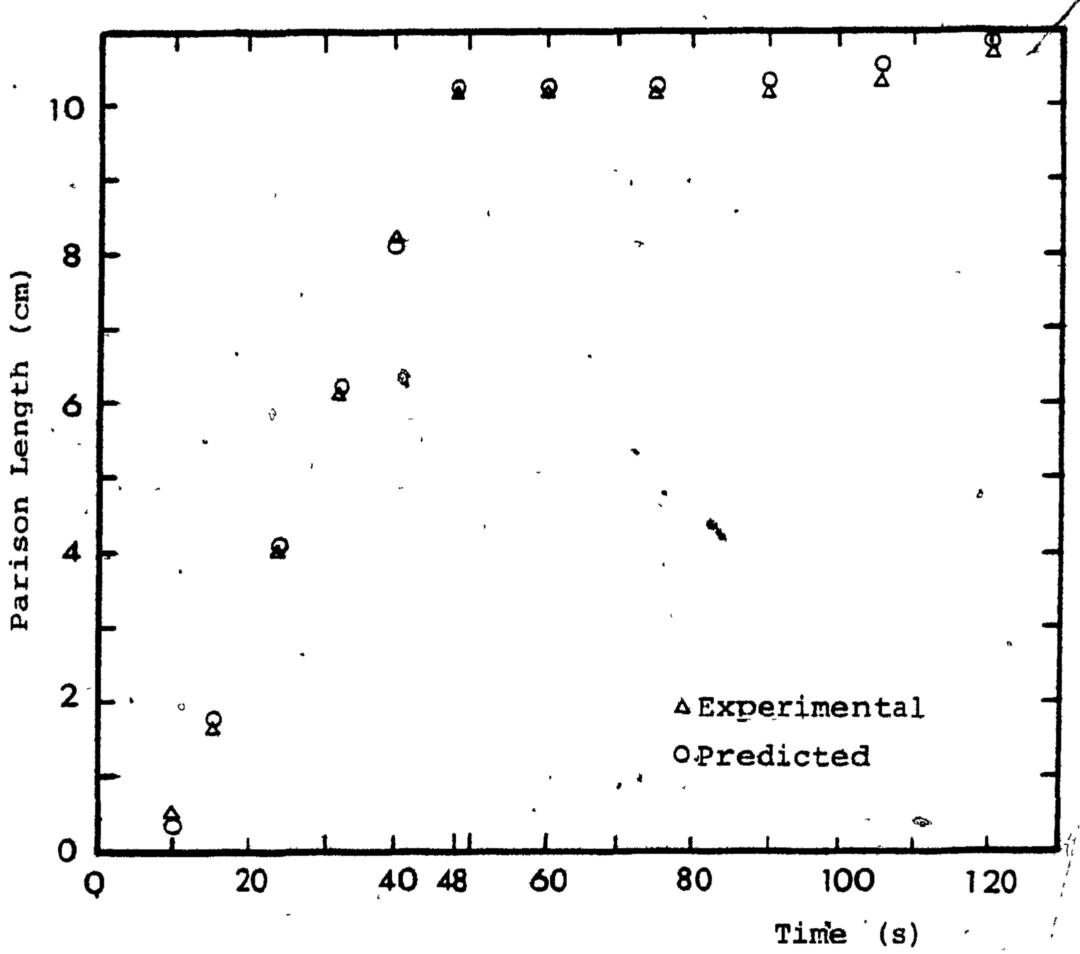

Figure 6.6 Comparison of Experimental and Predicted Values of Parison Length (Resin 27 Straight Die, m = 9 g, Q = 0.238 cm^3/s)

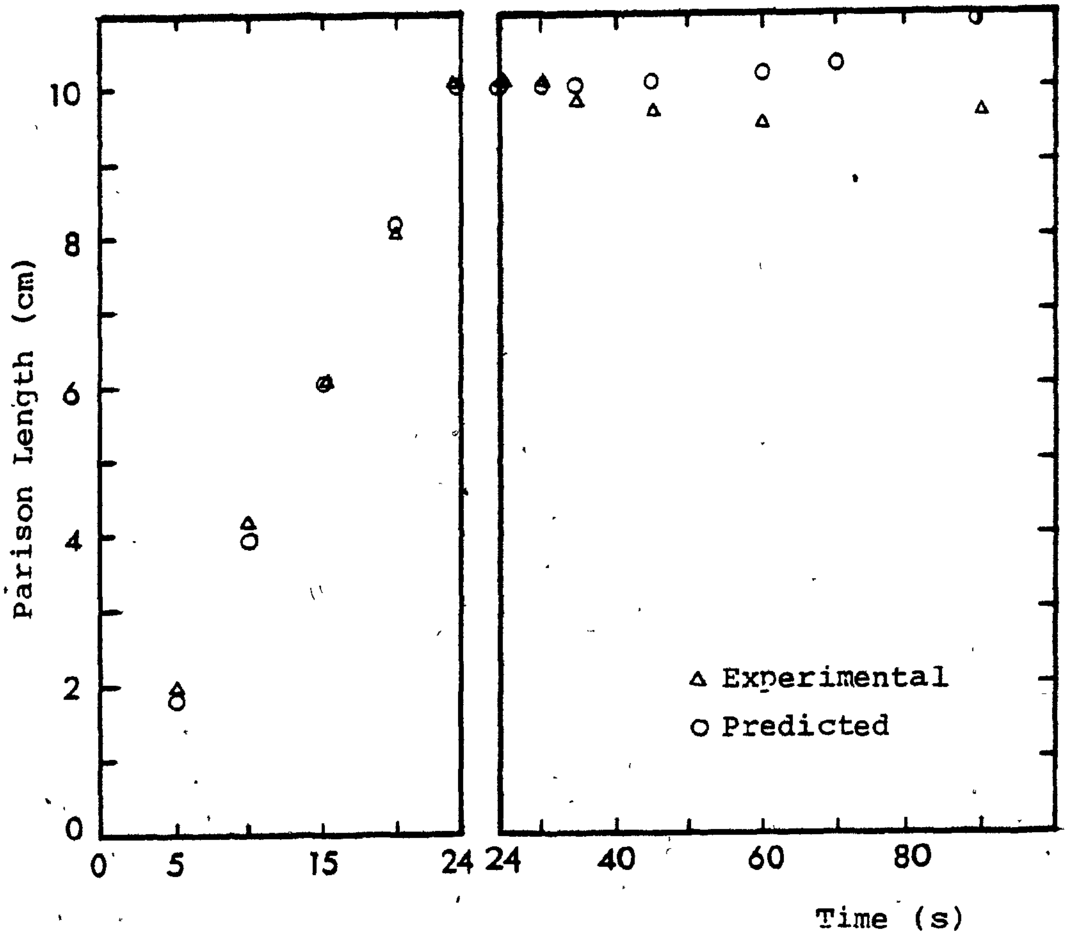

Figure 6.7 Comparison of Experimental and Predicted Values of Parison Length (Resin 27 Straight Die, m = 9 g, Q = 0.475 cm^3/s)

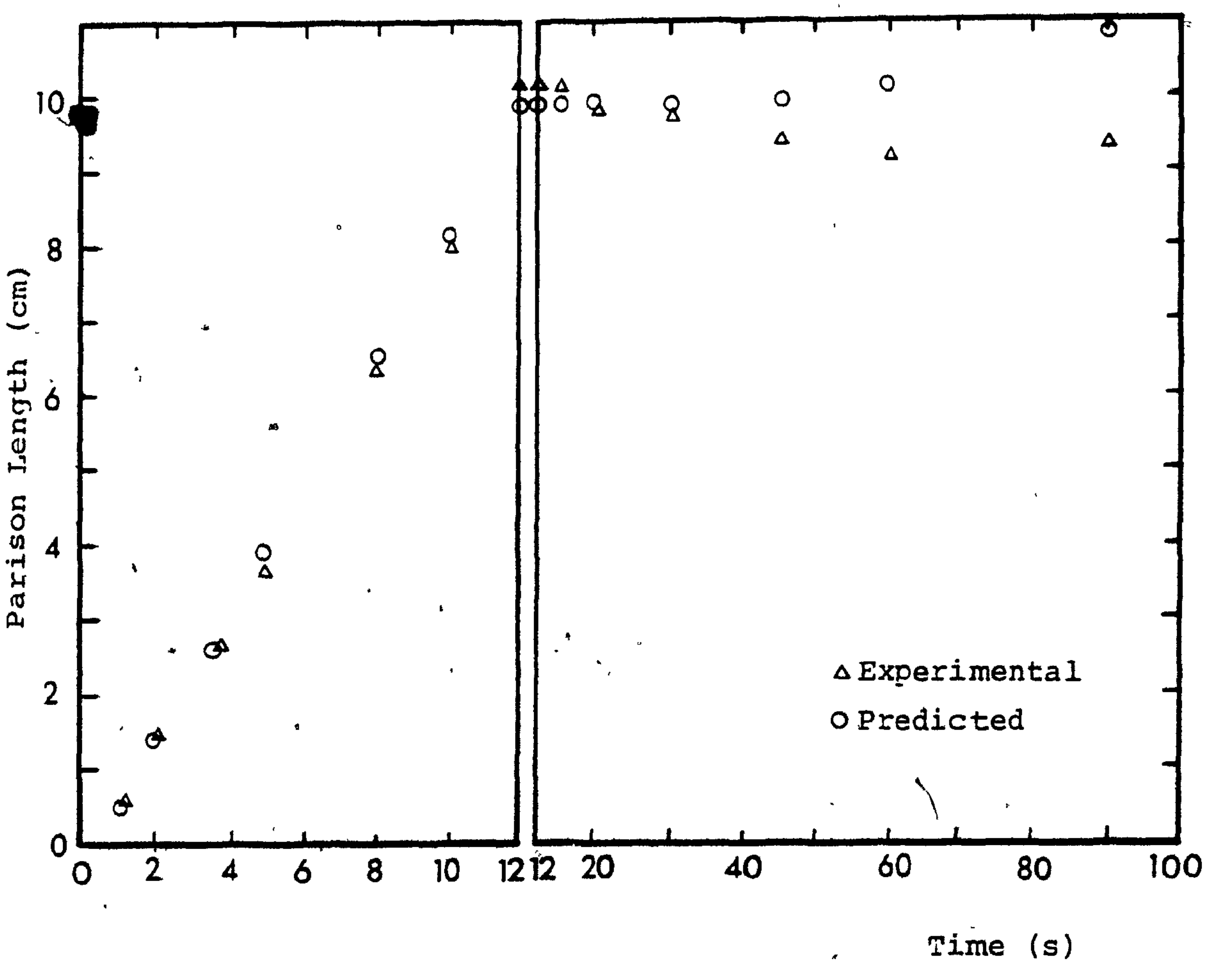

Figure 6.8 Comparison of Experimental and Predicted Values of Parison Length (Resin 27, Straight Die, $m = 9$ g, $Q = 0.950$ cm^3/s)

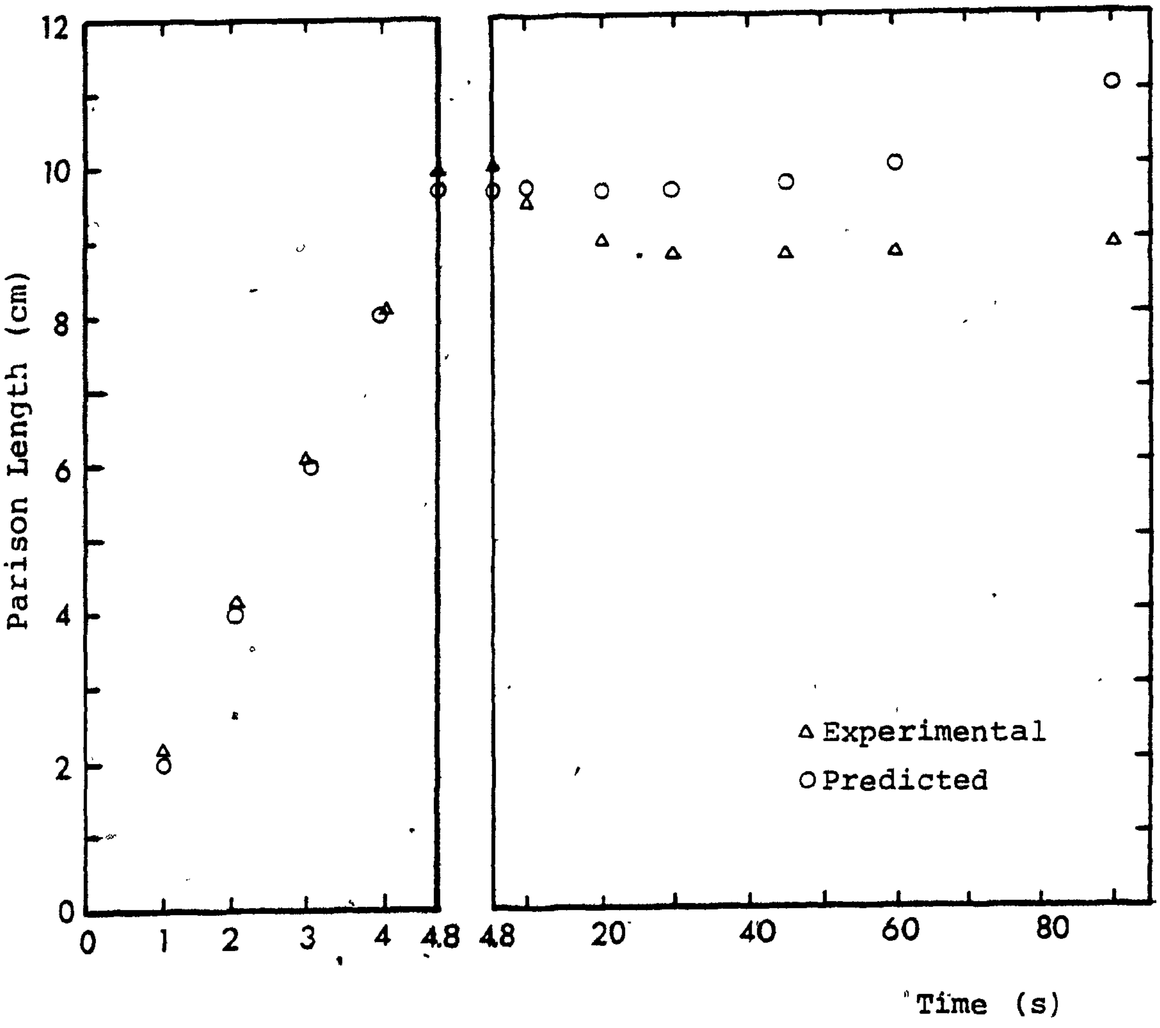

Figure 6.9 Comparison of Experimental and Predicted Values of Parison Length (Resin 27, Straight Die, $m = 9$ g, $Q = 2.375$ cm^3/s)

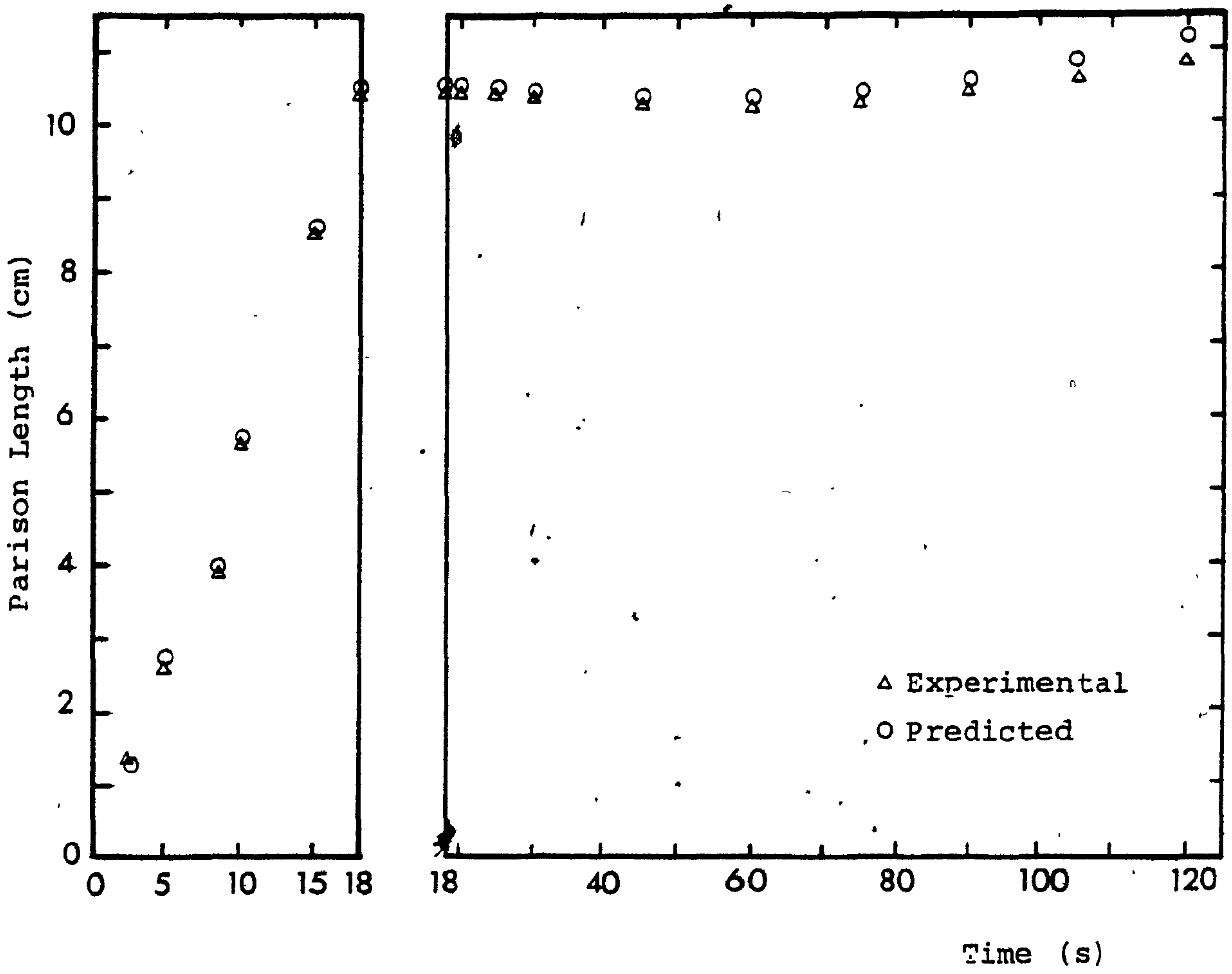

Figure 6.10 Comparison of Experimental and Predicted Values of Parison Length (Resin 27, Diverging Die, m = 6.8 g, Q = 0.475 cm^3/s)

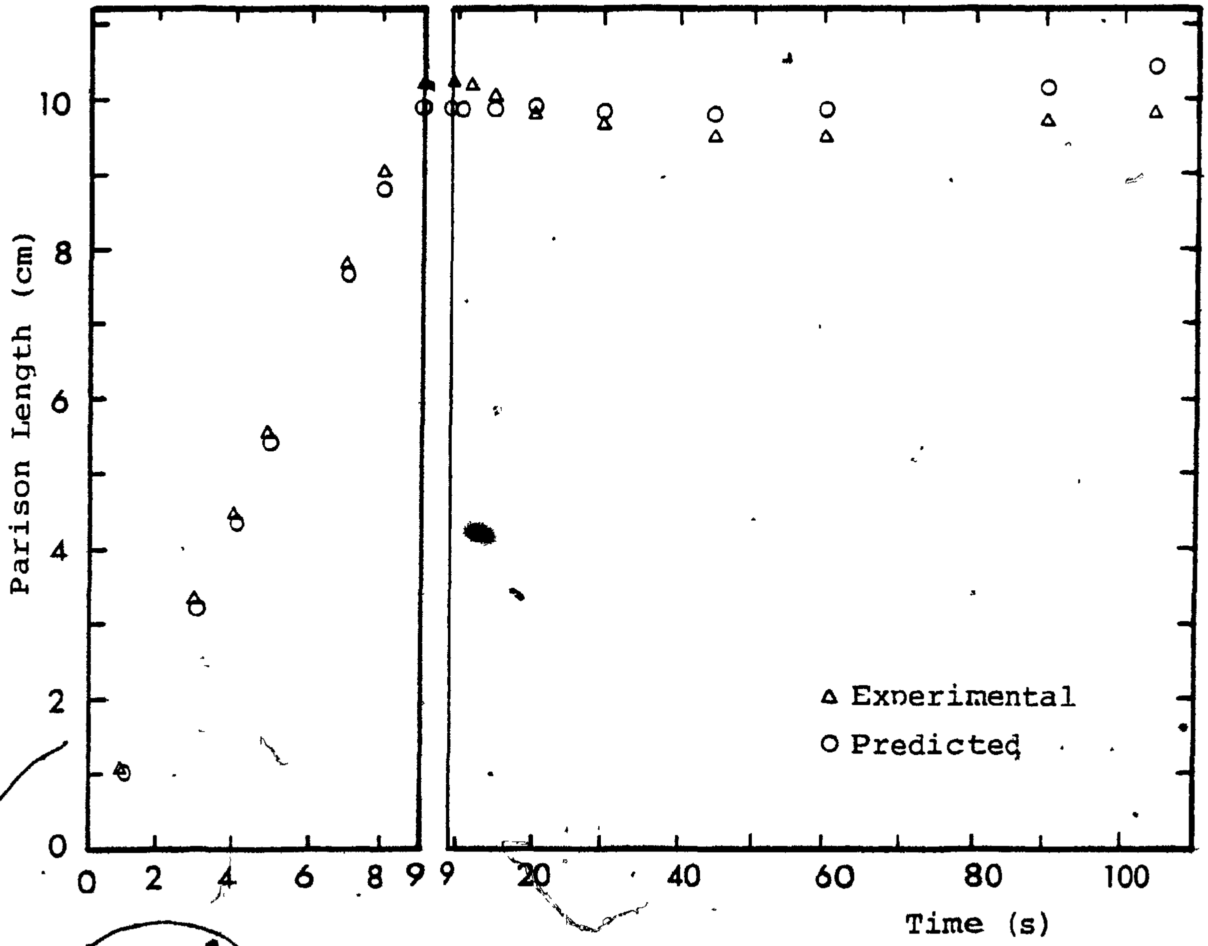

Figure 6.11 Comparison of Experimental and Predicted Values of Parison Length (Resin 27, Diverging Die, m = 6.8 g, Q = 0.950 cm^3/s)

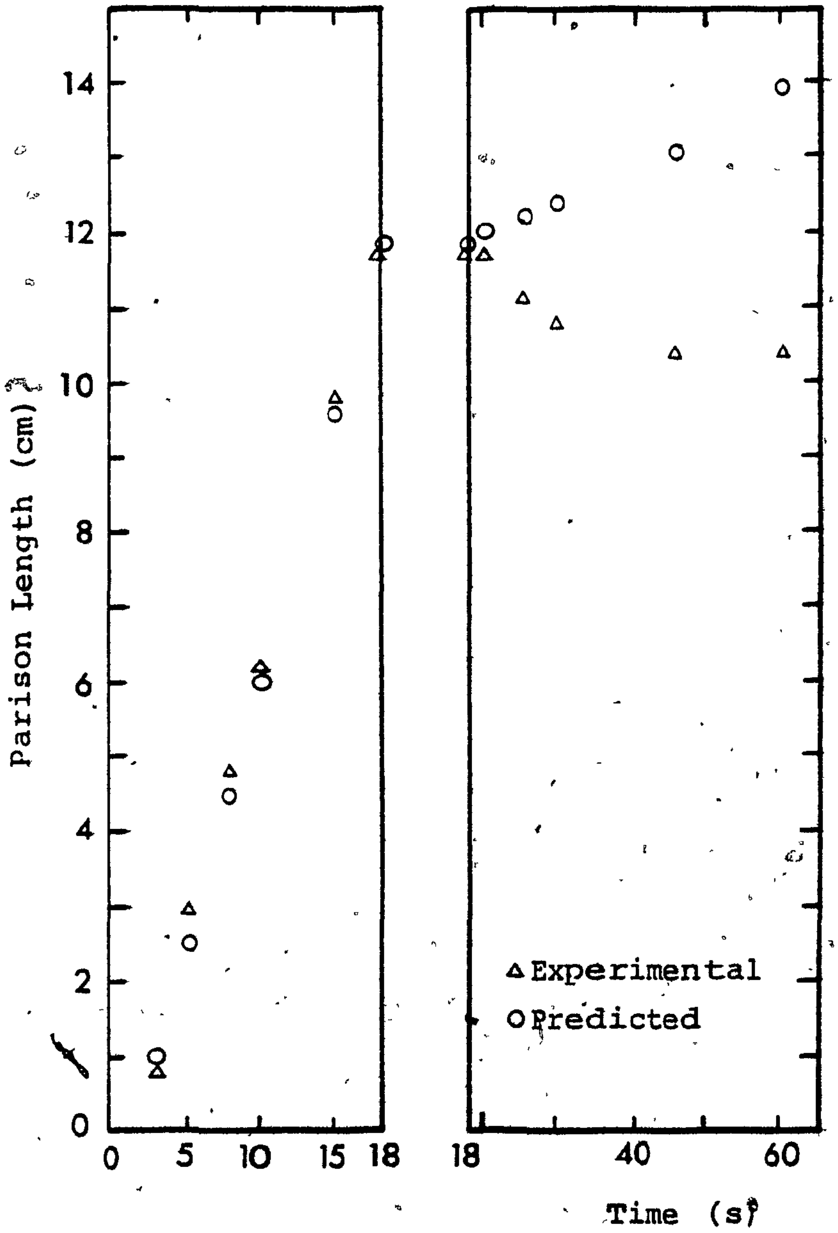

Figure 6.12 Comparison of Experimental and Predicted Values of Parison Length (Resin 27 20° Converging Die, m = 6.8 g Q = 0.475 cm^3/s)

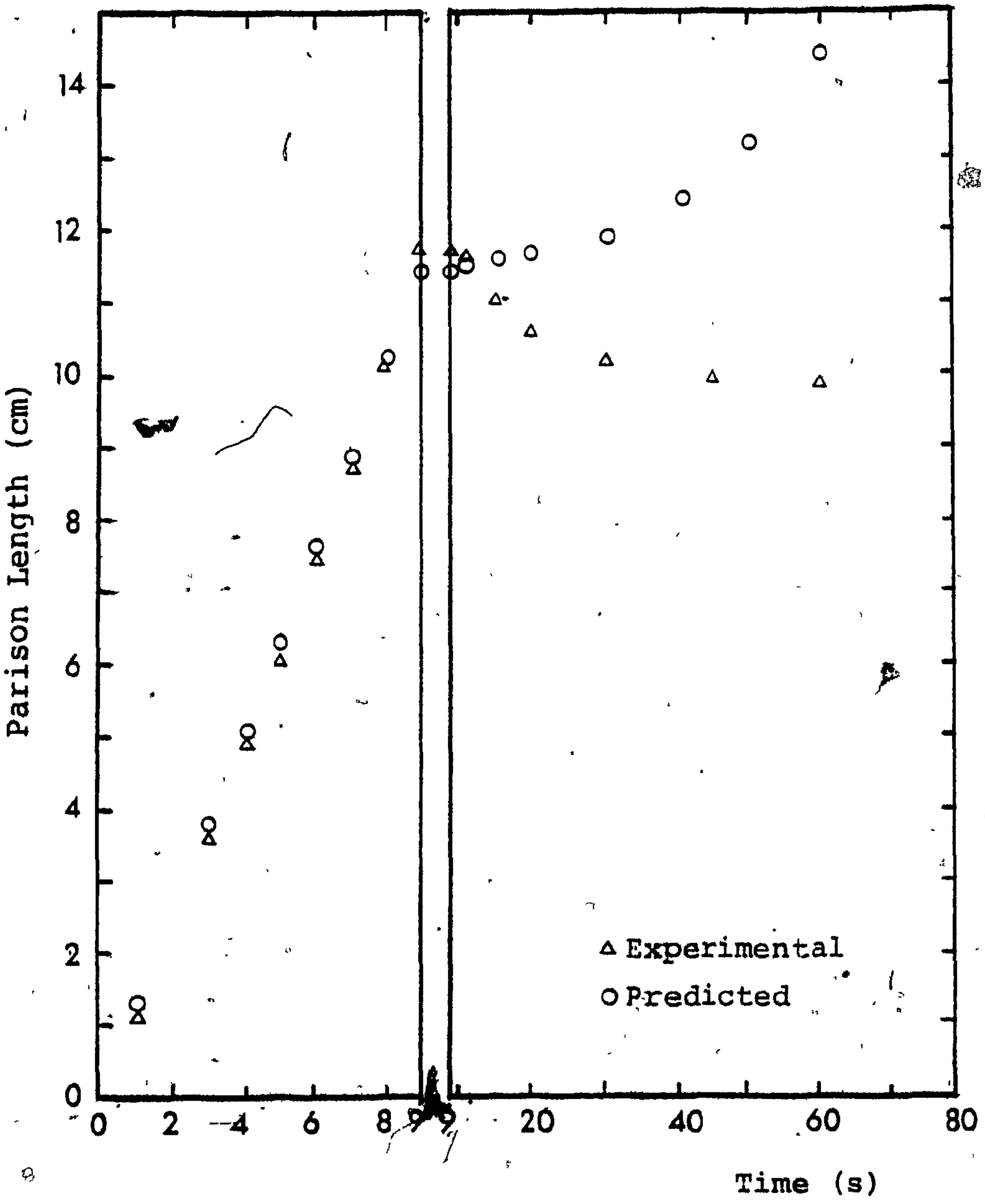

Figure 6.13 Comparison of Experimental and Predicted Values of Parison Length (Resin 27, 20° Converging Die, m = 6.8 g, Q = 0.950 cm^3/s)

in the case of the straight die, the model predictions and data are found to be in good agreement in the extrusion stage and at shorter times in the post-extrusion stage. At longer times the predictions are higher than the experimental data.

For the 20° converging die, it was observed that the model predictions are very poor in the post-extrusion stage. This is shown in Figures 6.12 and 6.13. The failure of the model for the 20° converging die is thought to result from the assumptions of the model. The large diameter swell obtained with this die renders invalid the assumptions that sag and swell are uncoupled and that sag is equivalent to uniaxial extension. In the actual case, of course, the two phenomena occur simultaneously and are coupled. In uniaxial extensional flow, there is a tendency of molecules to be oriented in the axial direction. Swell, on the other hand, is caused by a hoop orientation whereby the molecules tend to be oriented in the circumferential direction. Therefore, the assumptions that sag and swell are uncoupled and that sag is equivalent to uniaxial extension causes the model to over predict sag at longer times in the straight and diverging dies and leads to unacceptably large errors in the case of the 20° converging die where large values of swell are observed. To improve the predictions, sag and swell would have to be modelled as coupled phenomena. This would require elaborate calculations and a simple lumped parameter model would no longer be valid. Furthermore, it is not certain that such a sophisticated analysis would be successful since as was mentioned in section 4.2 current work attempting to model swell alone has not been successful to date.

Figure 6.14 shows parison behavior in the post-extrusion stage under different conditions. If there were no sag, the length of the parison would decrease continuously at a decelerating rate until the equilibrium swell value is obtained. This is represented by curve (1) of Figure 6.14. Curve (2) represents the case of no swell, and in this case the length of the parison in the post-extrusion stage will increase until it collapses. In the actual case the parison swells and sags simultaneously and this is shown by curve (3). The prediction of parison length depends on how the sag contribution is modelled. In the present model several alternatives were considered for the relation between elongational stress and strain. It was mentioned in section 6.3.1 that the possibility of using stress growth function in uniaxial elongation (at a constant strain rate) was examined. Lodge's rubber-like liquid model was used to evaluate the values of the stress growth function at a particular strain rate . An average value of strain rate was obtained for each element by trial and error. The predicted values of parison length using this method are

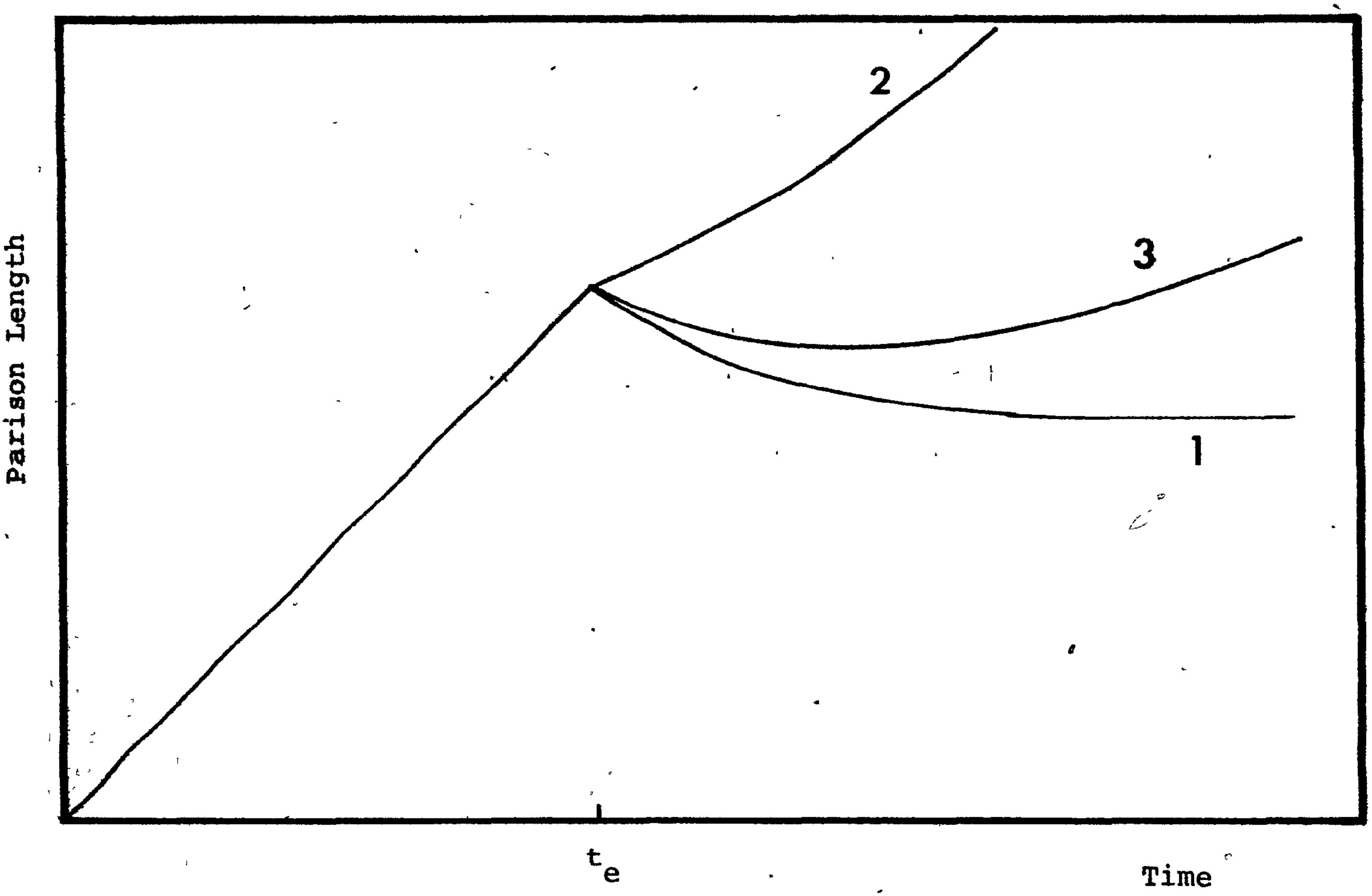

Figure 6.14 Parison Behaviour Under Different Conditions
(1): no sag, (2): no swell, (3): Actual case

shown in Figure 6.15. Also plotted on the same graph are the values of parison length obtained using Lodge's rubber-like liquid model for uniaxial extension in which the strain rate was taken to be both position and time-dependent and was integrated over the past history. The results show that the latter method gives better predictions and therefore this method was used for the rest of the calculations.

The relaxation spectrum (G_{ok}, λ_{ok}) used in Lodge's rubber-like liquid model was obtained from linear viscoelastic experiments. However, it is well known that the deformations the melt experience during its flow in the die alter its characteristics. Therefore, the possibility to account for such effects was also considered. For this purpose the model developed by Acierno et al. (1976) was used. This model has the distinctive feature of having relaxation times and moduli that depend upon the existing structure (i.e., strain history) with only one adjustable parameter. The model is a modified version of the convected Maxwell model, and it takes into account how the structure of the material changes with time when the material is deformed. This idea is represented by the concept of an entaglement density that varies with time. The structure-dependent relaxation spectrum (G_k and λ_k) is given by the following

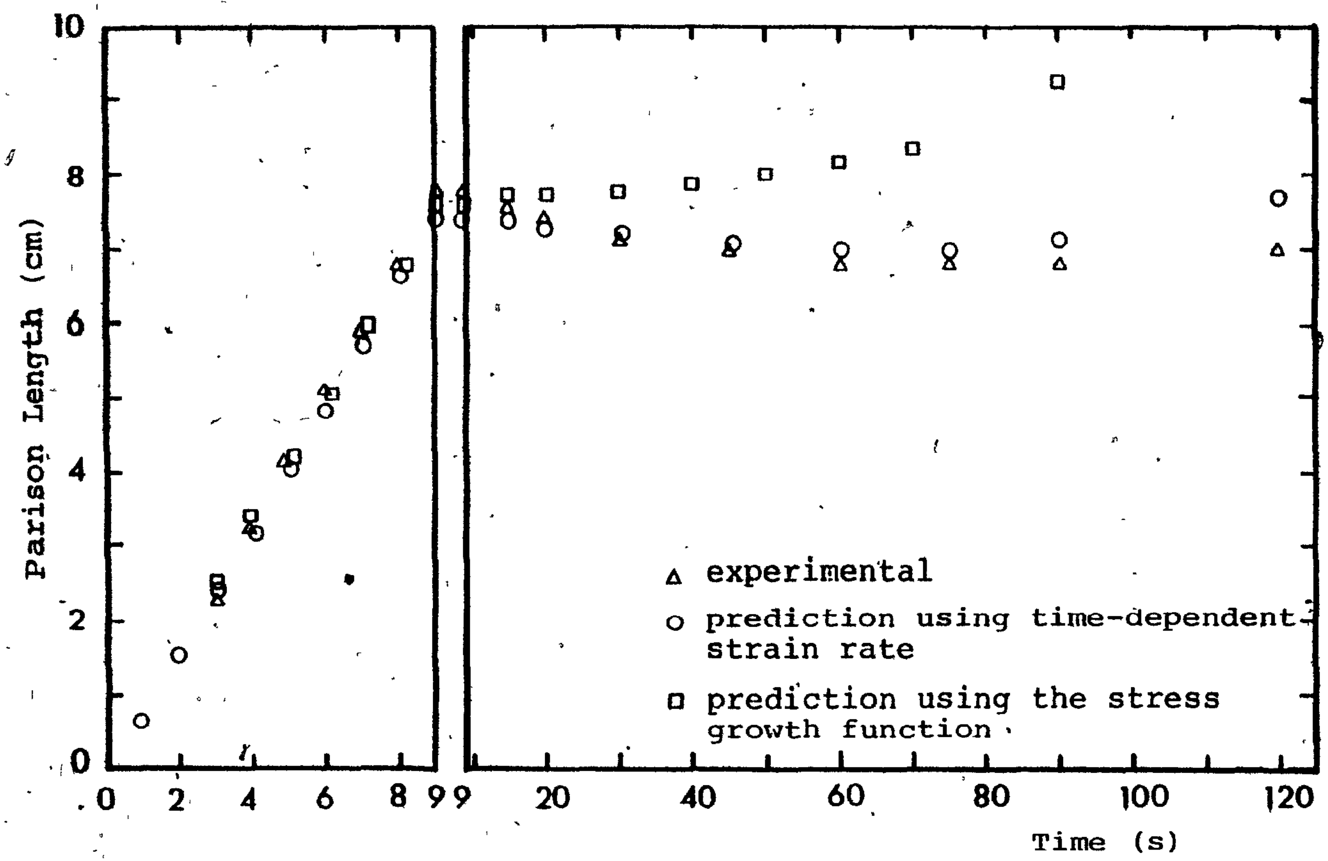

<u>Figure 6.14</u> Effect of the Relation Between Stress and Strain on Model Prediction (Resin 27, Straight Die, $m = 6.8$ g, $Q = 0.950\ cm^3/s$)

equations:

$$G_k = G_{ok}\, x_k \tag{6.4.1}$$

$$\lambda_k = \lambda_{ok}\, x_k^{1.4} \tag{6.4.2}$$

where the scalar quantity x_k is a structural parameter that describes how far the existing structure is from equilibrium ($x_k = 1$ is the equilibrium state). When the model equations are applied to steady shear flow the following equations are obtained for the viscosity and first normal stress difference (Acierno et al., 1976):

$$\eta_k = G_{ok}\lambda_{ok}x_k^{2.4} \tag{6.4.3}$$

$$N_{1k} = 2G_{ok}\lambda_{ok}^2\, x_k^{3.8}\, \dot{\gamma}^2 \tag{6.4.4}$$

$$N_1 = \Sigma N_{1k}\ , \quad \eta = \Sigma \eta_k \tag{6.4.5}$$

$$(1-x_k)/x_k^{2.4} = a'\lambda_{ok}\, \dot{\gamma} \tag{6.4.6}$$

where a' is the adjustable model parameter. The value of "a'" can be calculated using the above equations and the experimental η, N_1 data by trial and error procedure. This procedure is described in detail by Tsang (1981). In the present study the value of "a'" was found to be 1 using Tsang's (1981) procedure. The values of x_k were then calculated from equation 6.4.6 for each shear rate in the die. The structure dependent relaxation spectrum was calculated using equations 6.4.1 and 6.4.2 . However, using the structure-dependent relaxation spectrum did not improve the prediction of parison length. Therefore this method was not used in the calculations.

To summarize, a simple lumped-parameter model to predict the dimensions of the parison is developed and the capabilities and limitations of the model are studied. Previous reports of parison models have included very few comparisons with experiment, whereas the present model is tested using different die geometries, parison weights and extrusion velocities. The model predicts parison length with acceptable accuracy except in the case of the converging die.

CHAPTER 7

CONCLUSIONS AND RECOMMENDATIONS

7.1 Conclusions

In this section, the conclusions described in the previous chapters are summarized and presented in the same order in which they are presented in the main body of the thesis.

7.1.1 Conclusions regarding the pure swell experiments

1. Nearly 60-80% of both the diameter swell and thickness swell occurs in a short period of time after the parison is formed, but the equilibrium swell value is reached only after 5-8 minutes have elapsed. The exact relation between swell and time depends on the resin and die geometry.
2. Both diameter and thickness swells are increasing functions of shear rate, but the exact relation between swell and shear rate depends on the resin and die geometry.
3. Diameter swell at a given flow rate increases as die shape is altered in the following order: diverging, straight, converging.
4. A reduction in channel thickness along the length of the die enhances thickness swell.

5. Changing the mandrel of the die, while keeping the outer annular shell the same does not have a significant effect on diameter swell, i.e., diameter swell and thickness swell behave quite independently of each other.

6. The relation between die geometry and swell can be explained in terms of the tendency of the molecules, which have been oriented in the die, to return to a random configuration.

7. The ranking of the resins in terms of the magnitude of diameter swell was found to be the same for all the die geometries and extrusion rates used in this study.

8. The differences of behavior of resins in terms of swell cannot be explained in terms of the traditional rheological properties (e.g. shear viscosity, first normal stress difference and linear viscoelastic properties).

9. Swell was found to decrease with increasing weight average molecular weight and broadening molecular weight distribution.

10. The relation between diameter swell and thickness swell depends strongly on die design.

11. The diameter swell and thickness swell values are not equal, indicating that the swelling is not isotropic. The straight die and the 10° converging die give results closer to the isotropic case than the diverging and 20° converging dies.

12. The area swells evaluated at the same wall shear rate for two geometrically similar straight annular dies were nearly the same, but individual thickness and diameter swell values were quite different for the two cases.

7.1.2 Conclusions regarding swell combined with sag

1. The sag phenomenon can be modelled as a low strain rate uniaxial extensional deformation in which the strain rate is a function of time and position along the length of the parison, as long as the diameter swell is not too large.

2. The model predicts parison lengths with acceptable accuracy for different parison weights and extrusion rates except in the case of the converging die, for which the diameter swell is quite large.

7.2 Recommendations

1. The isothermal oil bath has to be modified to study very short-time swell phenomena.

2. A die similar to the obstructed flow die of Goettler et al. (1979), in which the channel thickness is increased, should be used to have a better understanding of the relation between die design and thickness swell.

3. Dies with different angles of divergence and convergence should be used.

4. Seperate experiments should be carried out to study the orientation caused by the particular dies which are used to obtain swell data.

7.3 Original Contributions

1. The time-dependency of diameter and thickness swell were determined.

2. The effects of die design, resin properties and extrusion rate on swell were determined.

3. The effect of die geometry on swell is explained qualitatively in terms of the orientation of the molecules caused by different die geometries.

4. A simple lumped-parameter model was developed to predict the length of the parison. The model uses swell data and storage modulus which can easily be obtained in the laboratory and the equations are simple enough to be solved using a desk computer. The applicabilty and limitations of the proposed model were determined using different die geometries, extrusion rates and parison weights.

REFERENCES

Acierno, D., LaMantia, F.P., Marucci, G., Titomanlio, G.,(1976), J. Non-Newt. Fl. Mech., 1,125

Ajroldi, G., (1978), Polym. Eng. Sci., 18(10),742

Bagley, E.B., (1957), J. Appl. Phys., 28, 624

Bagley, E.B., Duffey, H.J., (1970), Trans. Soc. Rheol., 14, 545

Basu, S., Rauwendaal, C., (1982), SPE Antec, 28, 720

Batchelor, J., Berry, J.P., Horsfall, F., (1973), Polymer, 14, 297

Bernhardt, E.C., (1959), "Processing of Thermoplastic Materials", Reinhold Publishing Co.

Bernstein, B., Kearsley, E., Zapas, L., (1963), Trans. Soc. Rheol., 7, 391

Billmeyer, F.W., (1971), "Textbook of Polymer Science", Wiley, NY

Bird, R.B., Armstrong, R.C., Hassager, O., (1977), "Dynamics of Polymeric Liquids", Volume I, Wiley, NY

Blower, K.E., Standish, N.W., (1973), Polym. Eng. Sci., 13, 222

Cancio, L.V., Hass, A.A., Shida, M., (1970), SPE Antec, 28, 148

Carnahan, B., Luther, H.A., Wilkes, J.O., (1969), "Applied Numerical Methods", Wiley, NY

Chang, H., Lodge, A.S., (1972), Rheol. Acta, 11, 127

Chang, P.W., Patten, T.W., Finlayson, B.A., (1979), Comp. Fluids, 7, 267

Chao, K.C., Wu, W., (1971), SPE J., 27, 37

Chee, K.K., Rudin, A., (1980), Rheol. Acta, 19, 76

Clifford, T.H., (1969), SPE J., 25, 32

Cogswell, F.N., (1970), Plast. Polym., (December 1970), 391

Cogswell, F.N., Webbs, P.C., Weeks, J.C., Maskell, S.G., Price, P.D.R., (1971), Plast.Polym., 39, 340

Coleman, C.J., (1971), J. Non-Newt. Fl. Mech., 8, 261

Cotten, G.R., (1979), Rubber Chem. Technol., 52, 187

Crochet, M.J., Keunings, R., (1980), J.Non-Newt. Fl. Mech., 7, 199

Crochet, M.J., Keunings, R., (1981), Proc. 2nd World Congr. Chem. Eng., Montreal, 285

Crochet, M.J., Keunings, R., (1982a), J. Non-Newt. Fl. Mech., 10, 339

Crochet, M.J., Keunings, R., (1982b), J.Non-Newt. Fl. Mech., 10, 85

Dealy, J.M., Garcia-Rejon, A., (1980), Proc. VIII th Int. Congr. Rheol., 3:63, Plenum Press, NY

Dealy, J.M., (1982), "Rheometers for Molten Plastics", Van Nostrand Reinhold Company, NY

Dutta, A., Ryan, M.E., (1982), J. Non-Newt. Fl. Mech., 10, 235

Ferry, J.D., (1980), "Viscoelastic Properties of Polymers", Wiley, NY

Fischer, E., (1981), SPE Antec, 27, 689

Franks, R.G.E., (1972), "Modelling and Simulation in Chemical Engineering", Wiley, NY

Garcia-Rejon, A., (1979), Ph.D Thesis, McGill University, Montreal

Goettler, L.A., Leib, R.I., Lambright, A.J., (1979), Rubber Chem. Technol., 52, 838

Graessley, W.W., Glasscock, S.D., Crawley, R.L., (1970), Trans. Soc. Rheol., 14, 519

Han, C.D., (1976), "Rheology in Polymer Processing", Academic Press, NY

Henze, E.D., Wu, W., (1973), Polym. Eng. Sci., 13, 153

Hoechst Plastics, (1976), "Blow Molding in Thermoplastics", 13

Horsfall, F., (1973), Polymer, 14, 262

Huang, D.C., White, J.L., (1979), Polym. Eng. Sci., 19, 609

Huang, D.C., White, J.L., (1980), Polym. Eng. Sci., 20, 182

Huang, D.C., Shroff, R.N., Shida, M., (1982), SPE Antec, 28

Instron Capillary Rheometer, (1976), Operating and Maintenance Instructions, Instron Co., Canton, MA

Kalyon, D., (1980), Ph.D Thesis, McGill University, Montreal

Kalyon, D., Tan, V., Kamal, M.R., (1980), Polym. Eng. Sci., 20, 773

Kamal, M.R., Tan, V., Kalyon, D., (1981), Polym. Eng. Sci., 21, 331

Leblanc, J.L., (1981), Rubber Chem. Technol., 54, 905

LeVan, N.T., (1972), M.S Thesis, McGill University, Montreal

Locati, G., (1976), Rheol. Acta, 15, 525

Lodge, A.S., (1974), "Body Tensor Fields in Continuum Mechanics", Academic Press, NY

Mendelson, R.A., Finger, F.L., (1975), J. of Appl. Polym. Sci., 19, 1061

Mendelson, R.A., Finger, F.L., Bagley, E., (1971), J. Polym. Sci., 35, 177

Mendelson, M.A., Yeh, P.W., Brown, R.A., Armstrong,R.C., (1982), J. Non-Newt. Fl. Mech., 10, 31

Middleman, S., Gavis, J., (1961), Phys. Fluids, 4, 355

Middleman, S., (1977), "Fundamentals of Polymer Processing", McGraw Hill, NY

Miller, J.C., (1975), Trans. Soc. Rheol., 19, 41

Nakajima, N., Shida, M., (1966), Trans. Soc. Rheol., 10, 299

Nakajima, N., (1974), Rheol. Acta, 13, 538

Nickell, R.E., Tanner, R.I., Caswell, B., (1974), J. Fluid Mech., 65, 189

Phuoc, H.B., Tanner,R.I., (1980), J. Fluid Mech., 98, 253

Plazek, D.J., Raghupathi, N., Kratz, R.F., Miller, W.R., (1979), J. Appl. Polym. Sci., 24, 1309

Pritchatt, R.J., Parnaby, J., Worth, R.A., (1975), Plast. Polym., (April 1975), 55

Racin, R., Bogue, D.C., (1979), J. Rheol., 23, 263

Reddy, K.R., Tanner, R.I., (1978), J. Rheol., 22, 661

Rheometrics Mechanical Spectrometer, Operations Manual, (1980), Rheometrics Inc.

Sheptak, N., Beyer, C.E., (1965), SPE J., 21, 190

Shroff, R.N., Shida, M., (1977), SPE Antec, 23, 285

Stratton, R.A., Butcher, A.F., (1971), J. Polym. Sci., A-2, 9, 1703

Suto, S., Fujimura, T., (1980), J. Appl. Polym. Sci., 25, 1509

Tadmor, Z., Gogos, C., (1979), "Principles of Polymer Processing", Wiley, NY

Tanner, R.I., (1970), J. Polym. Sci., A-28, 2067

Tanner, R.I., (1973), Appl. Polym. Symp., 20, 201

Tanner, R.I., (1982), J. Non-Newt. Fl. Mech., 10, 169

Terenzi, J.F., Griffith, R.M., Deeley, C.W., (1968), SPE J., 24, 37

Treloar, L.R.G., (1958), "The Physics of Rubber Elasticity", 2nd edition, Oxford Press

Tsang, W., (1981), Ph.D Thesis, McGill University, Montreal

Tschoegl, N.W., (1971), Rheol. Acta, 10, 582

Tschoegl, N.W., (1973), Rheol. Acta, 12, 82

Utracki, L.A., Kamal, M.R., Bakerdjian, Z., (1975), J.Appl. Polym. Sci., 19, 481

Vlachopoulos, J., Alam, M., (1972a), Polym. Eng. Sci., 12, 184

Vlachopoulos, J., Horie, M., Lidorikis, S., (1972b), Trans. Soc. Rheol., 16, 669

Vlachopoulos, J.,(1981a), "Reviews on the Deformation Behavior of Materials", Editor: P. Feltham, Freund Publishing, Tel-Aviv

Vlachopoulos, J., (1981b), Proc. 2nd World Congr. Chem. Eng., Montreal, 269

Walters, K., (1975), "Rheometry", Chapman and Hall, London

Wilson, N., Bentley, M., Morgan, B., (1970), SPE J., 26, 34

Winter, H.H., Fischer, E., (1981), Polym. Eng. Sci., 21, 366

Whipple, B.A., Hill, C.T., (1978), AIChE J., 24, 664

White, J.L., Roman, J.F., (1976), J. Appl. Polym. Sci., 20, 1005

White, J.L., Huang, D.C., (1981), Polym. Eng. Sci., 21, 1101

Worth, R.A., Parnaby, J., (1974), Trans. Instn. Chem. Engrs., 52, 368

NOMENCLATURE

a	Exponent in equation 5.3.7
a'	Acierno model adjustable parameter
A	Parameter of equation 5.3.7
A_b	Cross-sectional area of the barrel
A_d	Cross-sectional area of the die at the exit
A_i	Cross-sectional area of the i'th element
A_i'	Cross-sectional area of the unswollen element
B	Capillary die swell
B_A	Area swell
B_w	Weight swell
B_1	Diameter swell
B_2	Thickness swell
B_{1o}	Instantaneous diameter swell
B_{2o}	Instantaneous thickness swell
$B_{1\infty}$	Equilibrium diameter swell
$B_{2\infty}$	Equilibrium thickness swell
D	Diameter of capillary
D_p	Outside diameter of the parison
D_{od}	Outside diameter of the die at the exit
D_{id}	Inside diameter of the die at the exit
e	End correction (equation 2.3.9)
F	Force
G'	Storage modulus

G''	Loss modulus
G_k	k'th relaxation modulus
G_{ok}	k'th relaxation modulus at equilibrium
h_p	Thickness of the parison
h_o	Annular gap at the die exit
H	Thickness of the slit die
H_o	Relaxation spectrum
$\underline{H}^{-1}$	Finger tensor
J_o	Steady state shear compliance
L	Length of the parison; length of the die
L_i	Length of the i'th element
m	Weight of the parison
M	Torque
$\dot{M}$	Mass flow rate
$\bar{M}_w$	Weight average molecular weight
$\bar{M}_n$	Number average molecular weight
N	Number of parison elements that are fully extruded
N_1	First normal stress difference
N_2	Second normal stress difference
Q	Volumetric flow rate
R	Radius
R_{od}	Outside radius of the die at the exit
R_{id}	Inside radius of the die at the exit
R_{op}	Outside radius of the parison
R_{ip}	Inside radius of the parison

S_R	Recoverable shear strain
t	Time
t_e	Extrusion time
t_i	Time elapsed since the i'th element is fully extruded
t^*	Actual time (equation 6.3.24)
t'	Past time
v_e	Extrusion velocity in the barrel
v_d	Extrusion velocity at the die exit
z_i	Length of the hypothetical unswollen element

<u>Greek Symbols</u>

$\dot{\gamma}$	Shear rate
$\dot{\gamma}_A$	Apparent shear rate at the wall
$\dot{\gamma}_W$	Shear rate at the wall
δ	Mechanical loss angle
$\dot{\varepsilon}$	Extensional strain rate
$\dot{\varepsilon}_i$	Extensional strain rate of the i'th element
ζ_i	Characteristic time for swell (equation 6.3.11)
η	Viscosity
η_T^+	Stress growth function in extensional flow (constant strain rate)
η_T	Extensional viscosity
η^*	Complex viscosity
θ_o	Cone angle
$\Delta\theta$	Step-size for numerical integration

λ_k	k'th relaxation time
λ_{ok}	k'th relaxation time at equilibrium
ρ	Density
τ_{12}	Shear stress
τ_w	Shear stress at the wall
τ_{11}	Normal stress
τ_i	Stretching stress of the i'th element
ϕ_o	Displacement amplitude for rotational oscillation
Ψ_1	First normal stress difference coefficient
Ψ_2	Second normal stress difference coefficient
ω	Frequency (rad/s)
Ω	Rotational speed (rad/s)

Addenda

MWD	Molecular weight distribution
HDPE	High density polyethylene
LDPE	Low density polyethylene
PI	Polydispersity index
PP	Polypropylene
PS	Polystyrene

APPENDIX A1

Molecular Weight Distribution Curves for the Resins

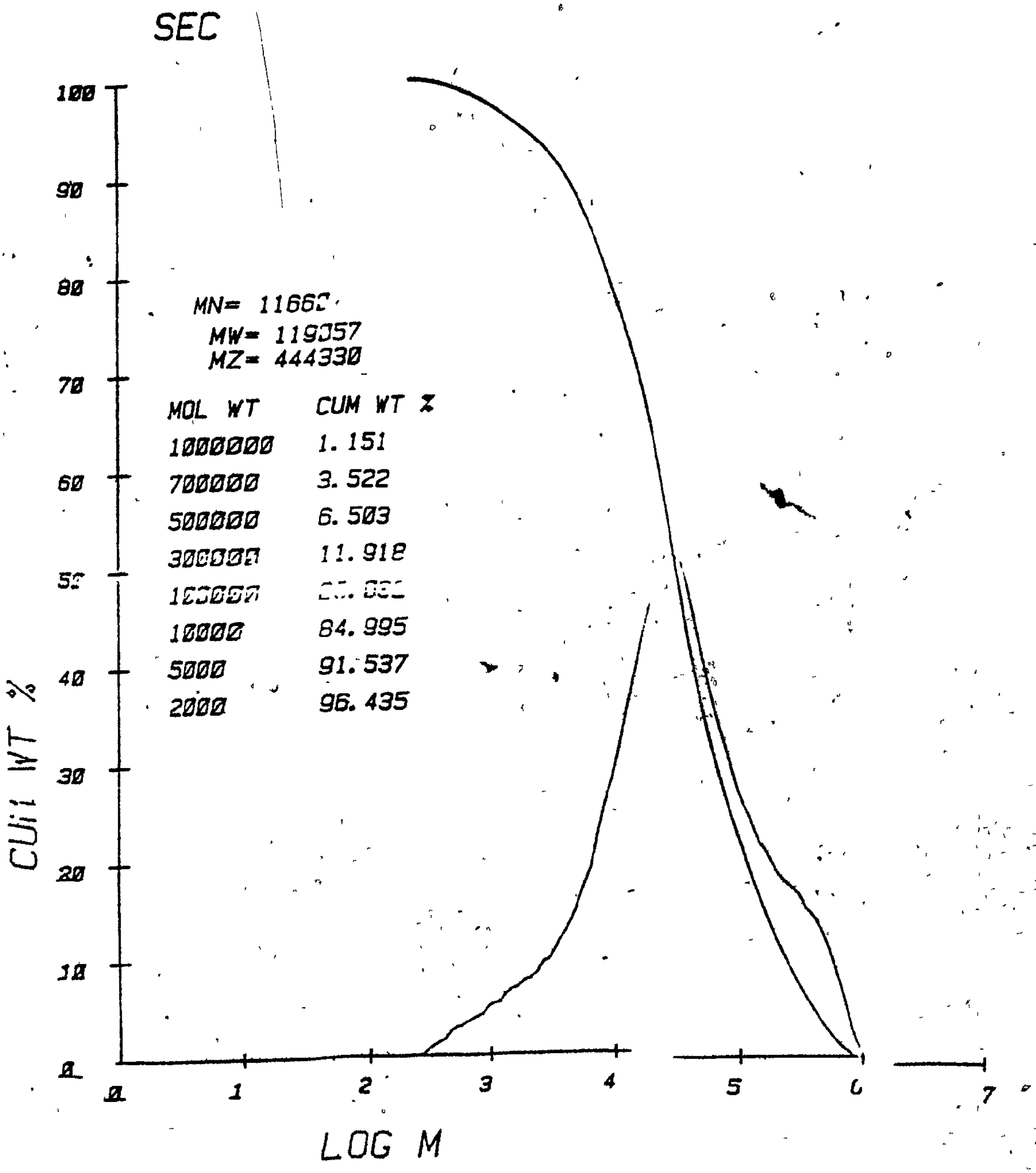

MN= 11660
MW= 119057
MZ= 444330

MOL WT	CUM WT %
1000000	1.151
700000	3.522
500000	6.503
300000	11.918
100000	[illegible]
10000	84.995
5000	91.537
2000	96.435

Figure A1.1 Molecular Weight Distribution of Resin 22A

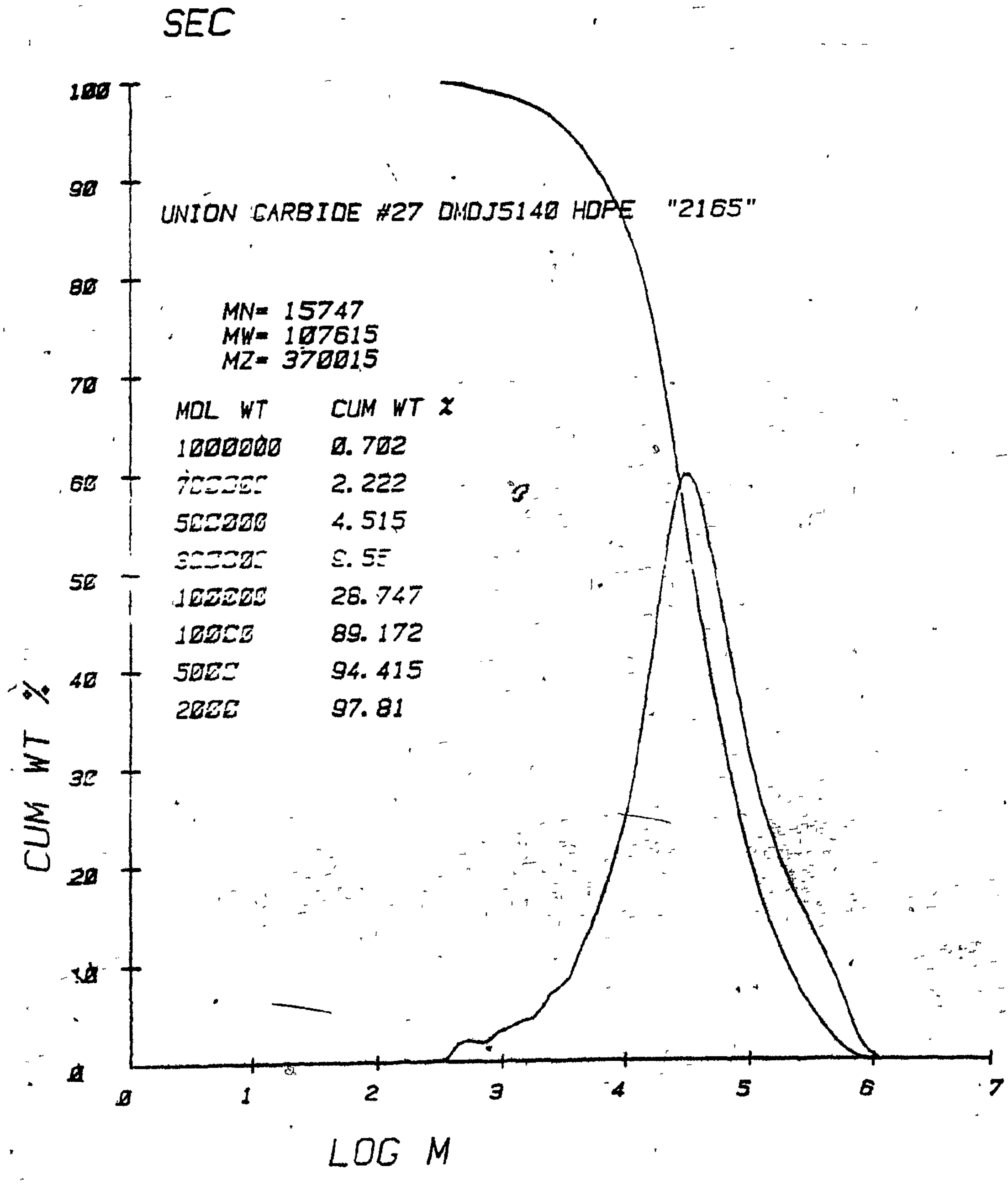

UNION CARBIDE #27 DMDJ5140 HDPE "2165"

MN= 15747
MW= 107615
MZ= 370015

MOL WT	CUM WT %
1000000	0.702
700000	2.222
500000	4.515
300000	8.5[illegible]
100000	26.747
10000	89.172
5000	94.415
2000	97.81

Figure A1.2 Molecular Weight Distribution of Resin 27

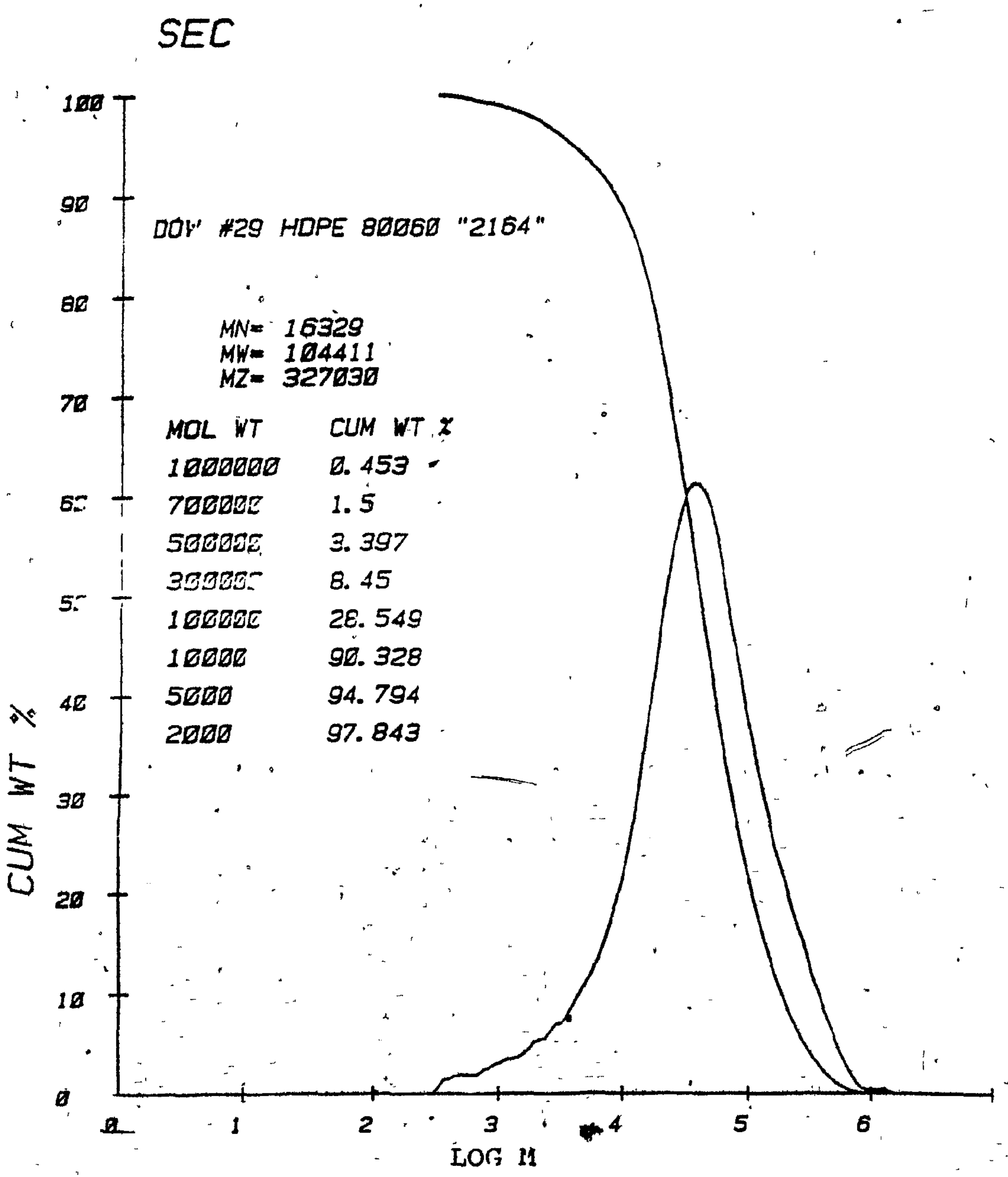

DOW #29 HDPE 80060 "2164"

MN= 16329
MW= 104411
MZ= 327030

MOL WT	CUM WT %
1000000	0.453
700000	1.5
500000	3.397
300000	8.45
100000	28.549
10000	90.328
5000	94.794
2000	97.843

Figure A1.3 Molecular Weight Distribution of Resin 29

APPENDIX A2

Rheological Characterization Data

TABLE A2.1 First Normal Stress Difference at 170°C

Shear rate (s^{-1})	N_1($Pa \times 10^{-3}$)		
	Resin 27	Resin 22A	Resin 29
0.063	3.064	2.060	4.395
0.100	3.989	3.101	5.990
0.158	5.194	4.429	7.214
0.251	6.101	5.494	8.920
0.398	7.991	7.856	11.130
0.631	9.928	11.900	11.930
1.000	12.140	16.690	13.160
1.585	17.540	22.000	16.070

TABLE A2.2 Shear Viscosity at 170°C

Shear rate (s^{-1})	η (Pa.s×10^{-3})		
	Resin 27	Resin 22A	Resin 29
0.063	33.060	31.850	47.180
0.100	29.070	28.780	37.780
0.158	24.720	25.720	29.950
0.251	20.700	22.910	22.370
0.398	16.490	19.880	17.290
0.631	13.040	16.720	13.390
1.000	10.470	13.310	10.500
1.585	9.012	9.078	8.316
2.9	7.746	6.848	7.896
6	5.479	4.964	5.957
12.5	4.242	3.474	4.441
34	2.560	1.985	2.542
70	1.651	1.381	1.717
149	1.061	0.839	1.092
405	0.571	0.423	0.618
880	0.310	0.266	0.366

TABLE A2.3 Complex Viscosity (η^*) at 170°C

Frequency (rad/s)	η^*(Pa.s×10^{-3})		
	Resin 27	Resin 22A	Resin 29
0.100	29.060	28.690	31.740
0.158	25.730	25.290	26.140
0.251	22.690	22.150	21.760
0.398	19.870	19.240	17.980
0.631	17.230	16.470	14.820
1.000	14.860	13.950	21.100
1.585	12.680	11.620	10.030
2.512	10.650	9.600	8.223
3.981	8.918	7.810	6.702
6.310	7.370	6.290	5.450
10.000	6.023	5.002	4.412

TABLE A2.4 Storage Modulus (G') at 170°C

Frequency (rad/s)	G' (Pa×10^{-3})		
	Resin 27	Resin 22A	Resin 29
0.100	1.980	1.115	1.822
0.158	2.873	1.668	2.423
0.251	3.980	2.496	3.254
0.398	5.113	3.705	4.315
0.631	7.100	5.386	5.704
1.000	9.200	7.701	7.432
1.585	11.900	10.820	9.994
2.512	15.000	14.960	13.150
3.981	18.200	20.250	17.250
6.310	22.230	27.000	22.680
10.000	26.210	35.400	29.710

APPENDIX A3

Data Obtained in the Pure Swell Experiments

TABLE A3.1 Swell as a Function of Time

(Straight Die, Resin 22A)

$Q = 0.024\ cm^3/s$			$Q = 0.095\ cm^3/s$		
t(s)	B_1	B_2	t(s)	B_1	B_2
1	1.06	-	1	1.08	-
3	1.08	-	3	1.11	-
5	1.10	-	5	1.12	-
10	1.11	-	30	1.19	1.10
120	1.19	1.11	45	1.23	1.13
150	1.21	1.13	75	1.24	1.16
225	1.25	1.15	120	1.28	1.20
300	1.30	1.20	150	1.30	1.25
360	1.31	1.22	225	1.34	1.27
480	1.33	1.26	300	1.36	1.27
540	1.33	1.26	360	1.38	1.29
600	1.33	1.26	420	1.38	1.29
			540	1.38	1.29
			600	1.38	1.29

TABLE A3.2 Swell as a Function of Time

(Straight Die, Resin 22A)

$Q = 0.238\ cm^3/s$			$Q = 0.475\ cm^3/s$		
t(s)	B_1	B_2	t(s)	B_1	B_2
1	1.15	-	1	1.20	-
3	1.18	-	3	1.24	-
5	1.20	1.05	5	1.26	1.10
10	1.23	1.08	10	1.30	1.12
30	1.26	1.11	30	1.34	1.15
45	1.28	1.14	45	1.36	1.19
75	1.31	1.17	75	1.38	1.24
120	1.33	1.23	120	1.41	1.30
150	1.37	1.25	150	1.44	1.32
225	1.40	1.27	225	1.46	1.37
300	1.42	1.29	300	1.48	1.40
360	1.44	1.31	360	1.51	1.41
480	1.46	1.34	480	1.53	1.43
540	1.46	1.34	540	1.53	1.43
600	1.46	1.34	600	1.53	1.43

TABLE A3.3 Swell as a Function of Time

(Straight Die, Resin 22A)

	$Q = 0.950$ cm^3/s			$Q = 2.375$ cm^3/s	
t(s)	B_1	B_2	t(s)	B_1	B_2
1	1.28	-	1	1.32	-
3	1.33	-	3	1.37	1.31
5	1.34	1.20	5	1.39	1.35
10	1.37	1.23	10	1.44	1.37
30	1.43	1.29	30	1.53	1.41
45	1.49	1.33	45	1.55	1.44
75	1.54	1.39	75	1.59	1.50
120	1.59	1.46	120	1.64	1.56
150	1.61	1.48	150	1.66	1.60
225	1.64	1.52	225	1.68	1.69
300	1.66	1.54	300	1.71	1.74
360	1.68	1.56	360	1.73	1.78
480	1.68	1.56	480	1.76	1.80
540	1.68	1.56	540	1.76	1.80
600	1.68	1.56	600	1.76	1.80

TABLE A3.4 Swell as a Function of Time

(Straight Die, Resin 27)

$Q = 0.024\ cm^3/s$

t(s)	B_1	B_2
2	1.10	–
5	1.14	–
120	1.24	1.26
150	1.27	1.28
225	1.33	1.35
300	1.36	1.42
360	1.37	1.46
420	1.38	1.50
480	1.38	1.54
540	1.39	1.54
600	1.39	1.54

$Q = 0.095\ cm^3/s$

t(s)	B_1	B_2
2	1.23	–
5	1.26	–
10	1.28	–
30	1.35	1.25
45	1.38	1.28
75	1.43	1.33
120	1.49	1.40
150	1.51	1.45
225	1.56	1.56
300	1.61	1.64
360	1.64	1.69
420	1.65	1.72
480	1.65	1.74
540	1.65	1.74
600	1.65	1.74

TABLE A3.5 Swell as a Function of Time

(Straight Die, Resin 27)

Q = 0.238 cm^3/s			Q = 0.475 cm^3/s		
t(s)	B_1	B_2	t(s)	B_1	B_2
2	1.25	-	2	1.28	-
5	1.30	1.26	5	1.33	1.40
10	1.34	1.28	10	1.37	1.43
30	1.42	1.32	30	1.48	1.49
45	1.45	1.35	45	1.53	1.53
75	1.49	1.42	75	1.59	1.60
120	1.56	1.49	120	1.65	1.66
150	1.59	1.54	150	1.69	1.70
225	1.65	1.65	225	1.71	1.75
300	1.69	1.70	300	1.73	1.80
360	1.71	1.75	360	1.75	1.83
480	1.71	1.79	480	1.76	1.89
540	1.71	1.79	540	1.76	1.89
600	1.71	1.79	600	1.76	1.89

TABLE A3.6 Swell as a Function of Time

(Straight Die, Resin 27)

$Q = 0.950\ cm^3/s$			$Q = 2.375\ cm^3/s$		
t(s)	B_1	B_2	t(s)	B_1	B_2
2	1.34	–	1	1.25	–
4	1.36	1.45	3	1.39	1.41
5	1.38	1.48	5	1.44	1.50
10	1.44	1.52	10	1.48	1.56
30	1.50	1.58	30	1.57	1.66
45	1.56	1.62	45	1.63	1.70
75	1.63	1.68	75	1.69	1.80
120	1.68	1.78	120	1.78	1.88
150	1.71	1.81	150	1.81	1.91
225	1.76	1.89	225	1.87	1.97
300	1.78	1.92	300	1.90	2.02
480	1.80	1.95	480	1.97	2.09
540	1.80	1.95	540	1.97	2.09
600	1.80	1.95	600	1.97	2.09

TABLE A3.7 Swell as a Function of Time (Straight Die, Resin 29)

$Q = 0.095\ cm^3/s$

t(s)	B_1	B_2
1	1.05	-
3	1.13	-
5	1.16	-
30	1.23	-
45	1.28	-
75	1.36	-
120	1.45	-
150	1.48	-
225	1.50	-
300	1.51	1.60
360	1.52	1.60
480	1.52	1.60
540	1.52	1.60
600	1.52	1.60

TABLE A3.8 Swell as a Function of Time

(Straight Die, Resin 29)

$Q = 0.238\ cm^3/s$			$Q = 0.475\ cm^3/s$		
t(s)	B_1	B_2	t(s)	B_1	B_2
1	1.12	-	1	1.14	-
2	1.18	-	2	1.18	-
3	1.20	-	3	1.20	-
5	1.21	-	5	1.25	-
10	1.24	-	10	1.33	-
30	1.32	-	30	1.40	-
45	1.37	-	45	1.45	-
75	1.44	-	75	1.52	-
120	1.52	-	120	1.58	-
150	1.53	-	150	1.59	-
225	1.54	-	225	1.60	-
300	1.55	-	300	1.61	-
360	1.56	-	360	1.63	-
480	1.56	1.76	480	1.63	1.96
540	1.56	1.76	540	1.63	1.96
600	1.56	1.76	600	1.63	1.96

TABLE A3.9 Swell as a Function of Time

(Straight Die, Resin 29)

$Q = 0.950\ cm^3/s$			$Q = 2.375\ cm^3/s$		
t(s)	B_1	B_2	t(s)	B_1	B_2
1	1.18	-	1	1.22	-
3	1.28	-	3	1.31	-
5	1.31	-	5	1.37	-
10	1.36	-	10	1.46	-
30	1.48	-	30	1.58	-
45	1.55	-	45	1.64	-
75	1.58	-	75	1.70	-
120	1.62	-	120	1.72	-
150	1.64	-	150	1.72	-
225	1.65	-	225	1.74	-
300	1.66	-	300	1.75	-
360	1.68	-	360	1.76	-
480	1.68	2.05	480	1.77	2.15
540	1.68	2.05	540	1.77	2.15
600	1.68	2.05	540	1.77	2.15

TABLE A3.10 Swell as a Function of Time

(Diverging die, Resin 22A)

$Q = 0.024\ cm^3/s$

t(s)	B_1	B_2
1	1.00	-
3	1.00	-
5	1.00	-
120	1.00	1.07
150	1.00	1.10
225	1.02	1.14
300	1.02	1.18
360	1.02	1.21
480	1.02	1.24
540	1.02	1.24
600	1.02	1.24

$Q = 0.095\ cm^3/s$

t(s)	B_1	B_2
1	1.00	-
3	1.00	-
5	1.00	-
30	1.00	1.05
45	1.00	1.07
75	1.01	1.09
120	1.02	1.13
150	1.03	1.16
225	1.05	1.20
300	1.07	1.24
360	1.09	1.27
480	1.11	1.29
540	1.11	1.29
600	1.11	1.29

TABLE A3.11 Swell as a Function of Time

(Diverging Die, Resin 22A)

$Q = 0.238\ cm^3/s$			$Q = 0.475\ cm^3/s$		
t(s)	B_1	B_2	t(s)	B_1	B_2
1	1.00	-	1	1.00	-
3	1.00	-	3	1.00	-
5	1.00	1.12	5	1.00	1.13
10	1.00	1.14	10	1.02	1.15
30	1.02	1.17	30	1.04	1.19
45	1.03	1.19	45	1.05	1.24
75	1.04	1.23	75	1.07	1.28
120	1.06	1.27	120	1.09	1.34
150	1.07	1.29	150	1.10	1.37
225	1.09	1.33	225	1.12	1.40
300	1.11	1.35	300	1.15	1.44
360	1.13	1.38	360	1.16	1.47
480	1.16	1.40	480	1.20	1.50
540	1.16	1.40	540	1.20	1.50
600	1.16	1.40	600	1.20	1.50

TABLE A3.12 Swell as a Function of Time

(Diverging Die, Resin 22A)

$Q = 0.950\ \text{cm}^3/\text{s}$			$Q = 2.375\ \text{cm}^3/\text{s}$		
t(s)	B_1	B_2	t(s)	B_1	B_2
1	1.00	-	1	1.00	-
3	1.00	1.05	3	1.00	1.14
5	1.00	1.17	5	1.00	1.21
10	1.00	1.23	10	1.00	1.30
30	1.04	1.33	31	1.06	1.40
45	1.07	1.37	45	1.09	1.44
75	1.10	1.42	75	1.12	1.50
120	1.13	1.46	120	1.15	1.57
150	1.15	1.49	150	1.17	1.60
225	1.17	1.52	225	1.20	1.62
300	1.19	1.55	300	1.21	1.64
360	1.20	1.57	360	1.23	1.64
480	1.23	1.57	480	1.25	1.64
540	1.23	1.57	540	1.25	1.64
600	1.23	1.57	600	1.25	1.64

TABLE A3.13 Swell as a Function of Time (Diverging Die, Resin 27)

$Q = 0.024\ cm^3/s$			$Q = 0.095\ cm^3/s$		
t(s)	B_1	B_2	t(s)	B_1	B_2
1	1.00	–	1	1.00	–
3	1.00	–	3	1.00	–
105	1.03	1.26	5	1.01	–
120	1.04	1.28	30	1.01	1.16
150	1.07	1.30	45	1.02	1.21
225	1.10	1.35	75	1.04	1.26
300	1.13	1.39	120	1.08	1.32
360	1.15	1.43	150	1.11	1.36
420	1.17	1.46	225	1.14	1.45
480	1.19	1.49	300	1.16	1.52
540	1.19	1.49	360	1.18	1.57
600	1.19	1.49	480	1.24	1.65
			540	1.24	1.65
			600	1.24	1.65

TABLE A3.14 Swell as a Function of Time
(Diverging Die, Resin 27)

$Q = 0.238\ cm^3/s$			$Q = 0.475\ cm^3/s$		
t(s)	B_1	B_2	t(s)	B_1	B_2
1	1.00	-	1	1.01	-
3	1.01	-	3	1.01	-
5	1.00	1.08	5	1.02	1.20
10	1.00	1.15	10	1.04	1.35
30	1.01	1.25	30	1.07	1.51
45	1.04	1.29	45	1.10	1.56
75	1.08	1.35	75	1.13	1.63
120	1.13	1.42	120	1.17	1.70
150	1.15	1.47	150	1.19	1.75
225	1.19	1.58	225	1.23	1.83
300	1.22	1.68	300	1.26	1.89
360	1.25	1.74	360	1.28	1.93
480	1.27	1.78	480	1.32	1.95
540	1.27	1.78	540	1.32	1.95
600	1.27	1.78	600	1.32	1.95

TABLE A3.15 Swell as a Function of Time

(Diverging Die, Resin 27)

Q = 0.950 cm^3/s			Q = 2.375 cm^3/s		
t(s)	B_1	B_2	t(s)	B_1	B_2
1	1.01	-	1	1.02	-
3	1.02	1.29	3	1.03	1.33
5	1.04	1.34	5	1.07	1.47
10	1.06	1.43	10	1.10	1.55
30	1.11	1.55	30	1.15	1.68
45	1.14	1.60	45	1.18	1.74
75	1.19	1.69	75	1.23	1.82
120	1.23	1.81	120	1.27	1.91
150	1.26	1.85	150	1.30	1.96
225	1.30	1.95	225	1.33	2.06
300	1.33	2.02	300	1.36	2.12
360	1.35	2.06	360	1.38	2.15
480	1.38	2.10	480	1.41	2.17
540	1.38	2.10	540	1.41	2.17
600	1.38	2.10	600	1.41	2.17

TABLE A3.16 Swell as a Function of Time

(Diverging Die, Resin 29)

$Q = 0.024\ cm^3/s$			$Q = 0.095\ cm^3/s$		
t(s)	B_1	B_2	t(s)	B_1	B_2
1	1.00	-	1	1.00	-
3	1.00	-	3	1.00	-
5	1.00	-	5	1.01	-
120	1.01	1.19	30	1.01	1.19
150	1.02	1.25	45	1.02	1.28
225	1.03	1.35	75	1.03	1.37
300	1.05	1.42	120	1.06	1.49
360	1.07	1.46	150	1.08	1.53
420	1.08	1.49	225	1.11	1.60
480	1.10	1.52	300	1.13	1.62
540	1.10	1.52	480	1.17	1.63
600	1.10	1.52	540	1.17	1.63
			600	1.17	1.63

TABLE A3.17 Swell as a Function of Time

(Diverging Die, Resin 29)

$Q = 0.238$ cm^3/s			$Q = 0.475$ cm^3/s		
t(s)	B_1	B_2	t(s)	B_1	B_2
1	1.00	-	1	1.00	-
3	1.00	-	3	1.00	-
5	1.00	1.05	5	1.00	1.15
10	1.00	1.13	10	1.02	1.33
30	1.04	1.29	30	1.05	1.43
45	1.05	1.37	45	1.08	1.47
75	1.08	1.46	75	1.10	1.54
120	1.11	1.58	120	1.15	1.64
150	1.12	1.62	150	1.17	1.69
225	1.16	1.68	225	1.20	1.83
300	1.18	1.73	300	1.22	1.93
360	1.21	1.74	360	1.24	1.96
540	1.21	1.74	480	1.24	1.98
600	1.21	1.74	540	1.24	1.98
			600	1.24	1.98

TABLE A3.18 Swell as a Function of Time

(Diverging Die, Resin 29)

$Q = 0.950$ cm^3/s			$Q = 2.375$ cm^3/s		
t(s)	B_1	B_2	t(s)	B_1	B_2
1	1.01	-	1	1.02	-
3	1.02	1.27	3	1.02	1.44
5	1.02	1.35	5	1.03	1.53
10	1.03	1.43	10	1.05	1.61
30	1.08	1.52	30	1.12	1.81
45	1.10	1.56	45	1.15	1.85
75	1.14	1.64	75	1.18	1.92
120	1.17	1.74	120	1.22	2.01
150	1.19	1.79	150	1.24	2.07
225	1.22	1.91	225	1.27	2.18
300	1.23	2.00	300	1.29	2.22
360	1.24	2.06	360	1.31	2.24
480	1.26	2.10	480	1.33	2.25
540	1.26	2.10	540	1.33	2.25
600	1.26	2.10	600	1.33	2.25

TABLE A3.19 Swell as a Function of Time
(20° Converging Die, Resin 22A)

$Q = 0.024\ cm^3/s$			$Q = 0.095\ cm^3/s$		
t(s)	B_1	B_2	t(s)	B_1	B_2
1	1.05	-	1	1.18	-
3	1.08	-	3	1.39	-
5	1.19	-	5	1.43	-
120	1.47	1.30	30	1.70	1.38
135	1.50	1.34	60	1.76	1.44
180	1.55	1.40	75	1.78	1.47
225	1.60	1.43	135	1.84	1.52
300	1.66	1.45	180	1.88	1.56
420	1.72	1.45	245	1.94	1.59
540	1.74	1.45	300	1.96	1.60
600	1.74	1.45	420	2.01	1.61
			540	2.04	1.61
			600	2.04	1.61

TABLE A3.20 Swell as a Function of Time

(20° Converging Die, Resin 22A)

$Q = 0.238\ cm^3/s$			$Q = 0.475\ cm^3/s$		
t(s)	B_1	B_2	t(s)	B_1	B_2
1	1.24	-	1	1.33	-
3	1.61	-	3	1.75	-
7	1.68	1.27	5	1.81	1.31
10	1.71	1.30	10	1.84	1.36
20	1.76	1.34	20	1.90	1.38
45	1.82	1.42	30	1.96	1.43
60	1.87	1.44	45	2.02	1.47
75	1.90	1.47	90	2.14	1.54
90	1.92	1.49	150	2.20	1.59
135	1.98	1.53	240	2.26	1.66
225	2.08	1.60	330	2.32	1.70
300	2.11	1.62	420	2.35	1.71
360	2.14	1.64	540	2.38	1.71
420	2.16	1.65	600	2.38	1.71
480	2.18	1.65			
540	2.18	1.65			
600	2.18	1.65			

TABLE A3.21 Swell as a Function of Time

(20° Converging Die, Resin 22A)

$Q = 0.950\ cm^3/s$			$Q = 2.375\ cm^3/s$		
t(s)	B_1	B_2	t(s)	B_1	B_2
1	1.39	-	1	1.55	-
3	1.83	1.35	3	1.95	1.45
5	1.89	1.39	5	2.15	1.51
10	1.98	1.43	10	2.27	1.57
30	2.11	1.51	30	2.33	1.71
75	2.24	1.61	45	2.39	1.77
150	2.33	1.70	90	2.45	1.89
210	2.39	1.73	150	2.52	1.96
300	2.46	1.78	210	2.58	1.98
420	2.49	1.83	300	2.65	1.99
480	2.52	1.85	480	2.68	2.01
540	2.53	1.85	540	2.68	2.01
600	2.53	1.85	600	2.68	2.01

TABLE A3.22 Swell as a Function of Time

(20° Converging Die, Resin 27)

$Q = 0.024$ cm^3/s			$Q = 0.095$ cm^3/s		
t(s)	B_1	B_2	t(s)	B_1	B_2
1	1.17	-	1	1.35	-
2	1.25	-	2	1.43	-
5	1.33	-	5	1.56	-
120	1.87	1.42	30	1.81	1.24
165	1.93	1.47	45	1.86	1.34
240	2.01	1.52	60	1.91	1.39
300	2.06	1.55	75	1.96	1.44
390	2.08	1.59	120	2.06	1.52
480	2.12	1.62	165	2.17	1.57
540	2.12	1.62	225	2.27	1.65
600	2.12	1.62	300	2.36	1.69
			360	2.43	1.71
			420	2.48	1.73
			480	2.53	1.75
			540	2.53	1.75
			600	2.53	1.75

TABLE A3.23 Swell as a Function of Time
(20° Converging Die, Resin 27)

$Q = 0.238\ cm^3/s$

t(s)	B_1	B_2
1	1.42	–
3	1.60	–
5	1.68	1.12
10	1.78	1.18
15	1.83	1.22
30	1.95	1.32
45	2.03	1.39
60	2.13	1.42
75	2.18	1.46
120	2.36	1.57
150	2.44	1.62
200	2.52	1.67
225	2.59	1.68
300	2.67	1.73
390	2.72	1.78
480	2.74	1.82
540	2.74	1.82
600	2.74	1.82

$Q = 0.475\ cm^3/s$

t(s)	B_1	B_2
1	1.63	–
3	1.73	–
5	1.86	1.17
7	1.88	1.20
10	1.93	1.22
20	2.03	1.32
30	2.13	1.37
45	2.23	1.42
60	2.29	1.48
75	2.36	1.53
100	2.44	1.60
120	2.49	1.63
150	2.54	1.67
225	2.64	1.73
300	2.72	1.78
390	2.78	1.83
480	2.82	1.87
540	2.82	1.87
600	2.82	1.87

TABLE A3.24 Swell as a Function of Time

(20° Converging Die, Resin 27)

$Q = 0.950\ cm^3/s$			$Q = 2.375\ cm^3/s$		
t(s)	B_1	B_2	t(s)	B_1	B_2
1	1.67	-	1	1.71	-
3	1.78	1.20	2	1.80	-
5	2.11	1.31	3	2.05	1.26
10	2.24	1.39	5	2.22	1.51
15	2.30	1.45	10	2.36	1.64
30	2.40	1.52	15	2.42	1.66
60	2.51	1.60	20	2.49	1.68
75	2.56	1.67	30	2.57	1.73
120	2.67	1.75	45	2.68	1.78
150	2.72	1.82	75	2.76	1.83
225	2.83	1.90	120	2.83	1.94
300	2.88	1.96	150	2.89	1.99
390	2.94	2.03	225	2.99	2.10
480	2.99	2.08	300	3.08	2.14
540	2.99	2.08	390	3.15	2.20
600	2.99	2.08	480	3.20	2.27
			540	3.20	2.31
			600	3.20	2.31

TABLE A3.25 Swell as a Function of Time

(20° Converging Die, Resin 29)

Q = 0.024 cm^3/s			Q = 0.095 cm^3/s		
t(s)	B_1	B_2	t(s)	B_1	B_2
1	1.12	-	1	1.29	-
2	1.15	-	2	1.34	-
3	1.19	-	3	1.40	-
5	1.26	-	5	1.48	-
105	1.87	1.31	10	1.61	-
150	1.90	1.33	20	1.84	1.23
225	1.96	1.37	45	1.90	1.31
270	1.99	1.39	75	2.00	1.38
360	2.02	1.41	120	2.11	1.43
420	2.05	1.43	180	2.22	1.48
480	2.08	1.43	225	2.26	1.52
540	2.11	1.43	300	2.32	1.56
600	2.11	1.43	360	2.38	1.59
			480	2.44	1.62
			540	2.44	1.62
			600	2.44	1.62

TABLE A3.26 Swell as a Function of Time

(20° Converging Die, Resin 29)

$Q = 0.238$ cm^3/s			$Q = 0.475$ cm^3/s		
t(s)	B_1	B_2	t(s)	B_1	B_2
1	1.49	-	1	1.59	-
2	1.55	-	2	1.69	-
3	1.62	-	3	1.73	-
5	1.69	1.21	5	1.83	1.26
10	1.87	1.25	10	2.00	1.29
15	1.92	1.28	20	2.06	1.34
30	2.04	1.33	30	2.12	1.37
45	2.16	1.36	60	2.29	1.45
75	2.22	1.41	90	2.35	1.52
105	2.30	1.45	120	2.43	1.56
120	2.33	1.48	150	2.46	1.60
150	2.39	1.51	225	2.52	1.66
225	2.45	1.58	300	2.58	1.72
300	2.51	1.63	360	2.61	1.75
420	2.60	1.68	420	2.64	1.78
480	2.62	1.68	480	2.68	1.79
540	2.62	1.68	540	2.68	1.79
600	2.62	1.68	600	2.68	1.79

TABLE A3.27 Swell as a Function of Time

(20° Converging Die, Resin 29)

Q_o = 0.950 cm^3/s

t(s)	B_1	B_2
1	1.68	-
2	1.81	1.23
3	1.85	1.25
5	1.97	1.29
7	2.02	1.31
10	2.12	1.34
30	2.32	1.44
60	2.46	1.55
90	2.51	1.63
120	2.57	1.67
150	2.62	1.72
225	2.71	1.79
300	2.75	1.85
360	2.77	1.89
420	2.81	1.92
480	2.81	1.96
540	2.81	1.96
600	2.81	1.96

Q = 2.375 cm^3/s

t(s)	B_1	B_2
1	1.78	-
2	1.92	1.26
3	2.00	1.30
5	2.06	1.37
10	2.29	1.42
15	2.41	1.45
30	2.52	1.55
45	2.58	1.60
60	2.63	1.65
80	2.69	1.72
120	2.75	1.79
150	2.78	1.84
180	2.81	1.86
245	2.86	1.91
300	2.90	1.93
360	2.92	1.96
420	2.95	2.00
480	2.98	2.02
540	3.02	2.05
600	3.02	2.05

TABLE A3.28 Swell as a Function of Time

(10° Converging Die, Resin 22A)

$Q = 0.024\ cm^3/s$

t(s)	B_1	B_2
1	1.18	–
2	1.21	–
5	1.27	–
120	1.50	1.51
150	1.55	1.54
180	1.58	1.58
240	1.60	1.63
300	1.63	1.67
330	1.65	1.69
450	1.70	1.74
540	1.75	1.75
600	1.75	1.75

$Q = 0.095\ cm^3/s$

t(s)	B_1	B_2
1	1.39	–
3	1.45	–
5	1.48	–
30	1.65	1.47
45	1.69	1.53
60	1.72	1.56
90	1.79	1.62
120	1.81	1.68
150	1.86	1.72
195	1.89	1.77
225	1.91	1.79
270	1.93	1.81
330	1.96	1.85
540	2.07	1.91
600	2.07	1.91

TABLE A3.29 Swell as a Function of Time

(10° Converging Die, Resin 22A)

$Q = 0.238\ cm^3/s$

t(s)	B_1	B_2
1	1.54	–
2	1.57	–
4	1.60	–
5	1.63	1.35
10	1.66	1.48
15	1.73	1.55
30	1.83	1.61
45	1.87	1.64
90	1.95	1.73
120	1.98	1.79
150	2.01	1.83
225	2.08	1.92
300	2.12	1.97
360	2.14	1.99
420	2.17	2.01
480	2.19	2.01
540	2.19	2.01
600	2.19	2.01

$Q = 0.475\ cm^3/s$

t(s)	B_1	B_2
1	1.61	–
2	1.63	–
3	1.69	–
5	1.77	1.38
10	1.87	1.59
15	1.90	1.67
30	1.94	1.77
60	1.99	1.87
80	2.04	1.92
105	2.07	1.95
120	2.09	1.97
150	2.12	2.01
210	2.19	2.06
240	2.21	2.08
300	2.26	2.12
360	2.29	2.15
420	2.31	2.16
480	2.34	2.17
540	2.34	2.17
600	2.34	2.17

TABLE A3.30 Swell as a Function of Time

(10° Converging Die, Resin 22A)

$Q = 0.950\ cm^3/s$			$Q = 2.375\ cm^3/s$		
t(s)	B_1	B_2	t(s)	B_1	B_2
1	1.69	-	1	1.76	-
2	1.76	-	2	1.81	-
3	1.82	-	3	1.84	1.73
5	1.93	1.46	4	1.91	1.81
15	2.03	1.70	6	1.96	1.83
40	2.13	1.89	10	2.05	1.86
60	2.18	1.98	15	2.12	1.91
105	2.24	2.09	30	2.19	2.00
120	2.26	2.12	45	2.24	2.10
150	2.29	2.16	60	2.27	2.16
225	2.34	2.21	90	2.34	2.25
300	2.36	2.26	120	2.39	2.29
360	2.39	2.29	150	2.43	2.34
480	2.44	2.32	210	2.51	2.39
540	2.46	2.32	300	2.58	2.44
600	2.46	2.32	360	2.60	2.48
			540	2.65	2.52
			600	2.65	2.52

TABLE A3.31 Swell as a Function of Time (10° Converging Die, Resin 27)

$Q = 0.024\ cm^3/s$			$Q = 0.095\ cm^3/s$		
t(s)	B_1	B_2	t(s)	B_1	B_2
1	1.22	-	1	1.33	-
2	1.25	-	2	1.40	-
3	1.30	-	3	1.49	-
5	1.35	-	5	1.54	-
120	1.82	1.80	30	1.80	1.85
180	1.90	1.89	45	1.87	1.90
240	2.00	1.95	75	1.95	2.00
300	2.05	2.00	90	2.02	2.02
375	2.10	2.05	135	2.15	2.08
480	2.20	2.10	165	2.20	2.13
540	2.20	2.10	210	2.27	2.18
600	2.20	2.10	300	2.40	2.25
			390	2.45	2.32
			480	2.50	2.38
			540	2.50	2.40
			600	2.50	2.40

TABLE A3.32 Swell as a Function of Time

(10° Converging Die, Resin 27)

$Q = 0.238\ cm^3/s$			$Q = 0.475\ cm^3/s$		
t(s)	B_1	B_2	t(s)	B_1	B_2
1	1.46	-	1	1.63	-
2	1.60	-	2	1.66	-
3	1.63	-	3	1.74	-
5	1.72	-	5	1.84	1.75
20	1.92	1.83	10	2.00	1.80
25	1.97	1.90	15	2.10	1.90
30	2.00	1.93	30	2.19	2.00
45	2.05	2.00	45	2.25	2.10
60	2.13	2.06	75	2.37	2.20
75	2.20	2.11	105	2.45	2.30
105	2.25	2.20	180	2.55	2.45
150	2.35	2.30	240	2.62	2.50
240	2.50	2.40	300	2.67	2.55
330	2.60	2.45	360	2.69	2.60
480	2.65	2.50	480	2.77	2.63
540	2.65	2.50	540	2.77	2.63
600	2.65	2.50	600	2.77	2.63

TABLE A3.33 Swell as a Function of Time

(10° Converging Die, Resin 27)

$Q = 0.950\ cm^3/s$			$Q = 2.375\ cm^3/s$		
t(s)	B_1	B_2	t(s)	B_1	B_2
1	1.66	–	1	1.71	–
2	1.73	–	2	1.78	1.79
3	1.74	1.74	3	1.93	1.84
5	2.00	1.80	5	2.11	1.90
10	2.17	1.90	10	2.28	2.05
15	2.20	2.00	20	2.39	2.18
25	2.35	2.10	25	2.44	2.24
45	2.50	2.20	45	2.59	2.40
90	2.60	2.36	90	2.69	2.60
135	2.68	2.50	150	2.80	2.76
180	2.75	2.60	240	2.90	2.90
240	2.82	2.65	300	3.00	2.95
310	2.96	2.70	360	3.05	2.98
360	2.95	2.74	480	3.10	3.00
480	2.98	2.79	540	3.10	3.00
540	2.98	2.79	600	3.10	3.00
600	2.98	2.79			

APPENDIX A4

Data Obtained in the Combined Effects of Sag and Swell Experiments and Comparison with Model Predictions

TABLE A4.1 Comparison of Experimental and Predicted Values of Parison Length (Resin 27, Straight Die, m=9 g)

$Q = 0.238\ cm^3/s$

t (s)	L (cm) Experimental	L (cm) Calculated
10	0.50	0.42
15	1.59	1.74
24	3.97	4.04
32	6.11	6.07
40	8.25	8.12
48*	10.16	10.24
60	10.16	10.29
75	10.16	10.30
90	10.16	10.38

$Q = 0.475\ cm^3/s$

t (s)	L (cm) Experimental	L (cm) Calculated
5	1.98	1.77
10	4.20	3.94
15	6.03	6.10
20	8.17	8.28
24*	10.10	10.03
30	10.12	10.05
35	9.76	10.05
45	9.60	10.07
60	9.52	10.20
90	9.60	10.93

---

* extrusion time

TABLE A4.2 Comparison of Experimental and Predicted Values of Parison Length (Resin 27, Straight Die, m=9 g)

Q = 0.950 cm^3/s

t (s)	L (cm)	
	Experimental	Calculated
1	0.63	0.53
2	1.45	1.41
3.5	2.62	2.61
5	3.57	3.90
10	8.01	8.10
12*	10.24	9.91
15	10.16	9.91
20	9.76	9.91
30	9.45	9.90
45	9.20	9.95
60	9.13	10.15
90	9.28	11.14

Q = 2.375 cm^3/s

1	2.20	1.99
2	4.16	3.97
3	6.10	5.97
4	8.10	7.98
4.8*	10.00	9.70
10	9.50	9.71
20	8.98	9.72
30	8.81	9.73
45	8.81	9.80
60	8.81	10.03
90	8.90	11.12

---

* extrusion time

TABLE A4.3 Comparison of Experimental and Predicted Values of Parison Length (Resin 27, Straight Die, m=6.8 g)

$Q = 0.238\ cm^3/s$

t (s)	L (cm) Experimental	L (cm) Calculated
10	1.20	1.32
14	2.40	2.36
20	4.02	3.89
25	5.20	5.17
30	6.35	6.44
36*	7.78	7.98
40	7.78	7.97
45	7.62	7.93
60	7.62	7.79
75	7.62	7.70
90	7.62	7.65
105	7.78	7.66
120	7.86	7.70

$Q = 0.475\ cm^3/s$

t (s)	L (cm) Experimental	L (cm) Calculated
5	1.74	1.77
8	3.09	3.08
10	4.04	3.94
15	6.19	6.12
18*	7.62	7.43
20	7.62	7.43
25	7.46	7.36
30	7.36	7.30
45	7.14	7.17
60	7.14	7.11
75	7.14	7.14
90	7.14	7.24
105	7.22	7.42
120	7.30	7.69

---

* extrusion time

TABLE A4.4 Comparison of Experimental and Predicted Values of Parison Length (Resin 27, Straight Die, m=6.8 g)

$Q = 0.950\ cm^3/s$

t (s)	L (cm)	
	Experimental	Calculated
3	2.35	2.40
4	3.17	3.16
5	4.13	4.08
6	5.08	4.82
7	5.87	5.74
8	6.82	6.62
9*	7.69	7.43
15	7.46	7.37
20	7.38	7.30
30	7.14	7.17
45	6.98	7.04
60	6.82	7.00
75	6.82	7.04
90	6.82	7.14
120	6.98	7.70

$Q = 2.375\ cm^3/s$

t (s)	Experimental	Calculated
1	1.90	1.79
2	3.97	3.77
3	5.85	5.78
3.6*	7.22	7.00
5	7.06	7.00
10	6.67	6.95
20	6.35	6.83
30	6.19	6.72
45	6.19	6.60
60	6.19	6.55
75	6.19	6.58
90	6.25	6.68
120	6.51	7.13

---

* extrusion time

TABLE A4.5 Comparison of Experimental and Predicted Values of Parison Length (Resin 27, Diverging Die, m=6.8 g)

$Q = 0.475\ cm^3/s$

t (s)	L (cm) Experimental	L (cm) Calculated
2.5	1.29	1.31
5	2.59	2.74
7	3.94	3.90
10	5.69	5.71
15	8.55	8.59
18*	10.45	10.41
20	10.45	10.47
25	10.45	10.47
30	10.37	10.45
45	10.29	10.40
60	10.29	10.38
75	10.29	10.44
90	10.45	10.59
105	10.61	10.84
120	10.77	11.20

$Q = 0.950\ cm^3/s$

t (s)	L (cm) Experimental	L (cm) Calculated
1	1.11	1.10
3	3.27	3.28
4	4.44	4.38
5	5.55	5.46
7	7.77	7.66
8	9.04	8.79
9*	10.31	9.88
12	10.23	9.95
15	10.00	9.95
20	9.84	9.95
30	9.68	9.91
45	9.52	9.87
60	9.52	9.89
90	9.68	10.18
105	9.88	10.48
120	10.16	10.91

---

* extrusion time

TABLE A4.6 Comparison of Experimental and Predicted Values of Parison Length (Resin 27, 20° Converging Die, m=6.8 g)

$Q = 0.475\ cm^3/s$

t (s)	L (cm) Experimental	L (cm) Calculated
3	0.80	1.00
5	2.94	2.47
8	4.79	4.51
10	6.19	5.97
15	9.74	9.57
18*	11.75	11.83
20	11.67	12.04
25	11.11	12.23
30	10.79	12.39
46	10.40	13.04
60	10.40	13.93

$Q = 0.950\ cm^3/s$

t (s)	L (cm) Experimental	L (cm) Calculated
2	2.54	2.55
4	4.91	5.06
5	6.03	6.30
6	7.54	7.59
7	8.81	8.84
8	10.00	10.19
9*	11.74	11.45
10	11.59	11.59
15	10.95	11.64
15	10.95	11.64
20	10.56	11.69
30	10.16	11.95
45	9.92	12.80
60	9.84	14.44

---

* extrusion time

APPENDIX A5

Lodge's Rubber-like Liquid Model: Application to uniaxial extension with time-dependent strain rate

The general form of Lodge's "rubber-like liquid" model is (Lodge, 1974; Bird et al., 1979):

$$\tau(t) = \int_{-\infty}^{t} \left(\sum \frac{G_{ok}}{\lambda_{ok}} e^{-(t-t')/\lambda_{ok}}\right) \underline{H}^{-1}(t,t')dt' \qquad \text{A5.1}$$

To determine the finger strain tensor, $\underline{H}^{-1}$, imagine a fluid flowing in a region with a space fixed cartesian coordinate system. At the present time t, a fluid particle has coordinates x_i (i = 1, 2, 3). At some past time t', that fluid particle had coordinates x_i' (i = 1, 2, 3). The displacements functions for a particular fluid element are defined as the functions giving the past coordinates of the particle in terms of the present coordinates, the present time and the past time, that is:

$$x_i' = x_i'(x , t, t') \qquad \text{A5.2}$$

The cartesian components of the fluid velocity, $\underline{v}(x',t')$ at the position x' at time t' are defined as the velocity components $v_i(x, t, t')$ of the particle (x, t) that happened to pass through the point x' at time t', that is:

$$v_i(x', t') = v_i(x, t, t') = \frac{\partial}{\partial t'} x_i'(x, t, t') \qquad \text{A5-3}$$

Alternatively, the displacement functions may be expressed in terms of the velocity field by integration of the above equations as follows:

$$x_i - x_i' = \int_{t'}^{t} v_i(x, t, t'')\, dt'' \qquad \text{A5-4}$$

The Finger strain tensor appearing in equation A5-1 can be found in terms of the displacement functions through the following relations:

$$\underline{H}^{-1} = \underline{C}^{-1} - 1 = (\underline{F}^{-1})(\underline{F}^{-1})^T - 1 \qquad \text{A5-5}$$

$$\underline{F}^{-1} = \frac{\partial x_i}{\partial x_j'} \qquad \text{A5-6}$$

where $\underline{C}^{-1}$ is the finger tensor, $\underline{F}^{-1}$ is the inverse of deformation gradient tensor and $(\underline{F}^{-1})^T$ is the transpose of $(\underline{F}^{-1})$.

Taking x_1 to indicate the principal strecth direction, the uniaxial extensional flow is described by the following velocity distribution:

$$v_1 = \dot{\varepsilon}(t)\ x_1 \qquad \text{A5-7a}$$

$$v_2 = -1/2\ \dot{\varepsilon}(t)\ x_2 \qquad \text{A5-7b}$$

$$v_3 = -1/2\ \dot{\varepsilon}(t)\ x_3 \qquad \text{A5-7c}$$

For the case under consideration, the extensional strain rate is:

$$\dot{\varepsilon}(t) = 0 \qquad \text{for } t<0 \qquad \text{A5-8a}$$

$$\dot{\varepsilon}(t) = \dot{\varepsilon}(t) \qquad \text{for } t\geq 0 \qquad \text{A5-8b}$$

Using equations A5-7 and A5-4 and the initial condition that $x_1' = x_1$ at $t' = t$, the following expressions are obtained for $0 \leq t' < t$:

$$x_1 = x_1' \exp \left\{ \int_{t'}^{t} \dot{\varepsilon}(t'')\ dt'' \right\} \qquad \text{A5-9a}$$

$$x_2 = x_2' \exp \left\{ -1/2 \int_{t'}^{t} \dot{\varepsilon}(t'')\ dt'' \right\} \qquad \text{A5-9b}$$

$$x_3 = x_3' \exp \left\{ -1/2 \int_{t'}^{t} \dot{\varepsilon}(t'')\ dt'' \right\} \qquad \text{A5-9c}$$

The length of the hypothetical unswollen element z can be introduced into the above equations using the definition of the extensional strain rate:

$$\dot{\varepsilon}(t) = \frac{1}{z}\frac{dz}{dt} = \frac{d\ln z}{dt} \qquad \text{A5-10}$$

Integrating the above equation we obtain:

$$\ln \frac{z(t)}{z(0)} = \int_0^t \dot{\varepsilon}(t'')dt'' \qquad -\infty \leqslant t' < 0 \qquad \text{A5.11}$$

$$\ln \frac{z(t)}{z(t')} = \int_{t'}^t \dot{\varepsilon}(t'')dt'' \qquad 0 \leqslant t' < t \qquad \text{A5.12}$$

where $z(t)$, $z(0)$, $z(t')$ denote the values of z at present time t, at $t=0$, and some past time t' respectively. Substitution of equation A5-12 into equations A5-9 gives:

$$x_1 = x_1' \; z(t)/z(t') \qquad \text{A5-13a}$$

$$x_2 = x_2' \; (z(t')/z(t))^{1/2} \qquad 0 \leqslant t' < t \qquad \text{A5-13b}$$

$$x_3 = x_3' \; (z(t')/z(t))^{1/2} \qquad \text{A5-13c}$$

For times $-\infty < t' < 0$ equations A5-13 can be evaluated at $t'=0$ using the continuity of the displacement functions. The following relations are obtained:

$$x_1 = x_1' \; z(t)/z(0) \qquad \text{A5-14a}$$

$$x_2 = x_2' \; (z(0)/z(t))^{1/2} \qquad -\infty \leqslant t' < t \qquad \text{A5-14b}$$

$$x_3 = x_3' \; (z(0)/z(t))^{1/2} \qquad \text{A5-14c}$$

Using the displacement functions the diagonal elements of the inverse of the deformation gradient tensor can be obtained from equation A5-6. Since all other terms except the diagonal terms are zero, $\underline{F}^{-1} = (\underline{F}^{-1})^T$. For $0 \leq t' < t$:

$$(\underline{F}^{-1}_{11})^T = \underline{F}^{-1}_{11} = \partial x_1/\partial x'_1 = z(t)/z(t') \qquad \text{A5-15a}$$

$$(\underline{F}^{-1}_{22})^T = (\underline{F}^{-1}_{33})^T = \underline{F}^{-1}_{22} = \partial x_2/\partial x'_2 = (z(t')/z(t))^{1/2} \qquad \text{A5-15b}$$

and the finger strain tensor is obtained from equation A5-5.

$$\underline{H}^{-1}_{11} = (z(t)/z(t'))^2 - 1 \qquad \text{A5-16a}$$

$$\underline{H}^{-1}_{22} = H^{-1}_{33} = (z(t')/z(t)) - 1 \qquad \text{A5-16b}$$

Using a similar procedure, the finger strain tensor for $-\infty < t' < 0$ is:

$$\underline{H}^{-1}_{11} = (z(t)/z(0))^2 - 1 \qquad \text{A5-17a}$$

$$\underline{H}^{-1}_{22} = \underline{H}^{-1}_{33} = (z(0)/z(t)) - 1 \qquad \text{A5-17b}$$

Combining equations A5-16, A5-17 and A5-1 the final equation is obtained as:

$$\tau_{11} - \tau_{22} = \left(\Sigma G_{ok} e^{-t/\lambda_{ok}}\right)\left(\frac{z^2(t)}{z^2(0)} - \frac{z(0)}{z(t)}\right) - \int_0^t \left(\Sigma \frac{G_{ok}}{\lambda_{ok}} e^{-(t-t')/\lambda_{ok}}\right)\left(\frac{z(t')}{z(t)} - \frac{z^2(t)}{z^2(t')}\right) dt' \qquad \text{A5-18}$$

APPENDIX A6

Computer Program (in Basic) Used to Solve the Model Equations

```
2 OPEN 2,4,2
3 OPEN 3,4,1
4 OPEN 4,4,2
5 OPEN 5,4,1
10 DIM Z(10),ZZ(10),E(10),F(5),H(5)
11 DIM G(10),Q(10),P1T(5,4),P2T(5,4)
12 REM ........................................
13 REM DATA INPUT:RELAXATION SPECTRUM
15 FOR M=1 TO 3
16 READ G(M)
18 NEXT
20 DATA 16956,6357,1420
24 PRINT#5,"RELAXATION SPECTRUM"
25 FOR MM=1 TO 3
26 READ Q(MM):PRINT#5,Q(MM),G(MM)
28 NEXT
30 DATA 0.316,3.16,31.6
31 REM ........................................
35 RO=.793:GR=9.81
37 REM ........................................
38 REM CONSTANTS OF EQUATION 6.3.11A
40 BI=1.7372:B0=1.3351:L1=56.86
41 REM ........................................
42 REM ........................................
43 REM CONSTANTS OF EQUATION 6.3.11B
45 TBI=1.9223:T0B=1.4270:L2=210.81
46 REM ........................................
50 VB=10:TE=17
55 DT=3.4:DELT=.20
60 BN=TE/DT
71 PRINT#1:PRINT#1:PRINT#1
75 VD=36*VB/(7*60)
76 REM ........................................
77 REM INITIAL VALUE OF Z(I)
80 FOR JJ=1 TO BN
82 ZZ(JJ)=VD*DT:Z(JJ)=3.1
84 NEXT
85 REM .......................
86 Z(1)=ZZ(1)
87 IDT=DT/2
90 IB=BI-(BI-B0)*EXP(-IDT/L1)
91 IC=TBI-(TBI-T0B)*EXP(-IDT/L2)
92 FOR KK=1 TO BN
93 FOR KY=1 TO 3
94 P1T(KK,KY)=0.0:P2T(KK,KY)=0.0
95 NEXT:NEXT
```

```
100 FOR TT=1.2 TO 200 STEP 0.2
101 T=TT-1
105 IF T>TE GOTO 140
110 AN=T/DT:BAN=INT(AN):HN=AN-BAN
115 IF (HN<0.001) THEN 122
120 N=INT(AN)
121 GOTO125
122 NN=AN-1:N=INT(NN)
125 LEXT=VD*(T-N*DT)/(IB*IC)
130 S0=LEXT
131 IF N=0 GOTO 250
135 GO TO 150
140 N=TE/DT
145 S0=0.0
150 FOR I=1 TO N
155 IT=T-I*DT
160 TS=IT+DT/2
165 IF I=1 GOTO 220
172 REM .......................................
173 REM SOLVING EQUATION 6.3.21
174 AT=0.0:FT=0.0:HT=0.0
176 FOR Y=1 TO 3
178 A=EXP(-IT/Q(Y))
180 AT=AT+(A*G(Y))
182 F(I)=Z(I)
184 FA=(DELT/2.0)*(ZZ(I)*A+F(I))+DELT*P1T(I,Y)
186 FB=(G(Y)/Q(Y))*FA
188 FT=FT+FB
190 H(I)=(1.0/(Z(I)↑2))
192 HA=(DELT/2.0)*(A/(ZZ(I)↑2)+H(I))+DELT*P2T(I,Y)
194 HB=(G(Y)/Q(Y))*HA
196 HT=HT+HB
200 NEXT
201 TAU=AT*((Z(I)/ZZ(I))↑2-ZZ(I)/Z(I))-FT/Z(I)+(Z(I)↑2)*HT
202 REM .......................................
203 ZC(I)=TAU/(RO*GR*(I-1)*10)
204 REM ......................................
205 REM CONVERGING Z(I)
208 GOSUB 1000
210 Z(I)=X
212 IF(NC=2) THEN 174
213 REM .........................
220 GOSUB 500
223 REM .......................................
224 REM AREA SWELL
225 SW=S5*S6
226 PRINT#5,"SW",SW,"Z",Z(I)
227 REM .......................................
230 W=Z(I)/SW
240 S0=S0+W
241 FOR K=1 TO 3
242 P1T(I,K)=EXP(-0.2/Q(K))*(P1T(I,K)+F(I))
243 P2T(I,K)=EXP(-0.2/Q(K))*(P2T(I,K)+H(I)):NEXT
245 NEXT
250 PRINT#5,TT,S0
251 S0=0.0:NEXT
300 STOP:END
```

```
498 REM ..................................................
499 REM SUBROUTINE TO CALCULATE PURE SWELL CONTRIBUTION
500 S5=BI-(BI-B0)*EXP(-TS/L1)
505 S6=TBI-(TBI-T0B)*EXP(-TS/L2)
510 RETURN
511 REM ..................................................
998 REM ..................................................
999 REM SUBROUTINE FOR WEGSTEIN'S METHOD OF CONVERGENCE
1000 IF(ABS((X-XC)/(X+XC)))<0.001 GOTO 1060
1005 IF(NC<=1) GOTO 1035
1010 XT=(XA(1)*XC-YA(1)*X)/(XA(1)-X+XC-YA(1))
1012 PRINT"XA,YA",XA(1),YA(1)
1013 PRINT"X,XC",X,XC
1015 XA(1)=X
1020 YA(1)=XC
1025 X=XT
1026 PRINT "XT",XT
1030 GOTO 1070
1035 XA(1)=X
1040 YA(1)=XC
1045 X=XC
1050 NC=2
1055 GOTO 1070
1060 X=XC
1065 NC=1
1070 RETURN
1071 REM ................................................
```